Teleoperation of Pneumatic Actuators: Design, Experimental Evaluation, and Stability Analysis

BY

Naghmeh Garmsiri

A thesis submitted to the Faculty of Graduate Studies of

University of Manitoba

In partial fulfillment of the requirement of the degree of

Doctor of Philosophy

Department of Mechanical and Manufacturing Engineering

University of Manitoba

Winnipeg

Abstract

Pneumatic systems are inexpensive, safe and require low maintenance. Because of the actuation material, air, they are potential candidates for dealing with external force. Teleoperation of pneumatic actuators can be very beneficial in applications in which the remote actuator needs to interact with the external force, e.g. telerehabilitation.

This thesis focuses on the teleoperation of a low-cost solenoid-driven pneumatic actuator. Firstly, a novel intelligent position controller is applied and experimented with on the pneumatic actuator and is later compared to two other controllers. The best among the three is chosen for the rest of the thesis. A unilateral pneumatic teleoperation system employing an electrically-actuated joystick is successfully developed and evaluated using impedance and admittance control schemes for dealing with the external force. Stability analysis is assured for autonomous and non-autonomous systems using the concept of Lyapunov Exponents (LEs). The concept of LEs allows the stability analysis of an available system, and as a result, it does not impose any limitations on the system parameters. In addition, it can show the effect of changing a certain parameter on the stability. Using this concept, the effect of changing a few parameters on stability is studied. The performances of admittance and impedance unilateral systems are then compared in terms of positioning accuracy, energy dissipation and fast response to the external force. It is shown that admittance unilateral teleoperation offers higher positioning accuracy and damping characteristics and reacts faster to the external force.

For the first time, a bilateral teleoperation system is applied to a solenoid valve-driven pneumatic actuator using an electrically-actuated haptic device. Unlike the last two methods, the slave robot does not deal with the external force independently. Instead, this

force is rendered on a haptic device and felt by the operator. By changing the admittance of the hand, the operator indirectly deals with the external force. Experimental verification shows the effectiveness of the developed bilateral teleoperation system.

Acknowledgments

I would first like to express my sincerest gratitude to my research supervisor, Dr. Nariman Sepehri, for giving me the opportunity to do my PhD under his supervision. I feel very fortunate for having this fabulous opportunity to work under an extremely knowledgeable and passionate supervisor and this research could not have been completed without his invaluable guidance, support, and encouragement.

My sincere thanks go out to the members of my advisory committee, Dr. Subramaniam Balakrishnan and Dr. Udaya Annakkage, for their careful review, comments and suggestions, which greatly improved this thesis.

I also would like to express my heartfelt appreciation to Dr. Christine Wu, who was always available to help by providing me with background knowledge and inspiring ideas. A special word of thanks is due to Dr. Pooya Sekhavat, Dr. Caixia Yang and Dr. Yuming Sun, from whom I received consistent support and encouragement in publishing the outcome of this research.

I would like to place on record my acknowledgment to the Natural Science and Engineering Research Council (NSERC) Canada and the University of Manitoba for providing financial support for this research.

I would like to thank my peers in the "Fluid Power and Telerobotics Research Laboratory" at the University of Manitoba, who helped make this journey more pleasant.

Finally, I would like to acknowledge my deepest gratitude to my family for their love, sacrifice, and support throughout my life.

. . . . to my parents.

Table of Contents

List of Tables

List of Figures

x

Nomenclature

Roman

A	Piston annulus area
A_i	Activation signal in the current iteration
Av_{eq}	Equivalent part of SMC
Av_{rb}	Robust part of SMC
b	Viscous damping coefficient
B	Damping coefficient of admittance/impedance control
b_m	Combined damping of the master manipulator
C_d	Valve coefficient of discharge
$e, e_x, \dot{e}, \ddot{e}, \dddot{e}$	Position error and derivatives
e_f	Force error
F_a	Actual force of the actuator
F_c	Coulomb friction
F_d	Desired force of the actuator
F_{ext}	External force
F_f	Dry friction
F_h	Force generated by the operator`s hand
F_m	Force applied to the operator's hand
F_s	Static friction
Fx	Associative variable in SMC
$f(x)$	Nonlinear function
K	Stiffness of admittance/impedance control
K_a	Learning rate of activation signals in BELBIC
K_{adm}	Stiffness term in the admittance model
K_{ext}	Stiffness coefficient of the environment
k_m	Combined stiffness of the master manipulator
K_o	Learning rate of inhibition signals in BELBIC
K_{rb}	SMC robustness gain
K_v	Valve spool position gain
L	Actuator stroke
m	Total mass of actuator`s moving parts
M	Inertia of admittance/impedance control
m_m	Combined inertia of the master manipulator
$\dot{m}_1, \dot{m}_2$	Air mass flow in actuator chamber 1 and 2
O_i	Inhibition signal in the current iteration
$P_1, P_2, \dot{P}_1, \dot{P}_2$	Air pressure in chamber 1 and 2 and derivatives
P_a	Atmospheric pressure
P_{cr}	Valve critical pressure ratio
P_s	Supply pressure
Px	Associative variable in SMC
R	Ideal gas constant
Rew_i	Reward signal at iteration i
$S, \dot{S}$	Sliding surface and derivative

SI_i	Sensory input signal at iteration i
T	Temperature of air source
u	Control signal
V_1, V_2	Instantaneous volume of air in actuator chamber 1 and 2
V_0	Cylinder inactive volume
v_{sv}	Stribeck velocity
w	Valve orifice area gradient
$x_d, \dot{x}_d, \ddot{x}_d, \dddot{x}_d$	Desired position and derivatives
$\vec{x}_{eq}$	Equilibrium vector
x_{ext}	Displacement corresponding to external force
x_i	State space variable of nonlinear equation
$x_m, \dot{x}_m, \ddot{x}_m$	Displacement, velocity, acceleration of the master actuator
$x_s, \dot{x}_s, \ddot{x}_s$	Displacement, velocity, acceleration of the slave actuator
$x_v, \dot{x}_v$	Displacement of the valve spool and derivative
$z, \dot{z}$	Average bristle deflection, derivative of z

Greek

α	Compressibility flow correction factor
δ	SMC control bandwidth
$\gamma, \bar{\gamma}$	Ratio of specific heats and a function of it
λ_i	The i-th Lyapunov exponent
σ_0, σ_1	Equivalent spring constant and damping coefficient of bristle
τ	Valve first-order time constant
$\dot{\emptyset}_1, \dot{\emptyset}_2$	mass flow per area unit in chambers 1 and 2

1. INTRODUCTION

1.1. Statement of the Problem

Teleoperation is widely used in different applications. Examples include carrying hazardous material [1] and delicate tasks such as microsurgery [2]. A teleoperated system is composed of a master device, operated by a human on one end, a slave manipulator on the other end that emulates the motion of the master, and a central controller that coordinates the system through a communication channel [3].

Teleoperation systems have two major categories: unilateral and bilateral. If the slave manipulator reflects the interaction force with the environment (called external force) back to the master, the teleoperation system is called bilateral [1]. The operator feels the external force and reacts accordingly by changing the stiffness of his/her hand. Although providing the haptic force at the master side enables the human operator to rely on their tactile senses along with other sensory information such as visual and audio information, it may make the stability of the overall teleoperation system more vulnerable [4]. If only the information of the master is transmitted to

the slave, the teleoperation system is called unilateral. Using a unilateral system eliminates the complexity of rendering the external force on the hand-controller. Furthermore, it also reduces the burden of dealing with external force on the operator side and helps the operator to focus on navigating the slave actuator. On the other side, the slave actuator should be able to deal with the external force independently.

Using pneumatic actuators in teleoperation systems offers several advantages. Pneumatic actuators are clean, inexpensive, easy to maintain, and are light for the amount of power they provide. Furthermore, the compressibility of air makes these actuators able to absorb unwanted force [5]. In addition to these properties, however, pneumatic actuators also have certain non-idealities, which make them less effective in accurate applications. These nonidealities include the compressibility of the air flow rate, dry friction and the overlapping of the valve spool that controls the air flow into and out of the actuator. Given these nonidealities, precise control of pneumatic actuators is challenging [6]. In a teleoperation system, the effect of dry friction and overlapping of the valve spool may delay motion of the slave in response to the master. Presence of delay might affect the feeling of being present to the operator.

In teleoperation applications, the slave manipulator requires extensive interaction with an environment and the motion of the manipulator is influenced by external force [7]. The stable interaction between the environment and the teleoperated slave manipulator is not always guaranteed [8]. This is very undesirable when the interaction is with fragile environments and potentially risky for both the slave actuator and the environment [9]. These facts justify the need for a tool that provides theoretical support for stability verification. Indeed, a quantitative indicator is required to show how stability changes as a result of variations in parameters such as controller gains or the physical parameters of the system.

The focus of this thesis is the interaction of a solenoid valve-driven pneumatic actuator with the environment over a local network. A commercial haptic device is used to navigate the pneumatic actuator. In summary, three main concerns are considered for effective teleoperation in this research:

(i) Control of pneumatic actuators is not easily achievable due to severe nonidealities. The positioning accuracy is of great interest in teleoperation systems.

(ii) Force interaction in a teleoperation system can be unilateral or bilateral. Each type comes with certain benefits and challenges.

(iii) Stability analysis of the whole teleoperation system is essential because of the presence of external force.

A potential application of a pneumatic teleoperation system can be telerehabilitation treatment. Telerehabilitation refers to the delivery of rehabilitation practices to a distant patient. In cases in which physiotherapists are located in a central clinic, patients can receive treatment in their homes through physical interaction with manipulators mounted in their residence. The physiotherapist navigates the remote manipulator through a master manipulator in a teleoperation manner. By using this method, the reach of physiotherapists will extend to almost anywhere, which is extremely beneficial for patients who have difficulty traveling. Pneumatic actuators are clean and affordable. Because of their actuation medium, air, they are suitable for force interaction. These characteristics make them able to be used for rehabilitation applications.

1.2. Objectives of this Thesis

The objectives of this thesis are:

I. For sake of being used in a human-haptic-pneumatic system, to find a suitable positioning method for a pneumatic actuator which works in a teleoperation system. It

should be noted that the performance of the teleoperation systems is strongly influenced by the positioning accuracy. The controller should provide reasonable position tracking accuracy, especially with hand-controller-generated trajectories, act robustly in the presence of external force, and have a simple structure.

II. To find a proper method of simultaneous control of force and position that (1) offers reasonable position tracking during the force interaction with the environment; (2) is able to provide a wide range of stiffnesses to the in-site operator in interacting with the slave; and (3) is stable.

III. To provide a theoretical approach for the stability analysis of the entire teleoperation system, the stability analysis method should have the following characteristics: (1) takes into account the complexity of the system as much as possible; (2) provides a quantitative measurement of the stability; and (3) does not impose conservative limitations on system parameters or control gains.

1.3. Methodologies and Approaches

This research is divided into three parts. The first part aims to address the first objectives, and includes the study of three position tracking methods. Firstly, a novel controller, the Brain Emotional Learning Based Intelligent Controller, BELBIC, is implemented and for the first time evaluated on a pneumatic actuator. BELBIC is model-free, and thus is robust to model uncertainties and external force [10]. Motivated by this fact, BELBIC is implemented in the positioning of the pneumatic actuator. The performance of BELBIC is compared to a Nonlinear Proportional Integral (NPI) controller. NPI was previously developed and evaluated on the same test rig as BELBIC [11]. Because both controllers are evaluated on the same test rig, a fair comparison is achievable. Later, BELBIC is experimentally compared to the Sliding Mode Controller, SMC, which is the most-established positioning method of pneumatic actuators

according to the literature [6]. Performance comparison is carried out on several tracking and regulating tasks.

Toward addressing the second objective, two unilateral and one bilateral teleoperation methods are considered. To evaluate each method, different experiments are done in which the actuator is navigated by the hand-controller and an external force is imposed on the actuator by a human subject. To deal with the external force in the unilateral teleoperation, impedance and admittance control schemes are implemented. The position controller for admittance unilateral teleoperation is obtained from the first part of the research. For impedance unilateral teleoperation, an SMC force controller is chosen based on the literature [12]. Different experiments are conducted for performance evaluation including dealing with high and low stiffness environments. The performances of these unilateral teleoperation methods are compared using the criteria mentioned in the previous section.

To address the third research objective, theoretical analysis using the concept of Lyapunov Exponents (LEs) is used that works based on the dynamic model. For each teleoperation method mentioned above, stability is assured by observing the evolution of an infinitesimally deviated system over a long period of time. In other words, LEs show the rate of separation of the originally infinitesimally close trajectories. The original system is stable if the deviated system behaves similarly to the original. An autonomous and a non-autonomous case are considered for each method. The concept of LEs shows the effect that changing any parameter has on the stability. Using this feature, some studies are done as examples to show how the system changes by changing a certain parameter.

1.4. Thesis Outline

The remainder of this thesis is divided into 9 chapters. A detailed literature review is presented in **Chapter 2**, which includes the present research on the position control, force control, simultaneous position and force control, teleoperation and stability analysis methods of teleoperation systems. In **Chapter 3**, a teleoperation system with the capability of working in unilateral and bilateral modes is described. A single degree of freedom double-rod pneumatic actuator is introduced as the key part of this research. **Chapter 4** describes a stability analysis method that is used later in the thesis.

In **Chapter 5**, the implementation of two position controllers for pneumatic actuators is presented followed by performance comparison in free motion and in the presence of external force. The most promising controller is later utilized by teleoperation systems. **Chapter 6** and **Chapter 7** address the development of unilateral teleoperation employing admittance and impedance control schemes, respectively. Stability analysis is conducted to assure the reliability of the control system. **Chapter 8** presents the development of a bilateral pneumatic teleoperation system followed by stability analysis. **Chapter 9** presents a comparison of the unilateral teleoperation methods that were discussed previously. Finally, **Chapter 10** outlines the contributions made so far, and future work.

2. RELEVANT BACKGROUND

This chapter describes the available approaches to control position, force, and simultaneous force and the position of the pneumatic slave manipulators. Then, the state-of-the-art methods used in teleoperation are presented followed by the methods available for the stability analysis of nonlinear systems.

2.1. Position tracking of Pneumatic Actuators

Prior works have extensively addressed the positioning of pneumatic actuators. Relevant research on this topic includes the design of a robust Proportional Integral (PI) controller using Quantitative Feedback Theory (QFT) to control a low-cost pneumatic actuator [11]. Back-stepping Sliding Mode Control (SMC) was a popular positioning tool for pneumatic positioning [13, 14]. A multi-objective controller was introduced to deal with pneumatic model uncertainties for motion tracking in the presence of a friction parameter change [15].

Implementation of a fuzzy controller was reported in [16]. Augmented controllers, which incorporate adaptive, predictive or observer-based components, have been utilized in this application. A state observer was coupled with an adaptive SMC to enhance the positioning of a pneumatic servo system [17]. A model-predictive approach was implemented for a hybrid pneumatic-electric actuator [18]. A Nonlinear Proportional Integral Derivative (NPID) controller was enhanced by a fuzzy part that is utilized to dynamically find NPID gains. It was shown that applying this method provides a faster response and less overshoot [19]. Using the descriptions of thermal processes, the idea of dynamic gain adaptation was implemented in adaptive back-stepping SMC [20].

Among the methods used to track the position of pneumatic actuators, SMC is the most popular scheme applied to position pneumatic actuators because of its robustness against model uncertainties and external disturbances [2, 21, 22, 23, 24]. These features make SMC compliant to position pneumatic actuators that are naturally hard to control because of the nonlinearity of air flow and friction [6]. With a few exceptions such as NPID, all above controllers including, require knowledge of system model and parameters. The augmented position controllers require effort to be designed and tuned. All in all, there is no simple-structured, model-free controller that is able to provide high position accuracy, despite extensive work on position tracking of pneumatic actuators.

2.2.   Teleoperation of Pneumatic Actuators

Research on teleoperation in pneumatic actuators has been limited to a few studies. A pneumatic slave manipulator with a solenoid on/off valve was designed that follows the motion of an identical pneumatic master manipulator in a bilateral manner [25]. A study on the stability of the same platform was conducted using the SMC condition for stability considering the external

8

force as model uncertainty [26]. This assumption is not always recommended, especially when the interaction with the environment changes the model structure, e.g., the order of the system [27].

A pneumatic slave actuator navigated by a pneumatic master actuator was designed in a bilateral way [7]. Stability was guaranteed by ensuring that the system was energetically passive [28] and that the environment was also passive [29]. Energetically passive systems such as dampers and brakes, unlike energetically active systems such as electrical motors, only dissipate, redirect or store energy. To position the slave, a modified PI controller was used which could provide satisfactory positioning in low speed movements. Tadano [2, 30] implemented unilateral pneumatic teleoperation for MRI applications, utilizing a pneumatic slave and electric/pneumatic master. The slave actuator was a high-performance actuator which was navigated by a lab-made electric master actuator with a force controller. The external force was not measured by a force sensor, but estimated using the position error. The reason is that the system was designed to work in the magnetic field, which enforces the minimum use of sensors. Without this limitation, a unilateral teleoperation system can take advantage of a force sensor in order to have a sense of the magnitude of the external force. To the best of our knowledge, no pneumatic unilateral teleoperation system was designed that measures the external force and feed it back to the control system. This

Further, all pneumatic bilateral teleoperation systems mentioned above employ a pneumatic master manipulator. A bilateral pneumatic slave which is navigated by an electric master is not been addressed in the literature.

2.3. Stability Analysis

There are different ways of studying the stability of dynamic systems. The Lyapunov direct method [31] is the best-known method for the stability analysis of nonlinear systems; however, it is highly limited because of the lack of a structure for deriving the Lyapunov function for complicated nonlinear systems. In the context of the stability analysis of teleoperation systems, stability analysis approaches were mostly passivity-based [32, 7, 25] or they considered a simplified model of the teleoperation network [33, 34]. Passivity-based methods limit the parameters of the controller and/or physical system as they are conservative. The analysis of oversimplified models is not enough because it does not include system complexity.

The concept of Lyapunov exponents (LEs) was first introduced by Lyapunov [31] to study the asymptotic behavior of nonlinear systems. It was later used to analyze the stability of many dynamic systems [35, 36, 37]. LEs can be calculated based on the time series [38] or dynamic model [36, 37]. Unlike many analysis methods, the concept of LEs can show the stability of an already-designed control system; therefore, it does not limit the parameters of the system. On the other hand, the calculation of LEs based on a mathematical model is limited because of model uncertainty and computational complexity. These properties make the concept of LEs a proper candidate to be applied to a teleoperation system. The essence of stability investigation for teleoperation systems is discussed before.

2.4. Summary

The majority of the existing researches on the bilateral teleoperation of pneumatic actuators consider identical pneumatic master and slave actuators. This research suggests using a commercial electrical hand-controller as the master in a bilateral manner. The reason is that electrical hand-controllers are available, noiseless and light-weight. Second, this research aims to

implement unilateral teleoperation on the pneumatic system. Unilateral systems are simple, more stable and independent of the operator's skillfulness. To achieve this goal, it is essential to employ an efficient force controller and position controller. The literature states SMC is the most popular method for the force control and position tracking of the pneumatic systems because of its robustness to model uncertainties of pneumatic actuators caused by the nonlinearity of the air. Alternatively, this research suggests applying a model-free position controller.

To study the stability of the entire teleoperation system including the pneumatic slave actuator, master actuator, external force and the operator's hand, the concept of LEs is suggested. Unlike many other stability analysis methods such as Lyapunov function, the concept of LEs does not require designing energy function and is applicable to already-designed systems.

3. EXPERIMENTAL SETUP AND MODELING

This chapter introduces the experimental setup of the pneumatic teleoperation system and relevant modeling. Each component of the experimental setup used for this research, i.e. slave manipulator, master manipulator, operator, and communication tool, is individually explained. In addition, two configurations of the teleoperation systems (bilateral and unilateral) are briefly explained.

3.1   Description of the Test Rig

The experimental setup used in this research is shown in Figure 3-1(a). It consists of a one degree-of-freedom, double rod (FESTO, DNC-40-500-PPV-A-S2) pneumatic actuator (Figure 3-1(b)) as the slave manipulator interacting with the environment, and a (PHANToM, 02350) omni-directional, haptic device, driven by an operator, as the master manipulator (Figure 3-1 (c)), and a PC (Figure 3-1(d)) equipped with a (QUANSER, Q8-137429) data acquisition board (Figure 3-1(e)) as the control station. The pneumatic actuator is driven by a five-port, three-way

proportional directional flow (FESTO, MPYE-5-1/8-HF-010-B) control valve as shown in Figure 3-1(f). The actuator rod has a 40-mm bore, with a 500-mm stroke. The maximum flow capacity of the control valve is 700 l/min at 7 bar (100 psi) absolute supply pressure. The above components are connected to a local network, which is assumed ideal, meaning the network characteristics such as time delay and packet loss are negligible. The sampling frequency is 500 Hz, which is estimated based on the least resolution among the resolutions of the sensors and dynamic of the system. The computer generates and forwards a control signal to the pneumatic actuator to move the slave according to the movement of the master. The computer also communicates with a (BOURNS, ENS1J-B28-L00256L) incremental rotary encoder (Figure 3-1(g)), a set of two (DURHAM, P1221-0025) pressure sensors (Figure 3-1(h)), and an (ARTECH, S type, 20210-500) load cell (Figure 3-1(i)). The sensors are assumed to be ideal, i.e. their dynamic does not have any effect on the dynamic of the overall system. To provide the environmental force interaction point, a shaft is attached to the pneumatic actuator (Figure 3-1(j)).

3.1.1   *Operator's hand and master manipulator*

The commercialized PHANToM haptic device, which is used as the master robot, is light-weight, affordable and noiseless. It is equipped with a graphical user interface, which provides easy setup and tuning of the manipulator. It is capable of serial communication using a high speed IEEE1394 communication protocol (FireWire), which is available on many industrial computers. Because these are well-known products, they can be easily interfaced to many prototyping software packages, i.e. QuarRC, which is developed by Quanser.

The master manipulator is moved by the operator`s hand, which, as a dynamic system, requires modeling. Because the operator`s hand and the master manipulator are attached, their

dynamic are interdependent [39]. Therefore, the combined dynamics of the master actuator and the operator`s hand in a single direction are described as follows [40]:

$$m_m \ddot{x}_m + b_m \dot{x}_m + k_m x_m = F_h + F_m \,, \qquad\qquad (3\text{-}1)$$
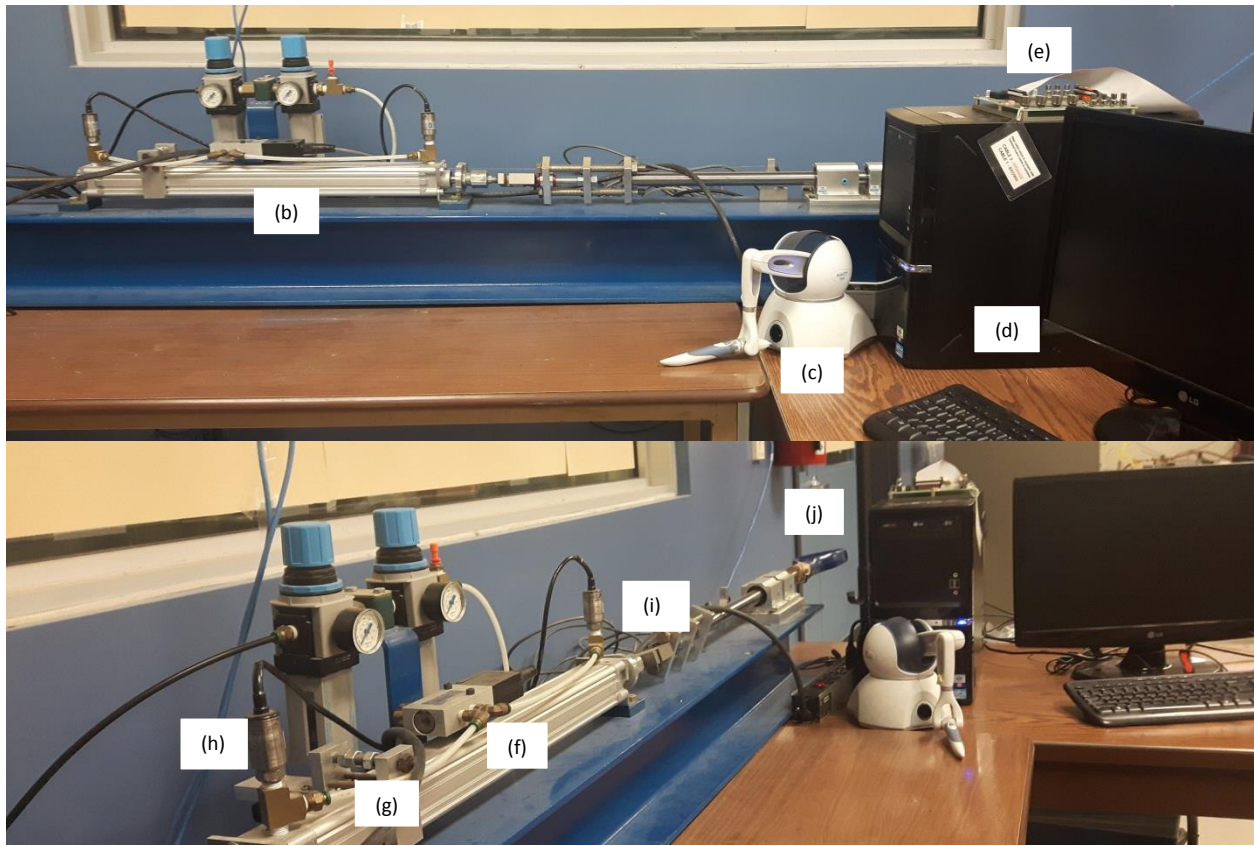
(a)
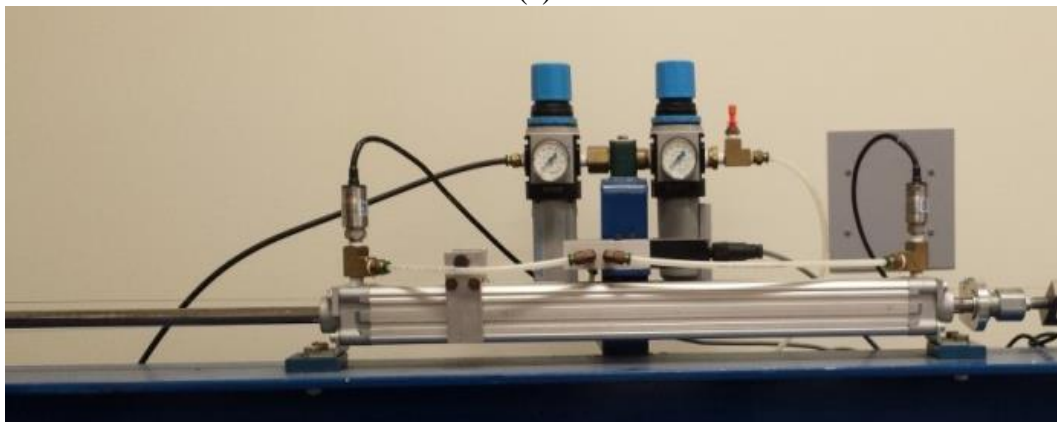
(b)
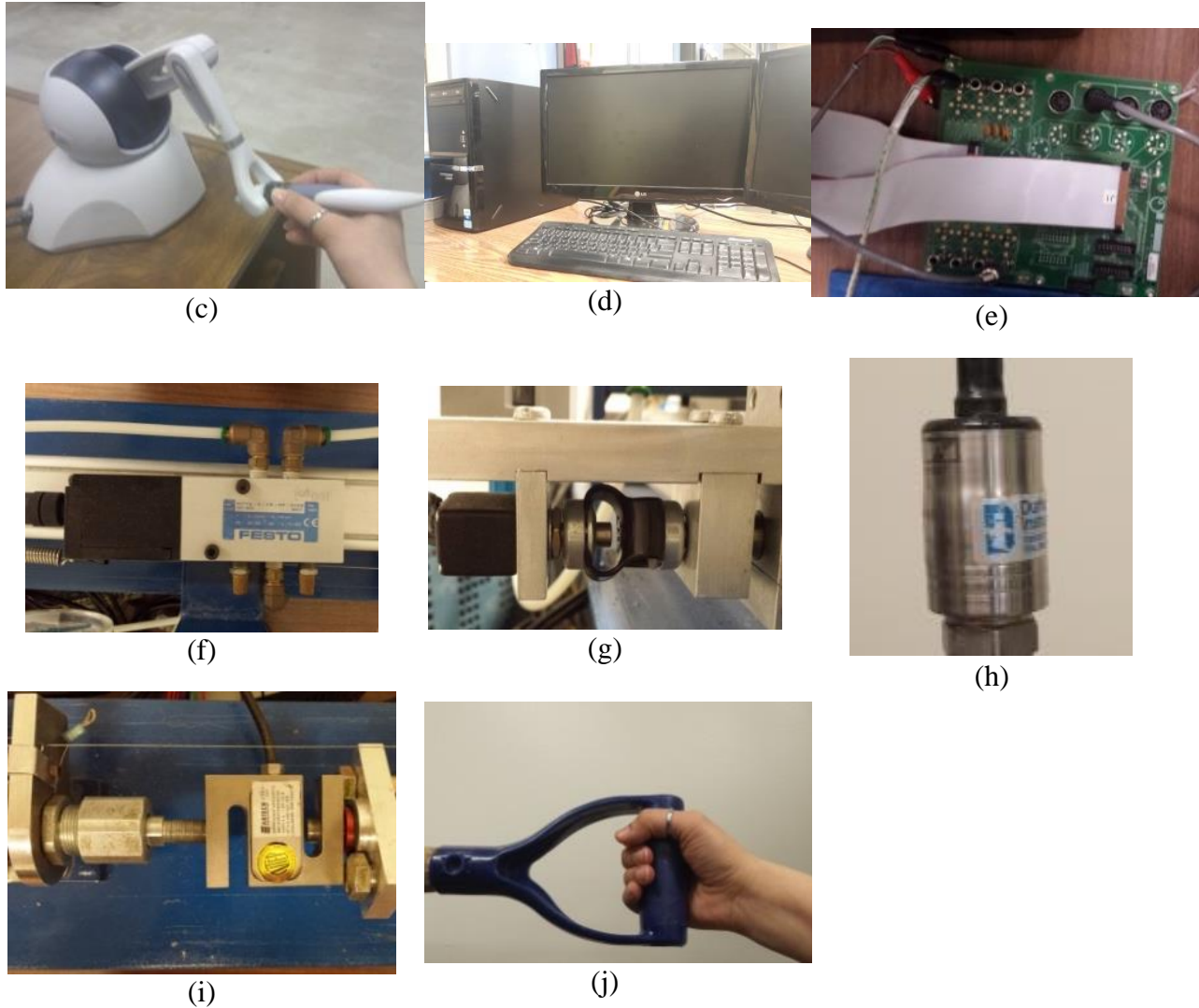
Figure 3-1. (a) Pneumatic teleoperation setup; (b) pneumatic (slave) actuator; (c) haptic device (master); (d) PC; (e) data acquisition board; (f) proportional valve; (g) encoder; (h) pressure sensor; (i) load cell; (j) environment force interaction point.

where m_m is the combined inertia of the master manipulator and the human arm, b_m is the combined viscous coefficient of the master manipulator and the human arm, and k_m is the combined stiffness of the human arm and the haptic device. F_h is the force generated by the operator's hand. F_m indicates the force applied to the operator's hand, which is generated by the built-in controller of the master manipulator and x_m is the displacement of the master actuator

15

and the operator`s hand as a result of F_h and F_m. F_m reflects the amount of force imposed to the slave by the environment. Therefore, it is proportional to the external force from the environment, F_{ext}. In the unilateral mode, no force is rendered on the hand-controller; thus, $F_m = 0$. As a result, the displacement of the master in the unilateral mode is only made by the operator force. Therefore, (3-1) does not appear in the modeling of the unilateral teleoperation.

3.1.2 Slave actuator

The slave actuator considered in this study is a solenoid-driven proportional directional valve-controlled pneumatic actuator. The schematic of a typical pneumatic actuator is given in Figure 3-2.
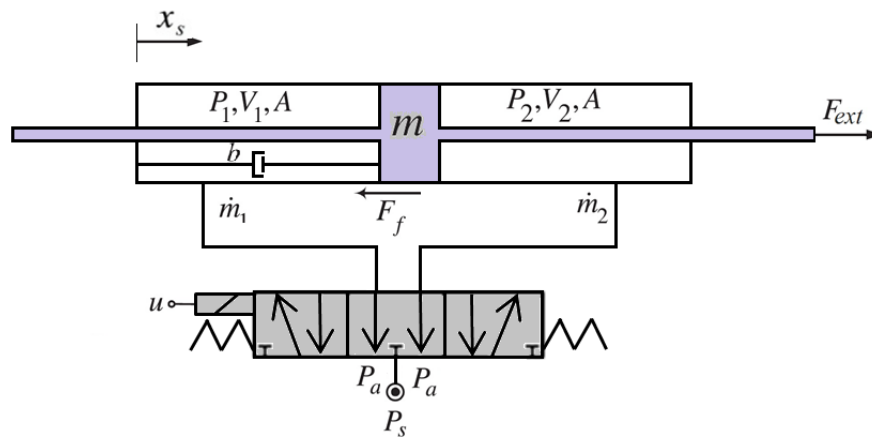
Figure 3-2. Schematic diagram of the pneumatic actuator.

The pneumatic actuator setup consists of three main components: the pneumatic power supply, the actuator, and the proportional valve. The pneumatic power supply delivers compressed air to the high pressure supply port of the valve at a constant pressure of 40 psi. An electrical control signal, u, is applied to the valve and allows the positioning of the valve spool, x_v. It modulates the flow of air into and out of the actuator chambers and creates a pressure differential across the piston. The force applied on the piston due to the differential pressure allows the piston position, x_s, to change.

16

Referring to Figure 3-2, the dynamic equation of the actuator is defined as:

$$m_p \ddot{x}_s = A(P_1 - P_2) + F_{ext} - \left(F_f + b\dot{x}_s\right), \tag{3-2}$$

where m_p is the combined mass of the piston-rod assembly, P_1 and P_2 are the absolute pressures in each of the actuator chambers and A is the annulus area of the piston. b is the viscous friction coefficient regarding the viscous friction force. The dry friction, F_f, is presented using the LuGre friction model [41] excluding the term related to viscous friction (note that the viscous friction is included as a separate term in (3-2)):

$$F_f = \sigma_0 z + \sigma_1 \dot{z}, \tag{3-3}$$

where σ_0 is the equivalent spring constant of bristle, z is the average bristle deflection, σ_1 is the equivalent damping coefficient of bristle in the LuGre friction model. The average bristle deflection z can be found by solving the following equation [41]:

$$\dot{z} = \dot{x}_s - \frac{\sigma_0 |\dot{x}_s| z}{F_c + (F_s - F_c)e^{-(\dot{x}_s/v_{sv})^2}}, \tag{3-4}$$

where F_c is the Coulomb friction, F_s is the static friction and v_{sv} is the Stribeck velocity. To position the actuator, the chamber pressures are varied by charging or discharging the appropriate volume of the air. The differential equations relating the chamber pressures to the air mass flows, $\dot{m}_1$ and $\dot{m}_2$ through the cylinder, are [42]:

$$\dot{P}_1 = \gamma RT \frac{\dot{m}_1}{V_1} - \alpha\gamma A \frac{\dot{x}_s P_1}{V_1}, \tag{3-5}$$

$$\dot{P}_2 = -\gamma RT \frac{\dot{m}_2}{V_2} + \alpha\gamma A \frac{\dot{x}_s P_2}{V_2}, \tag{3-6}$$

$$V_1 = V_0 + Ax_s, \tag{3-7}$$

$$V_2 = V_0 + A(L - x_s). \tag{3-8}$$

In equations (3-5) and (3-6), V_1 and V_2 are the instantaneous volumes of each actuator

chamber, which depend on the actuator position. L is the actuator stroke and V_0 is the cylinder inactive volume. γ is the ratio of specific heats, R is the ideal gas constant, T is the air temperature and α is known as the compressibility flow correction factor [11]. Defining $\bar{\gamma} = \sqrt{\frac{\gamma}{R}(\frac{2}{\gamma+1})^{(\gamma+1)/(\gamma-1)}}$, the nonlinear equation governing the mass flow rate of air through each control valve orifice is expressed as [43]:

$$\begin{cases} \dot{m}_1 = w x_v \, \dot{\varnothing}_1 \\ \dot{m}_2 = w x_v \, \dot{\varnothing}_2 \end{cases},$$

(3-9)

$$\dot{\varnothing}_1 = \begin{cases} \begin{cases} \dfrac{C_d P_s}{\sqrt{T}}\bar{\gamma}, & \dfrac{P_1}{P_s} \leq P_{cr} \\[2ex] \dfrac{C_d P_s}{\sqrt{T}}\bar{\gamma}\sqrt{1-(\dfrac{P_1/P_s - P_{cr}}{1-P_{cr}})^{(\gamma-1)/\gamma}}, & \dfrac{P_1}{P_s} > P_{cr} \end{cases}, & x_v \geq 0 \\[6ex] \begin{cases} \dfrac{C_d P_1}{\sqrt{T}}\bar{\gamma}, & \dfrac{P_a}{P_1} \leq P_{cr} \\[2ex] \dfrac{C_d P_1}{\sqrt{T}}\bar{\gamma}\sqrt{1-(\dfrac{P_a/P_1 - P_{cr}}{1-P_{cr}})^{(\gamma-1)/\gamma}}, & \dfrac{P_a}{P_1} > P_{cr} \end{cases}, & x_v < 0 \end{cases},$$

(3-10)

$$\dot{\varnothing}_2 = \begin{cases} \begin{cases} \dfrac{C_d P_2}{\sqrt{T}}\bar{\gamma}, & \dfrac{P_a}{P_2} \leq P_{cr} \\[2ex] \dfrac{C_d P_2}{\sqrt{T}}\bar{\gamma}\sqrt{1-(\dfrac{P_a/P_2 - P_{cr}}{1-P_{cr}})^{(\gamma-1)/\gamma}}, & \dfrac{P_a}{P_2} > P_{cr} \end{cases}, & x_v \geq 0 \\[6ex] \begin{cases} \dfrac{C_d P_s}{\sqrt{T}}\bar{\gamma}, & \dfrac{P_2}{P_s} \leq P_{cr} \\[2ex] \dfrac{C_d P_s}{\sqrt{T}}\bar{\gamma}\sqrt{1-(\dfrac{P_2/P_s - P_{cr}}{1-P_{cr}})^{(\gamma-1)/\gamma}}, & \dfrac{P_2}{P_s} > P_{cr} \end{cases}, & x_v < 0 \end{cases},$$

(3-11)

where w is the valve orifice area gradient, C_d is the control valve coefficient of discharge and $\dot{\varnothing}_i$ $(i = 1,2)$ governs mass flow per area unit. P_{cr} is the valve critical pressure ratio, P_s is the supply pressure and P_a is the atmospheric pressure. The valve orifice area gradient was

determined by partially dismantling the control valve, measuring the movement of the valve spool as the control signal was varied within its normal range and dividing this value by the nominal orifice diameter. The equation governing the control signal and valve spool displacement is as follows:

$$\dot{x}_v = \frac{1}{\tau}(-x_v + K_v u) \ ,$$
(3-12)

where τ is the valve first-order time constant and K_v is the valve spool position gain. The parameters of the test rig, described by the above equations, are shown in Table 3-1. The rationale for choosing their values has been reported in the previous works [40, 11].

Table 3-1. Parameters of the test rig [11, 40]

Parameter	Symbol	Value
Cylinder inactive volume	$V_0\ (m^3)$	1.64×10^{-4}
Piston annulus area	$A\ (cm^2)$	10.6
Actuator stroke	$L\ (m)$	0.5
Total mass of actuator`s moving parts	$m_p\ (kg)$	1.91
Valve coefficient of discharge	C_d	0.7
Valve critical pressure ratio	P_{cr}	0.2
Compressibility flow correction factor	α	1.2
Ratio of specific heats	γ	1.4
Ideal gas constant	$R\ (J/kgK)$	287
Temperature of air source	$T\ (K)$	300
Valve spool position gain	$K_v\ (mm/V)$	0.25
Valve first-order time constant	$\tau\ (ms)$	4.2
Atmospheric pressure	$P_a\ (Pa)$	1×10^5
Supply air pressure	$P_s\ (Pa)$	5×10^5
Valve orifice area gradient	$w\ (mm^2/mm)$	22.6
Viscous damping coefficient	$b(N.s/m)$	70
Coulomb friction	$F_c\ (N)$	32.9
Static friction	$F_s\ (N)$	38.5
Stribeck velocity	$v_{sv}\ (m/s)$	0.02
Equivalent spring constant of bristle	$\sigma_0\ (N/m)$	4500
Equivalent damping coefficient of bristle	$\sigma_1(N/m/s)$	93.13
Inertia of haptic and arm	$m_m\ (Kg)$	0.4
Viscous coefficient of haptic and arm	$b_m\ (Ns/m)$	5
Stiffness of haptic and arm	$k_m\ (N/m)$	1000

4. THEORY OF LYAPUNOV EXPONENTS

Lyapunov Exponents (LEs) are quantitative measures that demonstrate the asymptotic behavior of a nonlinear system. Introduced by Lyapunov to determine the stability of non-stationary solutions of ordinary differential equations [31], it has been widely applied to stability analysis of different dynamic systems [37, 35, 36, 44]. For a nonlinear system with n-dimensional state space, a set of n Lyapunov exponents exists. The steady state behaviour of the system (equilibrium point, limit cycle, quasi-periodic, or chaotic) is determined by the signs of LEs [45, 46]. All negative exponents show a stable system with the attracting fixed point. When all the exponents of a system are negative, except for one exponent, which is zero, the corresponding system has an attracting periodic orbit (limit cycle) [47]. Likewise, a stable quasi-periodic attractor with k frequencies has k zero Lyapunov exponents and the rest are negative [47]. In definition, a quasi-periodic system is an aperiodic, bounded system, which nearby orbits stay close to each other as time evolves [47]. In a two dimensional system:

- $\lambda_1 = 0$ and $\lambda_2 < 0$, the system has an attracting limit cycle.

- $\lambda_1 > 0$ and $\lambda_2 = 0$, the system has a repelling limit cycle

- $\lambda_1 < 0$ and $\lambda_2 > 0$, the system has a saddle point, i.e. trajectories move toward the point from one side, then repel from it from another side.

- $\lambda_1 < 0$ and $\lambda_2 < 0$, the system has an attractive or stable fixed point

- $\lambda_1 > 0$ and $\lambda_2 > 0$, the system has a repelling or unstable fixed point

In three more dimensional systems, all negative LEs infer a stable system with a fixed point. If all negative except one which is zero, the system is stable and has a limit cycle. A positive Lyapunov exponent refers to a chaotic system or a system which is highly sensitive to the initial conditions provided the system always stays within bounds [48]. Chaotic systems never converge to an attractive fixed point or limit cycle (like stable systems) nor move out of the bounded region (like unstable systems), but they show sustained unstable behaviour while remaining in a bounded region of the state space forever. In other words, a dynamic system is chaotic if it has three properties: 1) its orbits are bounded; 2) orbits are aperiodic; 3) nearby orbits diverge from each other fast in time [49]. Non-chaotic systems may have some of the above properties, but not all. An unstable system with a repelling fixed point has aperiodic orbits that separate fast, but it is not bounded. In the same line, quasi-periodic systems have aperiodic, bounded orbits but they diverge or converge from each other.

Although the above facts are considered for a smooth system, Kunze [50] showed that they can be extendable to nonsmooth systems provided some conditions are met. To explain the type of stability regarding Lyapunov exponents, some definitions are reviewed.

A point x is stable in the sense of Lyapunov (Lyapunov stable), if and only if for all $\epsilon > 0$, there exists $\delta > 0$ such that if $|x - y| < \delta$, then $|\varphi(x, t) - \varphi(y, t)| < \epsilon$ for all $t \geq 0$.

A point x is quasi-asymptotically stable, if and only if there exists $\delta > 0$ such that if $|x - y| < \delta$, then $|\varphi(x,t) - \varphi(y,t)| \to 0$ as $t \to \infty$.

A point x is asymptotically stable if and only if it is both Lyapunov stable and quasi-asymptotically stable.

For a system with all negative LEs, the nearby orbits always stay close to each other and eventually converge to a stable equilibrium point. Therefore, one can conclude asymptotic stability. If some exponents are zero and the rest are negative, the nearby orbits stay within a constant distance from each other, i.e. $|\varphi(x,t) - \varphi(y,t)| < \epsilon$. Therefore, the system is Lyapunov stable.

4.1.   Theory of Lyapunov exponents

Consider a smooth dynamic system in an n-dimensional state space, $\dot{x} = f(x)$, where $x \in \mathbb{R}^n$ is a state vector of the nonlinear system, and $f(x)$ is differentiable and continuous. To calculate LEs, the nonlinear equations of motion, $\dot{x} = f(x)$ are solved, from initial conditions $x(0) = x_0$. The solution is called "fiducial" trajectory. In the next step, principal axes are defined orthogonally on the fiducial trajectory. The lengths of the principal axes at each time instant show the behavior of the nonlinear system. Each LE is asymptotically defined as [51]:

$$\lambda_i = \lim_{t \to \infty} \frac{1}{T} \ln \frac{\|\delta x_i(t)\|}{\|\delta x_i(t_0)\|} \ . \tag{4-1}$$

In (4-1), the length of a principal axis in iteration i is shown by δx_i and T is the duration of the most recent observance. To calculate δx_i, linearized equations of motion are derived by calculating the Jacobian matrix, $F(t)$ [51]:

$$F(t) = \left.\frac{\partial f}{\partial x^T}\right|_{x=x(t)} , \tag{4-2}$$

$$\dot{\psi}_t = F(t)\psi_t \ . \tag{4-3}$$

With the initial condition equal to unity matrix, (4-3) is integrated to find principal axis $\delta x_i(t)$.

23

The nonlinear equations are also integrated simultaneously to provide the instantaneous state inputs for the Jacobian calculation [51]:

$$\begin{Bmatrix} \dot{x} \\ \dot{\psi}_t \end{Bmatrix} = \begin{Bmatrix} f(x) \\ F(t)\psi_t \end{Bmatrix} . \tag{4-4}$$

Figure 4-1 shows the infinitesimal two-dimensional hyper-ellipsoid. It is obvious that the lengths and directions of the principal axes change over time.
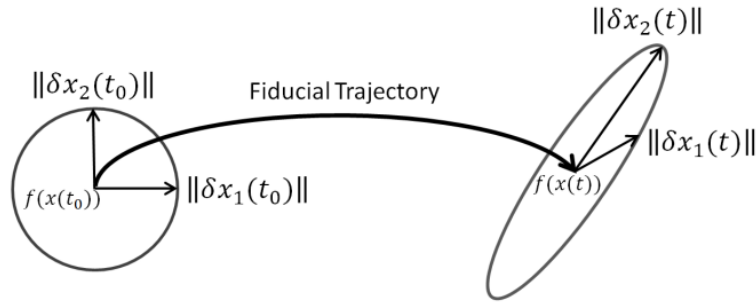
Figure 4-1. Evolution of principal axes for a two-dimensional system.

The principal axes tend to fall along the direction of the most rapid growth axis. When the orientations of the axes converge beyond the computer's limitation, they will not be distinguishable. To resolve the problem, the Gram-Schmidt scheme is used, which normalizes the length of each vector and then orthogonalizes them in each iteration [51].

It is important to note that LEs are global characteristics of the dynamical behavior of a system, although only one set of data is used in their calculation. According to the Theorem of Oseledec [52], LEs of a dynamical system with a hyperbolic equilibrium (all eigenvalues have non-zero real parts), once calculated using any fiducial trajectory, guarantee the stability of the dynamic system for any fiducial trajectory starting in the same stability region [52].

4.2. Procedure of calculating Lyapunov exponents

Consider a nonlinear mass-spring-damper described below:

$$\tilde{M}\ddot{x} + \tilde{B}\dot{x} + \tilde{K}x^2 = F(x) \ , \tag{4-5}$$

where x is the position of the spring. $\tilde{M}$, $\tilde{B}$ and $\tilde{K}$ are inertia, damping and stiffness coefficients and $F(x)$ is the force defined as

$$F(x) = K_p(X_d - x) \ , \tag{4-6}$$

X_d is the desired position and K_p is a positive coefficient. The state space model of the nonlinear mass spring damper is shown as follows:

$$\dot{x} = \begin{cases} \dot{x}_1 = x_2 \\ \dot{x}_2 = \dfrac{1}{\tilde{M}}(F(x) - \tilde{B}\dot{x} - \tilde{K}x^2) \end{cases} , \tag{4-7}$$

Assuming $\tilde{M} = 0.1$ Kg, $\tilde{B} = 5$ N. s/m, $\tilde{K} = 15$ N/m, $K_p = 50$ and $X_d = 1$ m, to calculate the Lyapunov exponents for (4-5), first, we should find the linearized equation.

$$\dot{\psi}_{x(t)} = \begin{bmatrix} 0 & 1 \\ -\dfrac{2\tilde{K}x_1x_2 + K_p}{\tilde{M}} & -\dfrac{\tilde{B}}{\tilde{M}} \end{bmatrix} \psi_{x(t)} \ . \tag{4-8}$$

Considering the initial condition $x^0 = \begin{bmatrix} 0 & 0 \end{bmatrix}$ and $\psi^0 = \begin{bmatrix} 1 & 0 \\ 0 & 1 \end{bmatrix}$, the iterative algorithm of calculating LEs is as follows:

Step 1: Integrate (4-7) and (4-8) over a time step. After $T = 0.01$ s, we have**:**

$$x^1 = \begin{bmatrix} 0.0212 & 3.9009 \end{bmatrix} \ , \tag{4-9}$$

$$\psi^1 = \begin{bmatrix} 0.2383 & 0.9499 \\ -1.5777 & -3.6920 \end{bmatrix} \ . \tag{4-10}$$

Step 2: Apply the Gram-Schmidt method [51] to make the principal axes of ψ^1 orthogonal in order to find the relevant growth of each principal axis of the infinitesimal 2-dimensional hyper-ellipsoid:

$$\psi^{1,orthogonal} = \begin{bmatrix} 0.2383 & 0.3834 \\ -1.5777 & 0.0579 \end{bmatrix} \ , \tag{4-11}$$

25

Step 3: Calculate LEs:

$$\lambda_1^1(t) = \frac{1}{0.01} \, ln \, \frac{\left\| \begin{bmatrix} 0.2383 \\ -1.5777 \end{bmatrix} \right\|}{\left\| \begin{bmatrix} 1 \\ 0 \end{bmatrix} \right\|} = 91.23 \quad, \tag{4-12}$$

$$\lambda_2^1(t) = \frac{1}{0.01} \, ln \, \frac{\left\| \begin{bmatrix} 0.3834 \\ 0.0579 \end{bmatrix} \right\|}{\left\| \begin{bmatrix} 0 \\ 1 \end{bmatrix} \right\|} = -569.88 \quad. \tag{4-13}$$

Step 4: Normalize the principal axes:

$$\psi^{1,normal} = \begin{bmatrix} 0.1494 & 0.9888 \\ -0.9888 & 0.1494 \end{bmatrix} \quad, \tag{4-14}$$

Step 5: Consider x^1 and $\psi^{1,normal}$ as initial condition; repeat steps 1 to 4.

After 100 seconds, the numerical values of LEs reach their steady values: $\lambda_1 = -13.25 \text{ s}^{-1}$ and $\lambda_2 = -34.75 \text{ s}^{-1}$. Since they are negative, the system described in (4-5) is stable.

4.3.   Linearization and Solution Analysis

The required conditions for the validity of applying the concept of Lyapunov exponents are, firstly, the existence of a solution of the nonlinear system should be proven; secondly, the linearized equation should have a solution which is unique. One should also be able to linearize the nonlinear system to find the Jacobian matrix [53].

4.3.1   Solution analysis for nonlinear equation

Let region $\Omega = R^n \times R$ and let D be an arbitrary compact set in Ω. The nonlinear equation has to be measurable, and bounded by $B(t)$, which is an integrable function on D. Thus, the nonlinear equation satisfies Filippov's solution theory [54] and according to that, for an arbitrary initial condition $x(t_0) = a$, where $(t_0, a) \in \Omega$, a solution for the equation exists which satisfies the

above initial condition. A function $: (X, \Sigma) \to (Y, T)$, where X and Y are equipped with Σ and

T σ-algebras respectively, is measurable, if $\forall E \in T, f^{-1}(E) := \{x \in X \mid f(x) \in T\} \in \Sigma$.

4.3.2 Solution analysis for linearized equation

The existence and uniqueness of the solution of the linearized equations of motion are addressed

using the theory of Caratheodory for differential equations [54]. According to this theory, if all

the elements of the linearized equations of motion are defined and piecewise continuous in x,

and measurable, and $|F(x(t)) \leq m(t)|$, where the function $m(t)$ is summable on each finite

interval, the solution for the linearized equation with the arbitrary initial condition $\psi_t(t_0) =$

$\psi_{t_0}(t \in [t_0, t_f])$ exists on the whole interval $[t_0, t_f]$ and is unique.

4.3.3 Linearization of dynamic model at nonsmooth instants

The nonlinear equations of motion cannot be linearized at the instants. To find the numerical

value of the principal axes' length, the extension method of calculating the variational equation

of nonsmooth systems [50, 55] is used. If all the states evolve continuously in time, the Jacobian

of the transition condition, G, is always the identity matrix. According to [56], the numerical

value of variational equations at nonsmooth instants can be defined as:

$$\delta x^+ = G(x^-)\delta x^- + [G(x^-)f_1(x^-) - f_2(x^+)]\frac{H(x^-)\delta x^-}{H(x^-)f_1(x^-)} \tag{4-15}$$

where δx^+ and δx^- are the numerical values of variational equations before and after the

nonsmooth instants. f_1 and f_2 are the nonlinear equations of motion before and after the

nonsmooth instant, and the plus and minus signs characterize the right and left-sided limits,

respectively. The matrix $H(x^-)$ is the Jacobian of the indicator function, $h(x)$, which indicates

the switching to the next manifold of motion [55]. If the nonlinear equations do not have

discontinuity, $f_1 = f_2 = f$, and (4-15) yields:

$$\delta x^+ = \delta x^- \tag{4-16}$$

It means at the nonsmooth instants of motion, where Jacobian does not exist, equation (4-16) can be used.

5. POSITION CONTROLLERS OF PNEUMATIC ACTUATOR

This chapter focuses on the position controllers applied to the pneumatic actuator. Model-free (BELBIC) and model-based (SMC) positioning methods are described and implemented experimentally. SMC is selected because it is the most popular position controller according to the literature [21, 22, 23]. BELBIC is selected because its independence on the model makes it robust to model uncertainties and external force. Further, the flexible structure allows the designer to add terms to controller formula if required. These controllers are compared to one other controller which was implemented in the same experimental setup [11]. The goal of this chapter is to find the most efficient method out of three for positioning a low-cost pneumatic actuator in a teleoperation system that is subject to significant friction and external force. It should be emphasized that the performance of the teleoperation system strongly depends on the positioning accuracy.

5.1　Brain Emotional Learning Intelligent Controller (BELBIC)[1]

This section presents a novel intelligent method, the Brain Emotional Learning Based Intelligent Controller, BELBIC. Similar to many intelligent control methods, the idea of BELBIC is inspired by natural science. It is based on the way psychologists modeled the way mammals learn to react to the environment according to various feelings such as stress, fear, enthusiasm, and interest [57]. They suggested a simple mathematical model of mammalian learning that divides all feelings into two categories: those that are generated in the amygdala and encourage the mammal to move forward, called activation feelings, and those which are generated in the orbitofrontal cortex and prevent action, known as inhibition feelings. According to the emotional learning model, mammals make decisions by comparing the intensity of activation and inhibition feelings at each moment [57]. This mathematical model was later adopted in control engineering and named BELBIC [58, 59, 60]. Instead of comparing activation and inhibition feelings, BELBIC generates and compares activation and inhibition signals that are quantitative measures of the relative success and failure of the control signal at each moment. Activation signals reward the controller for doing well, while inhibition signals quantify how risky the control action could be.

Activation and inhibition signals do not have any conventional formulation but finding suitable formulations for them is left to the controller designer. However, two crucial concepts are incorporated in their definition, which are also inspired by the mathematical model of mammalian learning: Sensory Input, *SI*, which is the quantified observation of the current situation and Reward, *Rew*, which determines the criteria by which we categorize *SI* as risky or beneficial. *SI* and *Rew,* collectively called `Emotional Signals`, should be defined by the controller designer based on the available knowledge of the dynamic system [57, 58].

---

[1] This section is written based on a published paper [81].

BELBIC can be a powerful tool in real-time control and decision systems due to its flexible definition and low computational load compared to intelligent controllers such as gradient-based methods [10]. Note that BELBIC may look like a version of reinforcement learning, since it works upon a reward signal [58]. However, even though they share this similarity in concept, BELBIC mimics a bio-inspired structure of decision making. It has its own unique method of applying reward signals to the controller. Further, the mathematical implementations of the two are quite different [61].

5.1.1 Mathematical implementation of BELBIC

Figure 5-1 shows the BELBIC output generation process.
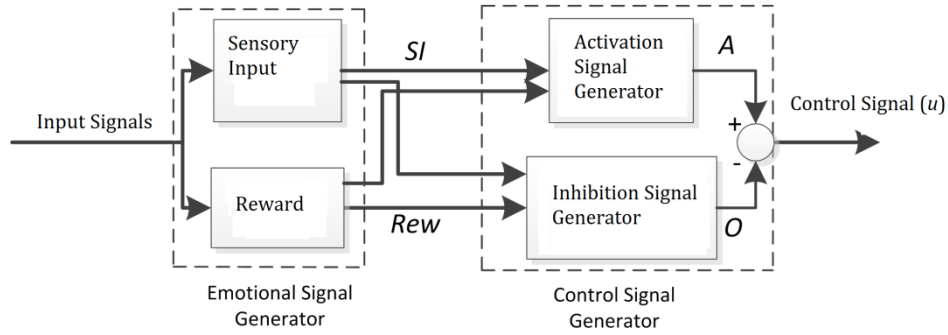
Figure 5-1. BELBIC output generation inspired by the mammals' brain learning model.

Mathematically, BELBIC generates the control signal in each iteration, u_i, by finding the difference of activation and inhibition signals [58]:

$$u_i = A_i - O_i \ ,$$ (5-1)

where A_i and O_i are activation and inhibition signals in the current iteration. The activation signal is formed by an iterative component, V_i, representing the difference of activation signal and reward and *SI*, which is a measure of the current situation of the system as follows [58]:

$$A_i = SI_i V_i \ ,$$ (5-2)

$$V_i = V_{i-1} + Y_i \ ,$$ (5-3)

$$Y_i = K_a max \{ 0, (Rew_i - A_{i-1}) \} ,$$ (5-4)

where K_a is the learning rate and Y_i is an associative variable. Likewise, the inhibition signal is formed by *SI* and a recursive term, W_i, which adds up the difference of reward and control signal as follows [58]:

$$O_i = SI_i W_i ,$$ (5-5)

$$W_i = W_{i-1} + X_i ,$$ (5-6)

$$X_i = K_o(u_{i-1} - Rew_i) ,$$ (5-7)

where K_o is the learning rate, and X_i and W_i are associative variables. Equation (5-6) shows that the inhibition signal is also recursive. Emerging recursive terms in a controller generally mean the controller is gradually learning to deal with new situations. Figure 5-2 shows the process of obtaining a control signal in the feedback loop using BELBIC.
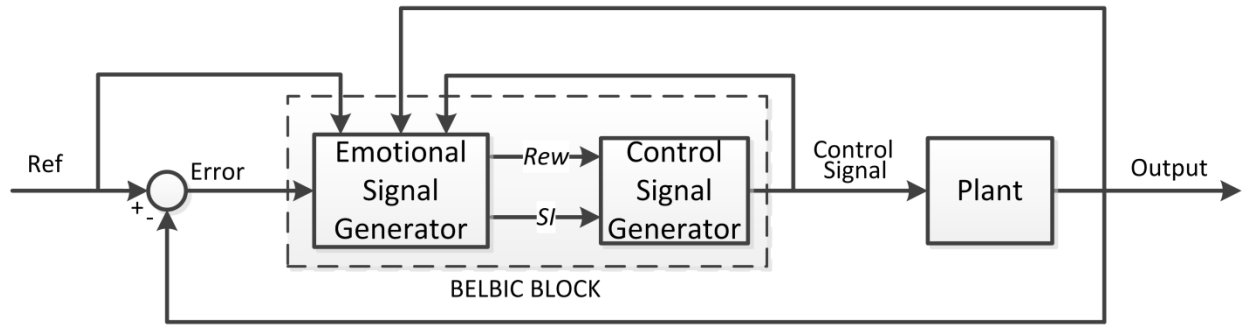
Figure 5-2. BELBIC in a feedback loop to control a plant.

Because BELBIC is utilized to apply to the position tracking of a pneumatic system, *SI* and *Rew* are chosen as a function of position error and the reference trajectory:

$$SI = 0.5e_x + 3\dot{R} + 0.001 \int e_x dt ,$$ (5-8)

$$Rew = 0.1e_x ,$$ (5-9)

$$e_x = R - X ,$$ (5-10)

where X is the actual output of the system, e_x is the position error and R is the reference trajectory. To set the coefficients, all were assumed to be zero (or very small) at the time except for one. In the next step achieving an acceptable performance was attempted through experiment. When each coefficient is tuned in this way, all the values were incorporated in the controller and slightly trimmed to get the desired performance. The numerical values of K_a and K_o were chosen to be 0.08 and 0.03, respectively [80].

5.2 Sliding Mode Controller

Sliding Mode Controller, SMC, is a robust controller which is designed based on the dynamic model of the system. It consists of two parts: the part derived from the dynamic model is known as the "equivalent" part, and the "robust" part which is responsible for dealing with the uncertainties, through which SMC is able to maintain control stability and provide a consistent performance in the presence of model uncertainty and disturbance [32].

5.2.1 Mathematical model of SMC for positioning the pneumatic actuator

The first step in applying SMC is to define a sliding surface. A sliding surface (sliding manifold) is a defined cross-section surface in the steady state which the dynamic system is desired to move to and stay on. A system on a sliding surface is said to be in sliding mode. The standard integral sliding surface which is derived based on Lyapunov stability theory for a third order system such as the pneumatic actuator, is defined as [21]:

$$S = (\frac{d}{dt} + \delta)^3 \int_0^t e \, d\tau \quad, \tag{5-11}$$

where δ is a positive constant known as the control bandwidth and e is the position error.

$$e = x_s - x_d \quad, \tag{5-12}$$

where x_d is the desired position and x_s is the position of the pneumatic piston as defined in Chapter 3. A robust control law, which is practically the area of the valve spool, can be obtained by combining the equivalent control component Av_{eq}, with a robust control component, Av_{rb}.

$$u = (Av_{eq} + Av_{rb})/(wK_v) , \qquad (5\text{-}13)$$

where K_v is the valve spool position gain and w is the valve orifice area defined in Section 2. The equivalent control component, Av_{eq}, is used to achieve the desired motion on the sliding surface where:

$$\dot{S} = 0 . \qquad (5\text{-}14)$$

This results in:

$$Av_{eq} = \frac{\ddot{x}_m - \delta^3 e - 3\delta^2\dot{e} - 3\delta\ddot{e} - Fx}{Px} , \qquad (5\text{-}15)$$

The associated variables Px and Fx are derived from the dynamic model and defined as:

$$Fx = -\frac{K\dot{x}_s + b\ddot{x}_s + \dot{F}_f - \dot{F}_{ext}}{m_p} , \qquad (5\text{-}16)$$

$$K = \alpha\gamma A^2 \left(\frac{P_1}{V_1} + \frac{P_2}{V_2}\right) , \qquad (5\text{-}17)$$

$$Px = \frac{\gamma RTA}{m_p} \left(\frac{\emptyset_1}{V_1} + \frac{\emptyset_2}{V_2}\right) . \qquad (5\text{-}18)$$

The time rate of the change of dry friction, F_f, is slow in comparison to the dynamics of the system. Therefore, $\dot{F}_f$ can be considered negligible in equation (5-16). Neglecting dry friction is mentioned in the previous application of SMC in positioning pneumatic actuators [23, 62, 63]. Since this simplification contributes to uncertainty, the robust part of SMC, Av_{rb}, will take more effort to compensate for the simplification. The formulation is as follows:

$$Av_{rb} = \frac{-K_{rb}}{Px} \text{sign} (S) , \qquad (5\text{-}19)$$

where K_{rb} is a robustness gain. For practical purposes, the discontinuous sign function is

approximated by the continuous hypertangant function as follows:

$$\text{sign}(S) \approx \tanh(aS) \ , \tag{5-20}$$

where a is a sufficiently large positive number [14].

5.3 Nonlinear Proportional-Integral Controller (NPI)

The Nonlinear Proportional Integral (NPI) controller is a Proportional Integral controller in which the integral term is augmented by compensation terms to reduce the effects of dead-band and dry friction of the pneumatic system. Karpenko et al. [11] applied NPI to control a pneumatic system. They successfully applied the method on the experimental test rig described in Chapter 3. Therefore, one can compare its performance to any other positioning method applied to the same test rig.

5.3.1 Mathematical model of NPI for positioning the pneumatic actuator

The formulation of the augmented integrator part of the NPI controller is only rewritten in its final form here, as reference [11]:

$$I(t) = \begin{cases} \dfrac{-u_{lower} - K_p e(t)}{K_i} & \dot{e}_{db} > \dot{e}_{min} \text{ and } u(t) > -u_{lower} \\ I(t - \Delta t) + e(t)\Delta t + K_a \ddot{x}_{braking}\Delta t & |\dot{e}_{db}| \leq \dot{e}_{min} \\ \dfrac{u_{upper} - K_p e(t)}{K_i} & \dot{e}_{db} > \dot{e}_{min} \text{ and } u(t) < -u_{upper} \\ 0 & \dot{x}_d(t) = 0 \text{ and } |e(t)| \leq \varepsilon \end{cases} \ , \tag{5-21}$$

$$\ddot{x}_{braking} = \begin{cases} \ddot{x}_d & \ddot{x}_d \dot{x}_d < 0 \\ 0 & \ddot{x}_d \dot{x}_d \geq 0 \end{cases} \ , \tag{5-22}$$

where $e(t)$ is the position error and $\dot{e}_{db}$ is the velocity error caused by dead-band and actuator friction. u_{lower} and u_{upper} are the lower and upper thresholds of the control signal, ε is the threshold of position error, K_p, K_i and K_a are control gains, and $\dot{e}_{min}$ is an experimentally determined threshold. $\ddot{x}_{braking}$ is the acceleration of braking and x_d is the desired position [11].

5.4   Comparison of Controllers

In this section, the performance of BELBIC, NPI and SMC are compared to choose the most efficient position controller for the pneumatic actuator. The performance criteria are position tracking error, smoothness of motion, simplicity of design, and robustness to the external force. Specifically, the performance of the controller in teleoperation configuration when an external force is applied to the actuator is of interest.

5.4.1   Comparison of BELBIC and NPI

The performance of BELBIC was compared with NPI. Experiments are proposed to evaluate their performance in the position tracking of two different reference trajectories. The presented experimental results of NPI are obtained from [11], and are limited to a few positioning tasks which were performed on the same experimental setup described in Chapter 3. Therefore, comparing BELBIC and NPI in terms of dealing with external force was not possible.

Figure 5-3 shows the performance of BELBIC vs. NPI in the tracking a smooth multiple-step trajectory consisting of five segments with different amplitudes separated by dwell periods and a multiple sharp step trajectory. This trajectory is selected because it provides the simultaneous tracking and regulating the position of the pneumatic actuator. As Figure 5-3 shows, both controllers track the reference trajectories successfully. NPI performs better in dealing with the delay caused by static friction at the beginning of motion. The reason is that NPI has some terms specifically defined to deal with the friction. The steady-state error in the first dwell segments is almost the same for both controllers, measured ±0.007 m as shown in Figure 5-3(b). For small dwell segments, the average steady-state error is 0.003 m for BELBIC vs. 0.004 m for NPI. The maximum and minimum position error of BELBIC is 0.02 m and 0.003 m respectively whereas these values are 0.013 m and 0.005 m for NPI. The root mean square is 0.0077 m for BELBIC

and 0.0065 m for NPI. In general, Figure 5-3 shows that while the performances of both controllers are comparable, BELBIC provides non-oscillatory tracking. NPI, on the other hand, provides better tracking accuracy than BELBIC when the friction is high. This is because of the presence of terms to deal with friction and undesired deadband effects in NPI formulation.
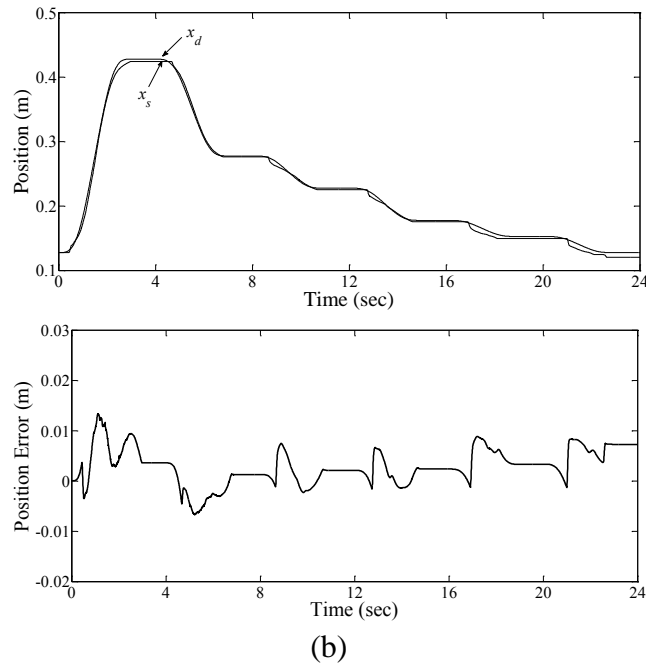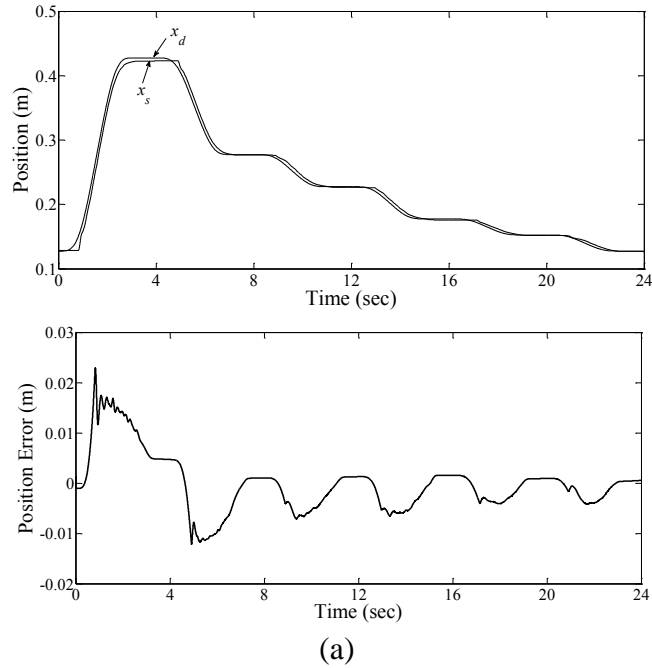
Figure 5-3. Position tracking of smooth multi-step trajectory by: (a) BELBIC; (b) NPI [11].

The performance of BELBIC and NPI in the tracking of the decaying sinusoidal trajectory is shown in Figure 5-4. By comparing the position error one can see that BELBIC maintains tracking of the reference trajectory better than NPI when the magnitude of the sinusoidal wave is small (from 24 s to 48 s). NPI causes big tracking errors in the 24 s to 48 s range. The reason can be explained by looking back at (5-21). The discontinuous definition of the controller caused by the switching between the control rules and also the discontinuous definition of (5-22) leads to sharp hikes in the NPI control signal. The maximum and minimum position error of BELBIC is 0.025 m and 0.004 m. These values are measured 0.023 m and 0.005 m for NPI. The root mean square is 0.0082 m for BELBIC and 0.0122 m for NPI. For small magnitudes of reference trajectory, hikes of control signal cause overshoot in the output. The position error of BELBIC is obviously lower but more oscillation can be observed in motion. Referring to Figure 5-3 and, one can conclude that BELBIC performs better than NPI in position tracking. In terms of implementation burden, the design of BELBIC requires some knowledge of the system dynamics, whereas NPI is rather simple but tuning the physical gains in (5-21) is challenging.
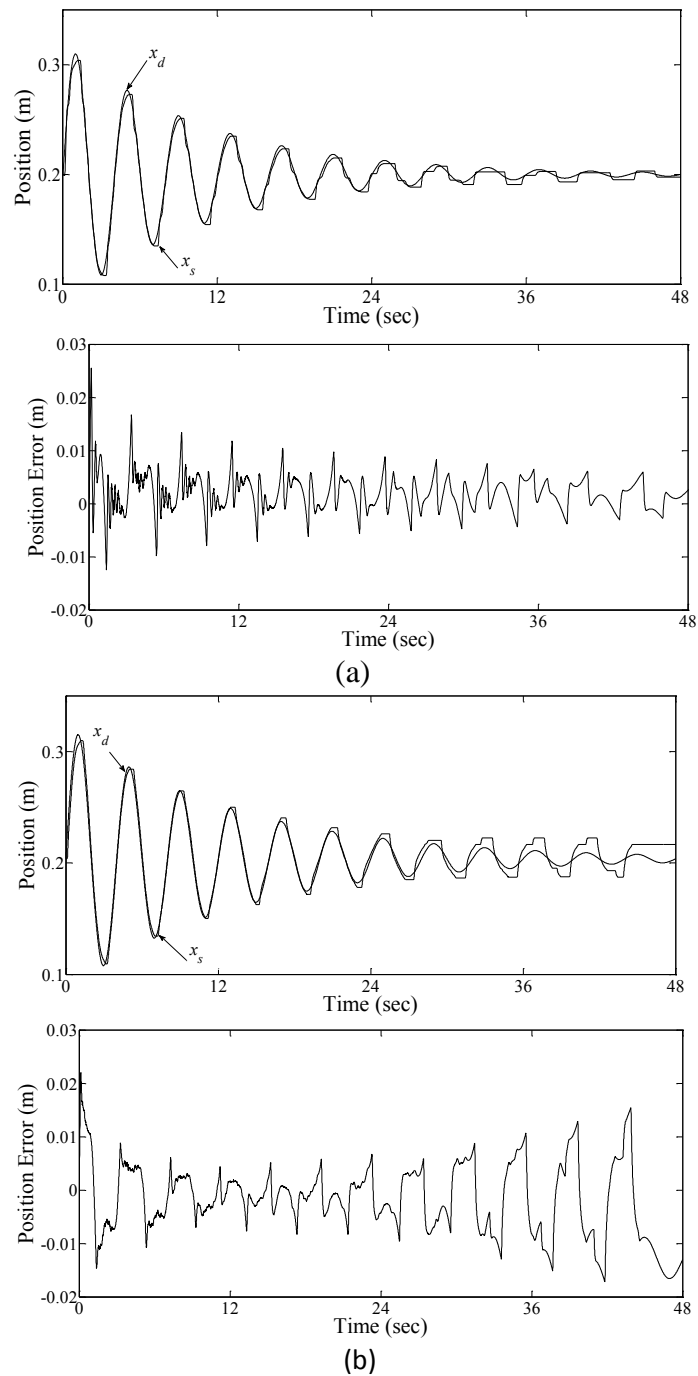
Figure 5-4. Position tracking of a decaying sinusoidal wave by: (a) BELBIC; (b) NPI [11].

5.4.2   Comparison of BELBIC and SMC

Experiments are conducted to demonstrate the performance of BELBIC and SMC in comparison to each other. All experiments are performed on the setup detailed in Chapter 3. To

make SMC more practical for reference trajectories such as sharp step, the higher derivatives of the equivalent control component, Av_{eq}, in (5-15) are ignored.

Figure 5-5 shows the experimental results of BELBIC and SMC position tracking. The desired reference trajectory is a sinusoidal wave with a frequency of 1 rad/s. As shown in Figure 5-5(a), BELBIC provides less oscillatory motion compared to SMC. The maximum tracking error for both control schemes was observed to occur at the point where the piston changes its direction of motion. This relates to the static friction as well as the undesirable effect of the valve dead-zone. Further experiments showed that the piston has an asymmetric static friction. The magnitude of static friction was measured 40 N at the start of the 'left to right' motion, and 5 N at the start of the 'right to left' motion. Compared to SMC, BELBIC has a smaller error at these points. Also, the error of 'left to right' and 'right to left' motion is almost equal for BEBLIC. The average tracking error for the region away from these points was 0.002 m for SMC vs. 0.007 m for BELBIC. The maximum and minimum of the position error are 0.026 m and 0.0025 m for SMC and 0.0013 m and 0.00045 m for BELBIC. The root mean square is 0.0083 for BELBIC and 0.0056 m for SMC. The control signals for both schemes were observed to be within ± 5 V and unsaturated. The oscillatory behaviors around the region whereby the piston changes its direction of motion can be understood as the controller's efforts to overcome the effect of valve dead-zone as well as static friction as mentioned before [14]. In general, this experiment showed the provided tracking accuracy of SMC was higher than BELBIC. However, by being model-free, BELBIC can handle the static friction better than SMC.

(a)

(b)
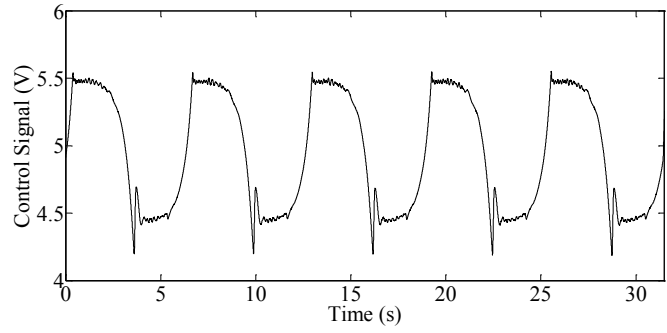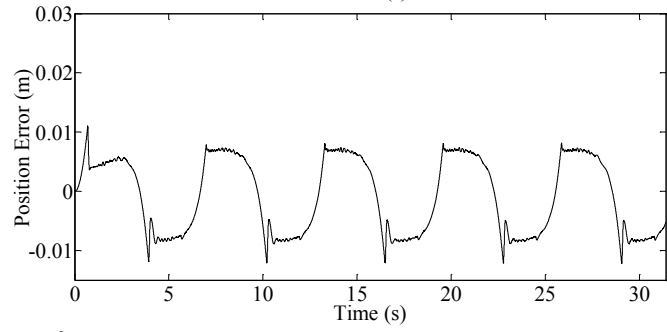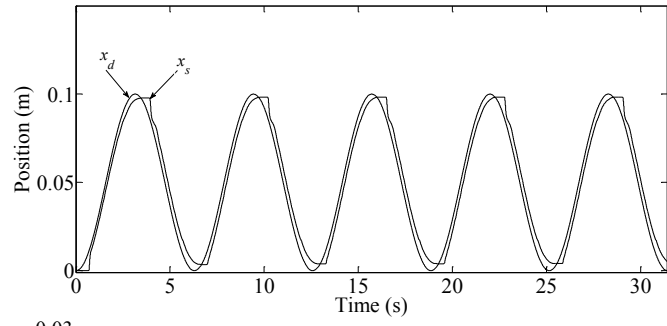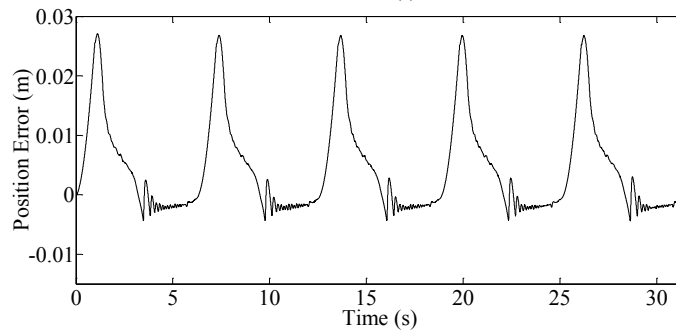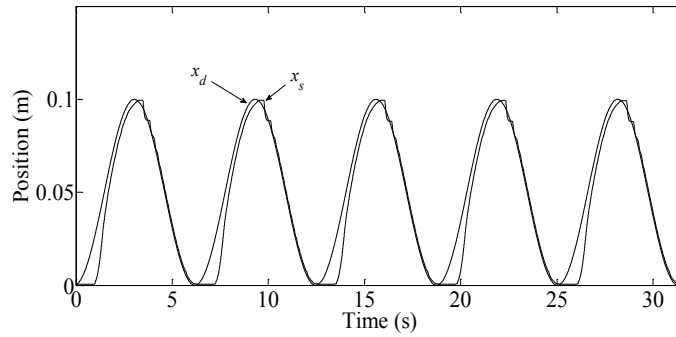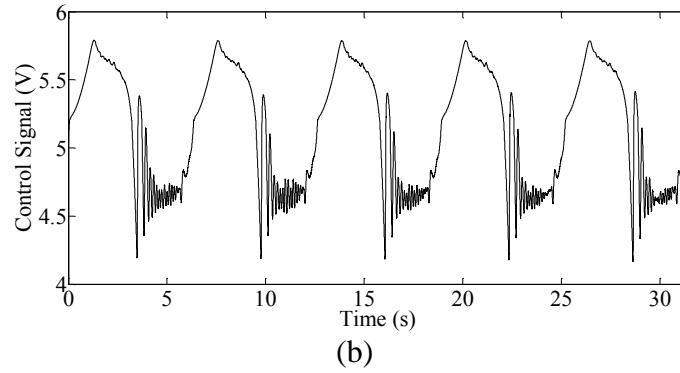
Figure 5-5. Position tracking of a sinusoidal wave by: (a) BELBIC; (b) SMC.

The performance of BEBLIC and SMC in the tracking of a smooth multiple steps trajectory is presented in Figure 5-6. Similar to the previous experiment, the maximum position errors for both control schemes were observed to occur at the point where the piston starts its motion and BELBIC outperforms SMC at this point. The average steady-state errors on dwell segments are observed to be equal (0.005 m) for both controllers. Note that the effects of the control valve dead-zone and stick friction prevent the controllers from achieving zero steady-state error. The maximum and minimum of the position error is 0.073 m and 0.003 m for SMC and 0.0013 m and 0.004 m for BELBIC. The root mean square is 0.0073 m for BELBIC and 0.0054 m for SMC. Figure 5-6 shows that for the parts away from the direction change point, the position errors of SMC and BELBIC are more or less comparable. The oscillation of motion is observed in tracking task by SMC.
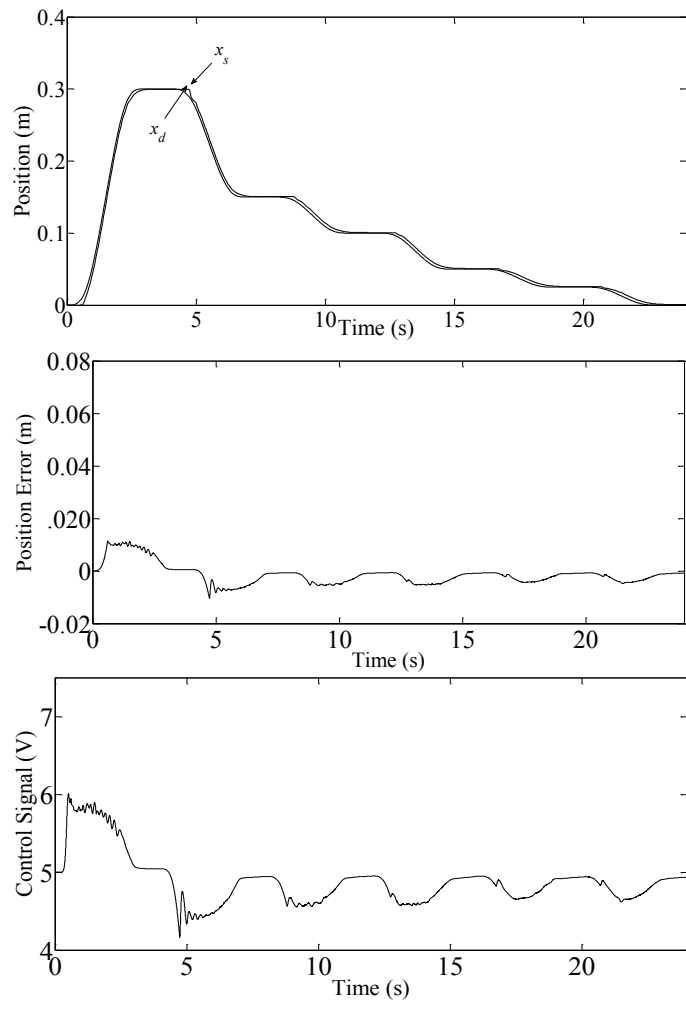
(a)
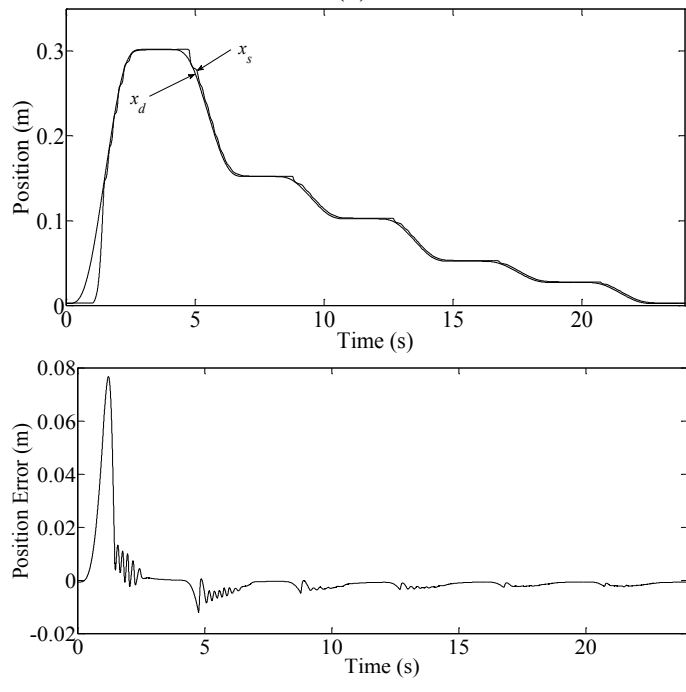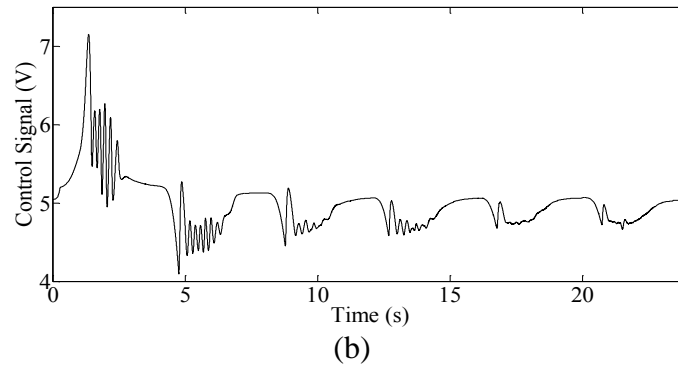
Figure 5-6. Position tracking of a smooth step wave by: (a) BELBIC; (b) SMC.

The tracking of a sharp multi-step reference trajectory is experimented with to observe the performance of controllers in regulating. As shown in Figure 5-7, BELBIC reaches the steady state value much faster than SMC. It settles on the dwell part rapidly while SMC has up to 50% overshoot and a notable settling time. The average steady-state error is 0.003 m for BELBIC and 0.005 m for SMC. The maximum and minimum of the position error are 0.0071 m and 0.003 m for BELBIC and 0.0078 m and 0.002 m for SMC. The root mean square if the position error is 0.0041 m for BELBIC and 0.0058 m for SMC. It is evident that BELBIC outperformed SMC in this experiment. This can be due to the simplification of the SMC control formulation, which removed the term related to the derivative of the desired position, $\ddot{x}_m$, from (5-15).
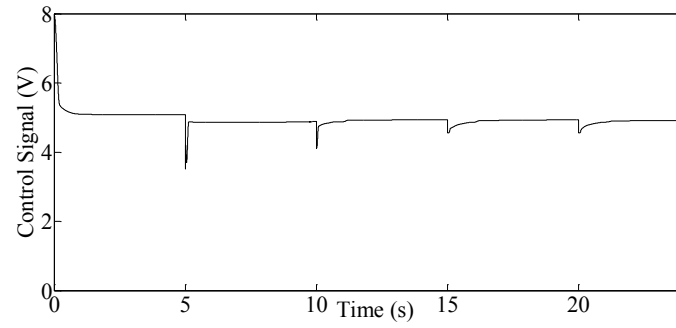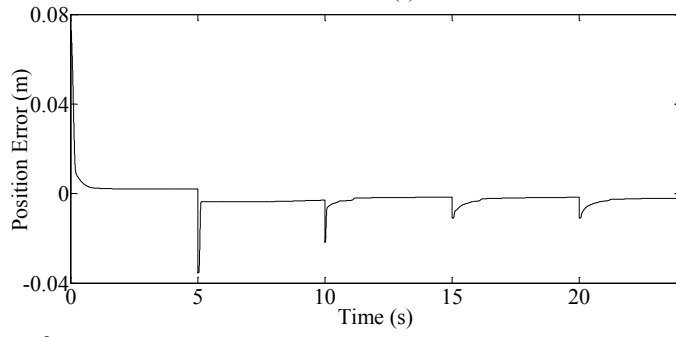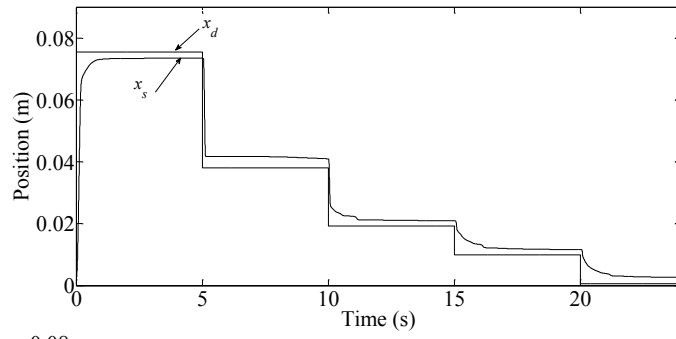
(a)
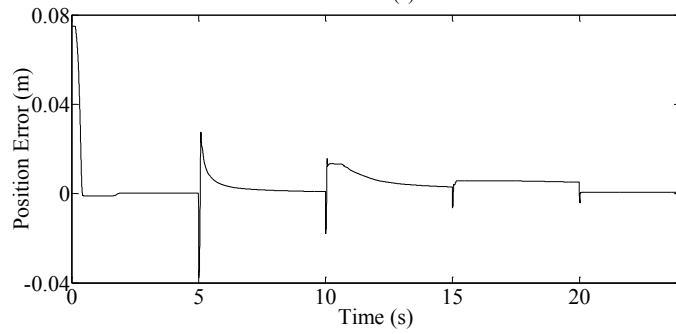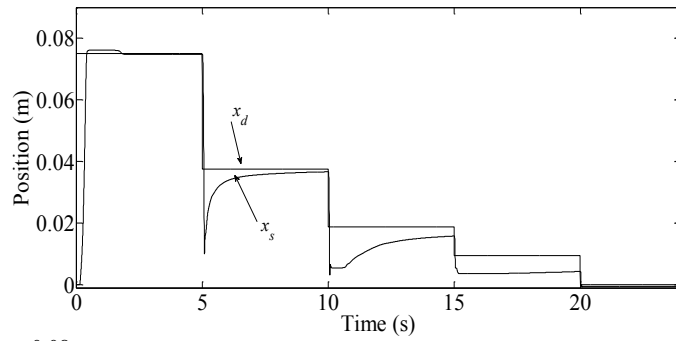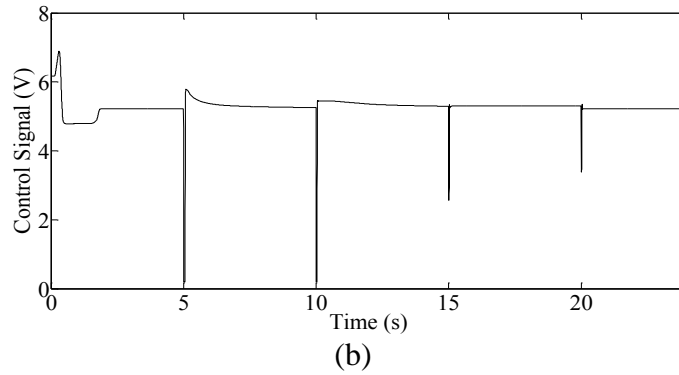
Figure 5-7. Position tracking of a step wave by: (a) BELBIC; (b) SMC.

To evaluate the performance of two controllers on a teleoperation set up, more experiments are conducted using the reference input trajectory generated by a commercialized PHANToM hand-controller driven by an operator. The joystick-generated trajectories are untidy compared to predefined functions such as sinusoidal because they are based on human hand motion. Using the joystick, however, the operator has the opportunity to plan the motion based on real time evaluation of the situation. Therefore, the motion of the joystick should be rather slow and uneven since the operator needs time to decide and move the joystick.

The first experimental result using a joystick-generated trajectory is presented in Figure 5-8. The piston moves slowly in a sinusoidal-like motion. The human operator tried to make the joystick motion almost identical for all the experiments in terms of range and speed of the motion. Nevertheless, the unavoidable small differences in smoothness and speed of motion show the system is capable of handling a wide range of trajectories. According to Figure 5-8, SMC significantly outperformed BELBIC with an average position error of 0.002 m vs. 0.009 m. The maximum and minimum position errors are 0.014 m and 0.0027 m for BELBIC and 0.018 m and 0.004 m for SMC. The root mean square is 0.0083 m for BELBIC and 0.0043 m for SMC. The large position error at the beginning of rightward motion is still observed for SMC. Both controllers show unsaturated control signals.

(a)

(b)
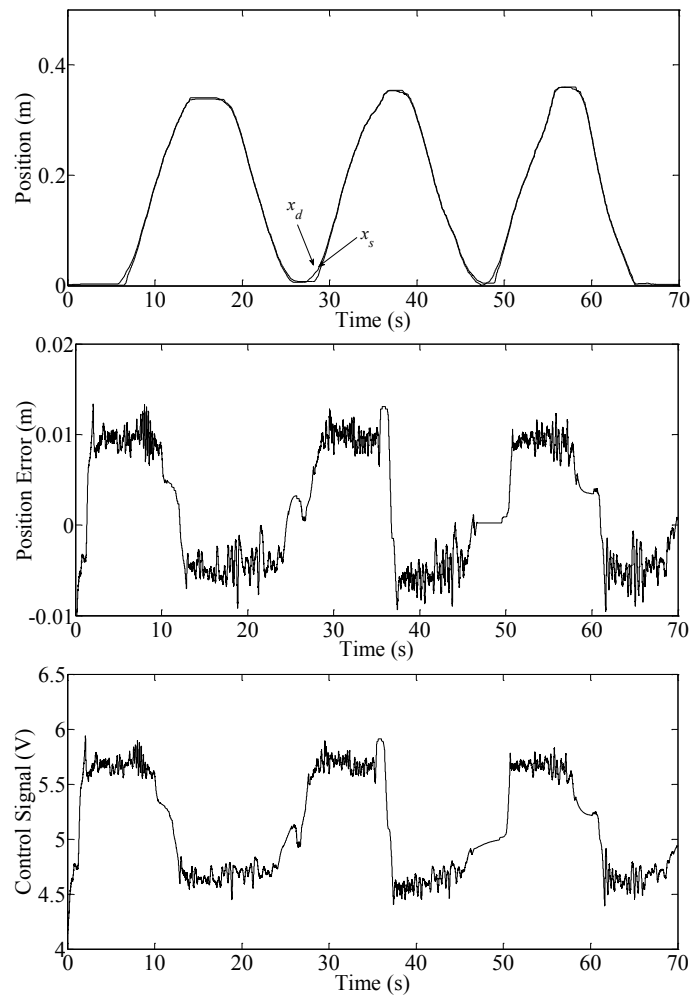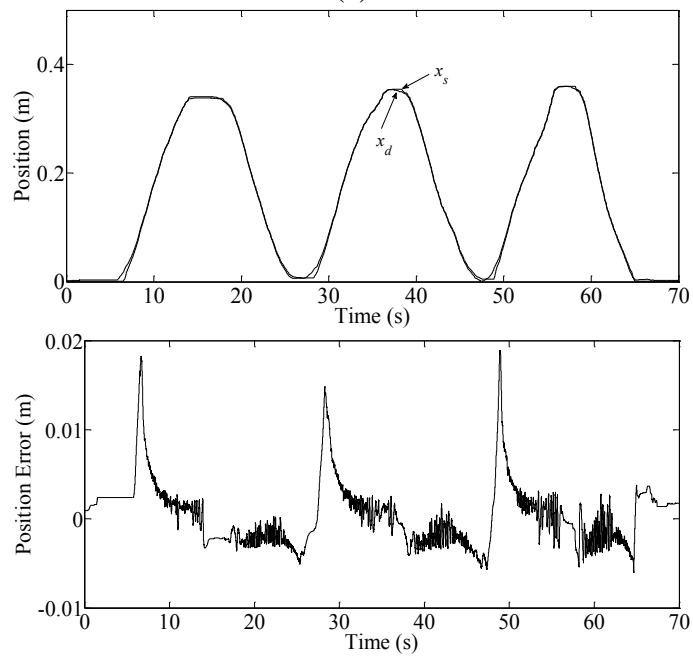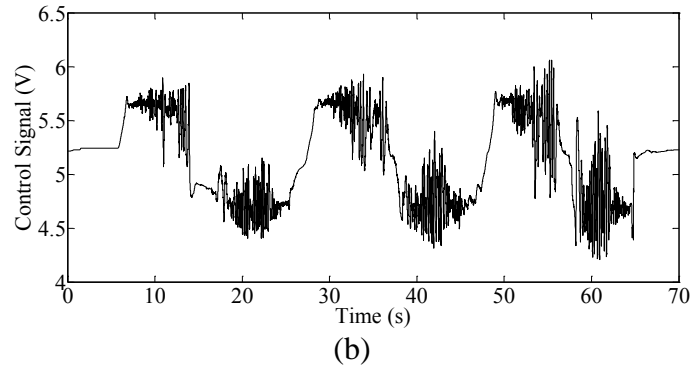
Figure 5-8. Position tracking of a joystick-generated trajectory by: (a) BELBIC; (b) SMC.

The latter experiment is accomplished with a joystick-generated trajectory. The piston is subject to a variable external force generated by a human through a handle attached to the piston tip. The force is measured by a load cell mounted between the handle and the piston. Because this experiment includes the interaction of a robot and a human, the motion is slow. Figure 5-9 shows the experimental results. The maximum and minimum position errors are 0.0011 m and 0.002 m for BELBIC and 0.0018 m and 0.0008 m for SMC. The root mean square is 0.0048 m for BEBLIC and 0.0039 m for SMC. The average position error of BELBIC is 0.006 m, while this value is 0.004 m for SMC. This confirms that SMC performs better than BELBIC in position tracking when an external force is imposed on the piston. Both controllers show non-oscillatory tracking and a bounded and unsaturated control signal.

(a)
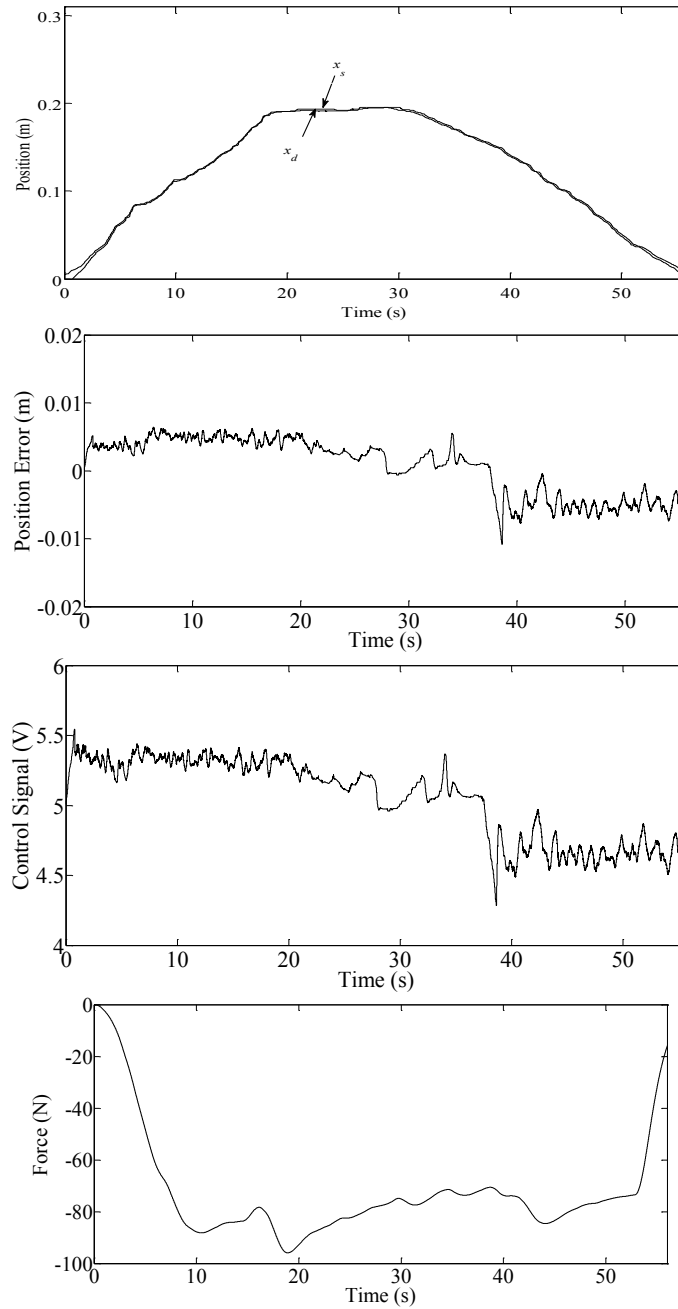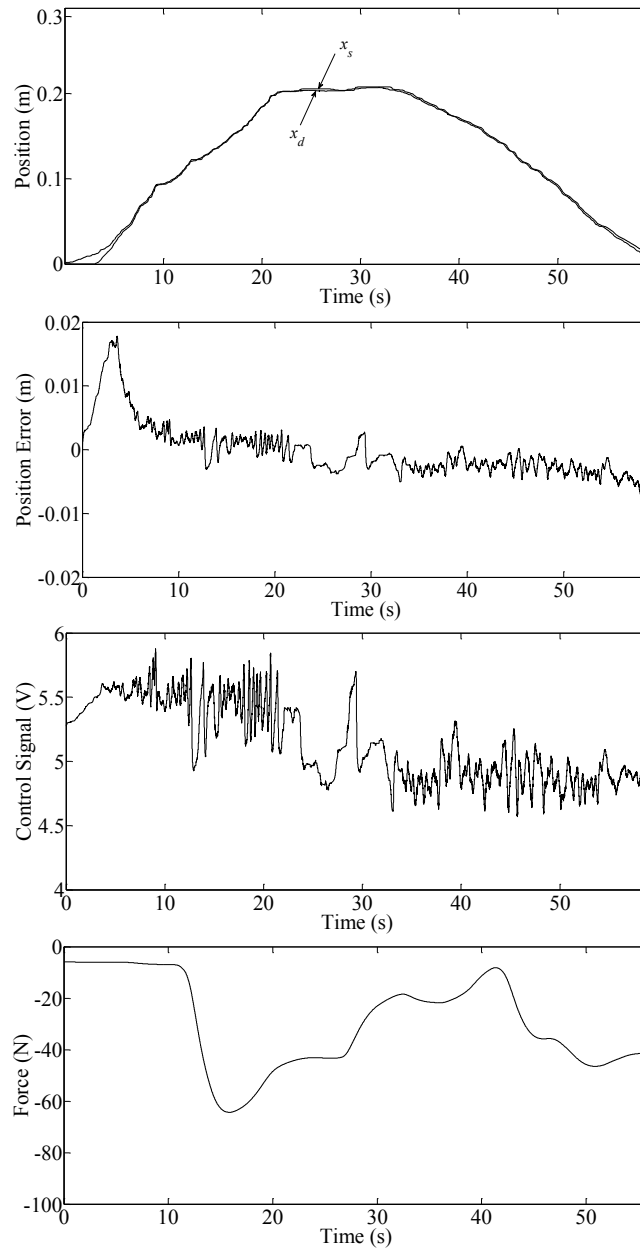
Figure 5-9. Position tracking of a joystick-generated trajectory in the presence of variable external force by: (a) BELBIC; (b) SMC.

5.5 Summary

This chapter aims to find the most efficient position controller for teleoperation application. A novel intelligent controller (BELBIC) was applied to position a pneumatic actuator subject to external force and friction. An SMC was also implemented to the same actuator. The

performances of BELBIC and SMC and a previously-applied position controller, NPI, were compared.

Comparing NPI and BELBIC showed that BELBIC performed better than NPI in terms of position tracking accuracy. With regard to the ease of implementation of controllers, the proper tuning of NPI gains is a challenge. These gains should be changed if the system slightly changes. Therefore, one can conclude that BELBIC is preferred over NPI.

BELBIC and SMC were compared through several position tracking tasks in free motion and in the presence of the external load. The experimental results showed that SMC generally performs better than BELBIC, except for in tracking sharp steps. Specifically, SMC was significantly more accurate than BELBIC in tracking joystick-generated trajectories. SMC requires knowledge of system physical parameters which are sometimes difficult to obtain. BELBIC has a simple structure and does not need a dynamic model. In conclusion, SMC was chosen to be used for the positioning of pneumatic actuators in this research because SMC outperformed BELBIC in tracking joystick-generated trajectories. This is in line with the fact that the focus of this research is on teleoperation, which implies the tracking of joystick-generated trajectories.

The contribution of this chapter was the successful implementation of BELBIC to the control of pneumatic actuators for the first time and also applying it to a bilateral pneumatic system following the comparison of NPI, BELBIC, and SMC positioning techniques.

6 UNILATERAL TELEOPERATION OF PNEUMATIC ACTUATORS; IMPLEMENTATION OF ADMITTANCE CONTROL[1]

This chapter focuses on the design and development of a unilateral teleoperated pneumatic actuator based on admittance (position-based) interaction control. Unilateral is one of the configurations of teleoperation systems; it features a simple structure, independence from the skill of the operator and less chance of instability [4]. Unlike its counterpart, bilateral teleoperation, which is popular due to its offering a feeling of force interaction on the remote side to the human operator, unilateral teleoperation relies on the slave manipulator for managing the external force.

Simultaneous control of force and position in the same direction is not possible since one prevents the other. However, many applications are required to reasonably interact with the environment while moving along a certain position trajectory. A few methods have been introduced to address this issue. An approach was proposed where position trajectories were

---

[1] This chapter is written based on a paper under review [83].

compromised due to force demands [64]. A hybrid force/position tracking strategy was introduced in which force was controlled in constrained directions, while the position was controlled in unconstrained directions. When the robot was operating in a constrained environment the controller would have behaved purely as a force controller [65]. The crucial concern of these methods is stability at the moment of switching between force and position tracking [64, 65, 27].

Introduced by Hogan [66], "Impedance/admittance control" combines the desired force and position through a mass, spring and damper characteristics model. Impedance/admittance control considers both force and position continuously; therefore, it does not have stability issues at the instant of switching. Further, one can achieve different stiffness by tuning the mass, spring and damper gains. These features have made impedance/admittance control the best-known method of force/position tracking, especially during human-manipulator interactions [67, 39]. If the force is handled using a positioning loop, the method is called position-based impedance control or "admittance control". Conversely, the term "impedance control" refers to a force loop which handles both force and position.

An admittance control scheme is utilized to interact with the external force while the actuator is tracking a trajectory given by a joystick. In nonlinear systems, admittance, or position-based impedance control, is the opposite pair of force-based impedance control, which is also known simply as impedance control. This means that the roles of input and output (cause and effect) are exchanged. For a dynamic system, cause and effect are force and displacement. It should be noted that, although being complementary concepts, admittance is not necessarily the inverse of impedance and vice versa [27].

Admittance control simultaneously maintains the desired force and position in the same direction [66]. It provides the system with a function which converts the external force, F_{ext}, to a corresponding position called the external position, x_{ext}. Figure 6-1 shows the general block diagram of admittance control, where x_{ext} is added to the primary desired position, x_m, determined by the master manipulator. In this approach, the position controller tracks a modified desired trajectory, x_d, which is the combination of the primary desired trajectory, x_m, and the displacement corresponding to the external force, x_{ext} ($x_d = x_m + x_{ext}$). The relationship between the external force, F_{ext}, and the corresponding displacement, x_{ext}, is usually defined by a second-order linear mass-spring-damper model as follows:

$$\frac{x_{ext}}{F_{ext}} = \frac{1}{Ms^2 + Bs + K} \ ,$$ (6-1)

where $\boldsymbol{M}, \boldsymbol{B}$ and $\boldsymbol{K}$ are admittance parameters corresponding to desired inertia, damping and stiffness characteristics of the actuator while exposed to the environmental force and $\boldsymbol{s}$ is the Laplace operator. Displacement of the manipulator in response to external force can be tuned by tuning admittance parameters.
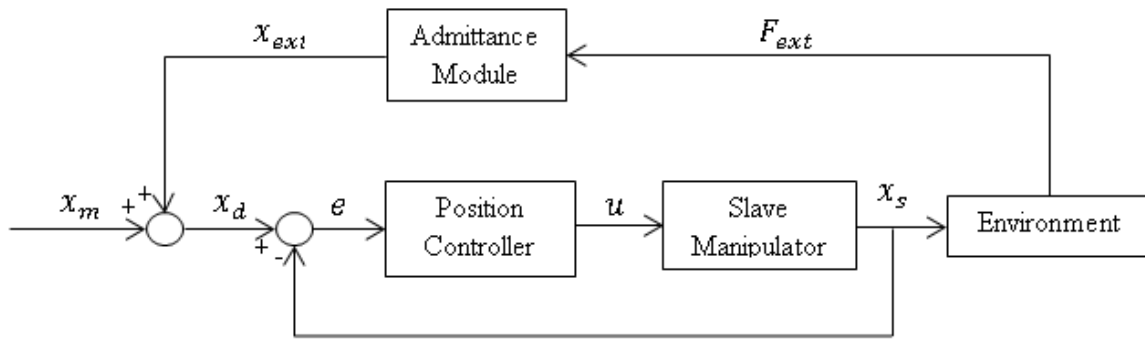
Figure 6-1. General block diagram of admittance control.

6.1 Simulation Studies and Stability Analysis

6.1.1 Autonomous System

Simulation studies

The performance of the proposed unilateral pneumatic system is first evaluated through simulation. Referring to Figure 6-1, the teleoperated control system receives the displacement of the master, x_m, and the external force imparted to the slave from the environment, F_{ext}. The environment is considered spring-dominant in simulation, which means F_{ext} is proportional to the slave position:

$$F_{ext} = -K_{ext}x_s \ , \tag{6-2}$$

where K_{ext} is the stiffness coefficient of the environment. A simplified admittance model is employed whereby the external force is related to the external position by a virtual spring:

$$x_{ext} = F_{ext}/K_{adm} \ , \tag{6-3}$$

where K_{adm} is a positive coefficient corresponding to the stiffness term in the admittance model.

Step tracking simulation results for the admittance control are shown in Figure 6-2. The system step input, x_m, is 0.1 m, as shown in Figure 6-2(a). The environment is considered a spring with the stiffness coefficient of $K_{ext} = 100$ N/m. This value is chosen by assuming the environment to be a human arm, interacting with the slave actuator, that moves 0.01 m for 1 N of actuator force. Accordingly, the external force, F_{ext}, is shown in Figure 6-2(b). The external position, x_{ext}, is derived from (6-3) and shown in Figure 6-2(c). The desired stiffness in the admittance model is considered $K_{adm} = 2000$ N/m, i.e. it is desired that the displacement of the slave in response to the external force be small. This value is selected considering the characteristics of a rehabilitation test rig. The modified desired trajectory, x_d, is obtained by adding the primary desired trajectory, x_m, and the external position, x_{ext} as shown in Figure 6-2(d).
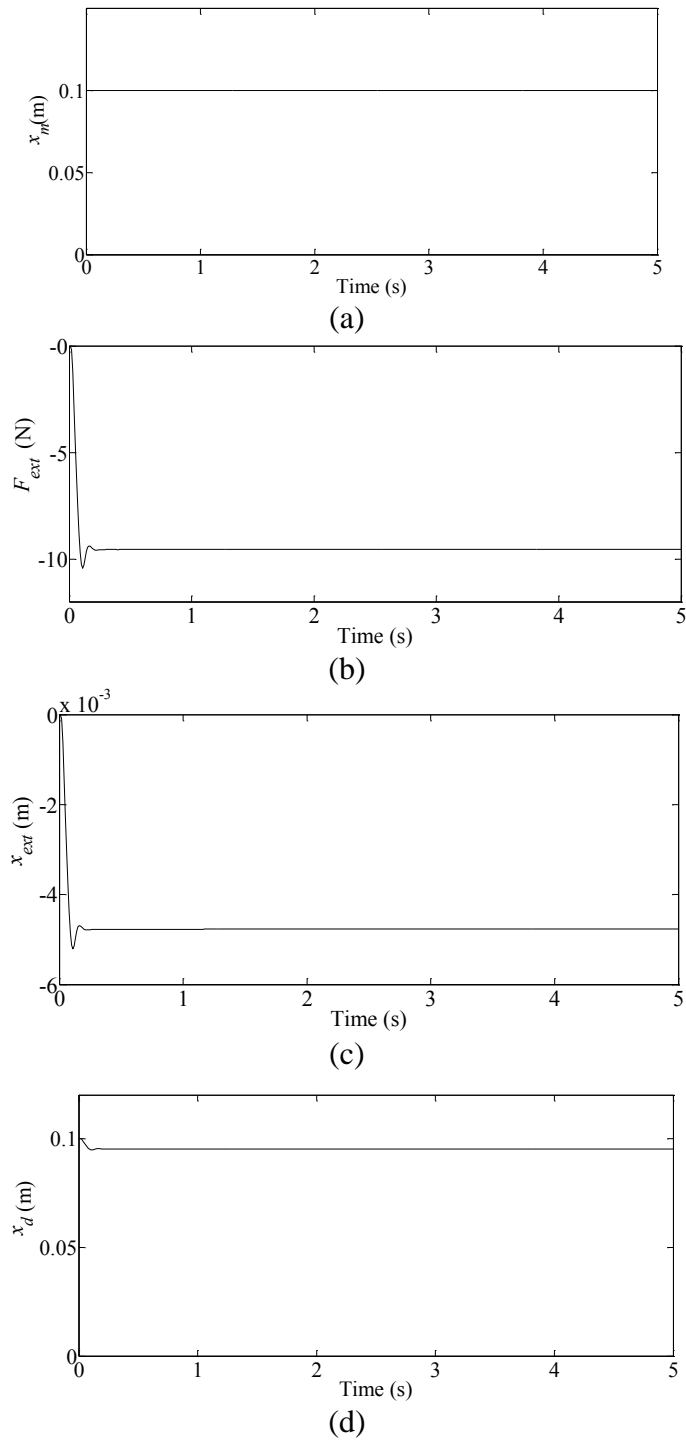
Figure 6-2. Admittance control variables pertaining to step tracking: (a) primary desired trajectory provided by the master manipulator, x_m; (b) external force, F_{ext}; (c) displacement corresponding to the external force, x_{ext}; (d) desired trajectory achieved from the admittance model, x_d.

Figure 6-3 shows the corresponding slave manipulator variables. The SMC position controller is detailed in 5.2. The controller parameters are $\delta = 80 \text{ s}^{-1}$ and $K_{rb} = 2000 \text{ m/s}^3$. To set the control parameters, one was assumed to be zero and the other was adjusted to achieve an acceptable performance. Both parameters were considered and tested on several desired trajectories. The value of parameters was slightly tuned to get the desired performance. The slave position, x_s, is shown in Figure 6-3(a). The air pressures in cylinder chambers are shown in Figure 6-3(b). The control signal applied to the slave actuator is shown in Figure 6-3(c) and does not saturate. The control signal of this system changes within the range of 0-10 V. Hence, with the 5 V control signal, the valve is fully closed. The position tracking error is shown in Figure 6-3(d). It is seen that there is a reasonable agreement between the motions of the slave and master actuators.
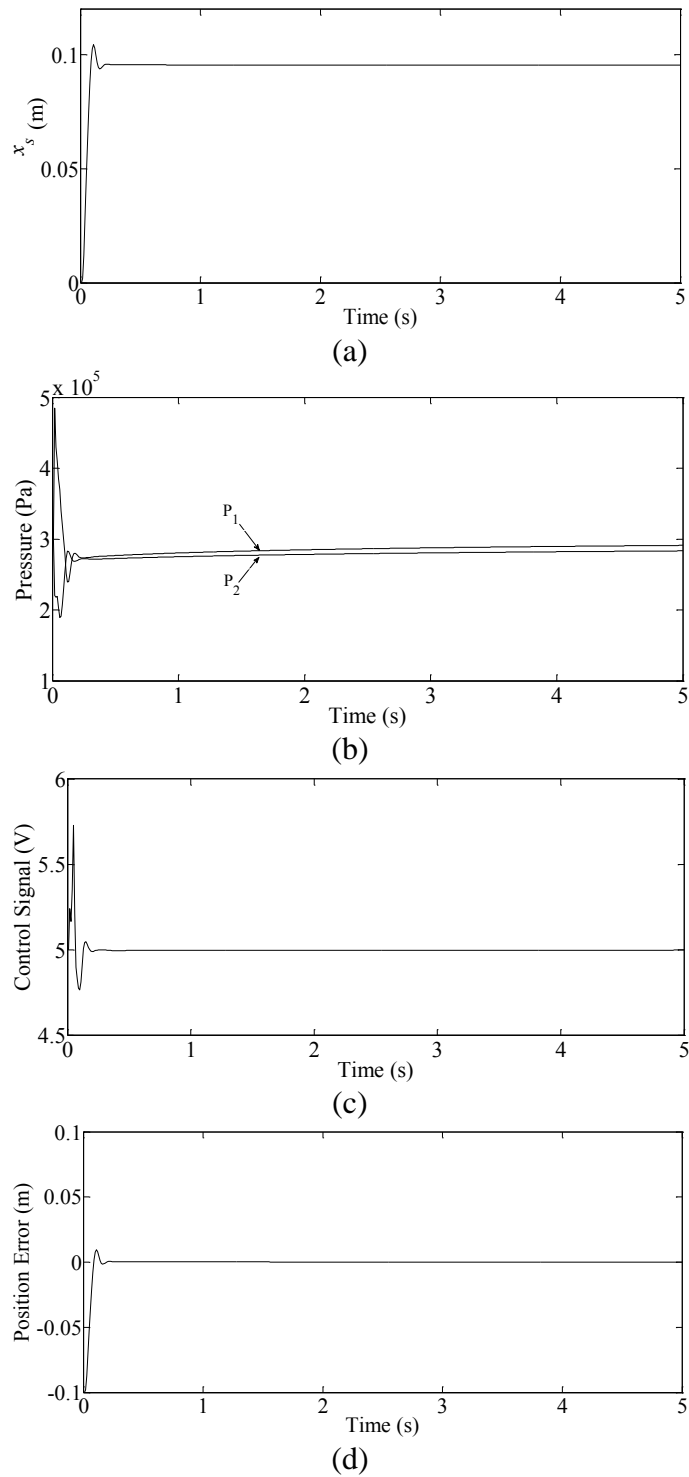
Figure 6-3. Step tracking with SMC: (a) piston position; (b) chamber pressures; (c) control signal; (d) position error

Stability analysis

The stability analysis of the entire admittance unilateral teleoperation system is conducted. The state space model is formed by defining the state space vector as:

$$\vec{x} = [x_1 \ x_2 \ x_3 \ x_4 \ x_5 \ x_6 \ x_7]^T = [x_s \ v_s \ P_1 \ P_2 \ x_v \ z \ \int_0^t e \, d\tau]^T \ , \tag{6-4}$$

where x_s and v_s are the displacement and the velocity of the piston, P_1 and P_2 are air pressures in each actuator chamber, x_v is the displacement of the spool valve as a result of the control signal, z is the average bristle deflection and e is the position error. Using the state variables, (6-1) to (6-3), and equations (3-2) to (3-12), the state space model is constructed as:

$$\begin{cases} \dot{x}_1 = x_2 \\ \dot{x}_2 = \dfrac{1}{m_p}\left[A(x_3 - x_4) + F_{ext} - \left(\sigma_0 x_6 + \sigma_1\left(x_2 - \dfrac{\sigma_0|x_2|x_6}{F_c + (F_s - F_c)e^{-(x_2/vs)^2}}\right) + bx_2\right)\right] \\ \dot{x}_3 = +\gamma RT \dfrac{wx_5 \, \dot{\varnothing}_1}{V_0 + Ax_1} - \alpha\gamma A \dfrac{x_2 x_3}{V_0 + Ax_1} \\ \dot{x}_4 = -\gamma RT \dfrac{wx_5 \, \dot{\varnothing}_2}{V_0 + A(L - x_1)} + \alpha\gamma A \dfrac{x_2 x_4}{V_0 + A(L - x_1)} \\ \dot{x}_5 = \dfrac{1}{\tau}(-x_5 + K_v u) \\ \dot{x}_6 = x_2 - \dfrac{\sigma_0|x_2|x_6}{F_c + (F_s - F_c)e^{-(x_2/vs)^2}} \\ \dot{x}_7 = e \end{cases} \tag{6-5}$$

The control signal in terms of state space variables is defined as:

$$u = \frac{1}{wK_v}\left(\frac{\dddot{x}_d - \delta^3 e - 3\delta^2 \dot{e} - 3\delta \ddot{e} - Fx - K_{rb} \, tanh(S)}{\dfrac{\gamma RTA}{m_p}\left(\dfrac{\dot{\varnothing}_1}{V_0 + Ax_1} + \dfrac{\dot{\varnothing}_2}{V_0 + A(L - x_1)}\right)}\right) . \tag{6-6}$$

The associated variables in (6-5) are defined as:

$$\ddot{x}_d = \frac{-K_{ext}}{K_{adm}m_p}(A(\dot{x}_3 - \dot{x}_4)) - \frac{b}{m_p}(A(x_3 - x_4) - K_{ext}x_1 - bx_2 - F_f) \tag{6-7}$$
$$- K_{ext}x_2)$$

$$Fx = -\frac{\alpha\gamma A^2}{m_p}\left(\frac{x_3}{V_0 + Ax_1} + \frac{x_4}{V_0 + A(L - x_1)}\right)x_2 - \frac{K_{ext}}{m_p}x_2 - \frac{b}{m_p^2}(A(x_3 - x_4)) \tag{6-8}$$
$$- K_{ext}x_1 - bx_2 - F_f)$$

59

$$S = \delta^3 x_7 + 3\delta^2 e + 3\delta\dot{e} + \ddot{e} \ , \tag{6-9}$$

$$e = (1 + \frac{K_{ext}}{K_{adm}})x_1 - x_m \ , \tag{6-10}$$

$$\dot{e} = (1 + \frac{K_{ext}}{K_{adm}})x_2 \ , \tag{6-11}$$

$$\ddot{e} = \frac{1}{m_p}(1 + \frac{K_{ext}}{K_{adm}})\dot{x}_2 \ . \tag{6-12}$$

The dry friction in the state space is as follows:

$$F_f = \sigma_0 x_6 + \sigma_1 x_2 - \frac{\sigma_0 \sigma_1 |x_2| x_6}{F_c + (F_s - F_c)e^{-(x_2/v_{sv})^2}} \ . \tag{6-13}$$

The mass flow rate per area unit in the state space is defined as:

$$\begin{cases} \dot{\emptyset}_1 = \begin{cases} \dfrac{C_d P_s}{\sqrt{T}}\bar{\gamma}, & \dfrac{x_3}{P_s} \leq P_{cr} \\ \dfrac{C_d P_s}{\sqrt{T}}\bar{\gamma}\sqrt{1 - (\dfrac{x_3/P_s - P_{cr}}{1 - P_{cr}})^{(\gamma-1)/\gamma}}, & \dfrac{x_3}{P_s} > P_{cr} \end{cases} \\[2em] \dot{\emptyset}_2 = \begin{cases} \dfrac{C_d x_4}{\sqrt{T}}\bar{\gamma}, & \dfrac{P_a}{x_4} \leq P_{cr} \\ \dfrac{C_d x_4}{\sqrt{T}}\bar{\gamma}\sqrt{1 - (\dfrac{P_a/x_4 - P_{cr}}{1 - P_{cr}})^{(\gamma-1)/\gamma}}, & \dfrac{P_a}{x_4} > P_{cr} \end{cases} \qquad x_5 \geq 0 \\[2em] \dot{\emptyset}_1 = \begin{cases} \dfrac{C_d x_3}{\sqrt{T}}\bar{\gamma}, & \dfrac{P_a}{x_3} \leq P_{cr} \\ \dfrac{C_d x_3}{\sqrt{T}}\bar{\gamma}\sqrt{1 - (\dfrac{P_a/x_3 - P_{cr}}{1 - P_{cr}})^{(\gamma-1)/\gamma}}, & \dfrac{P_a}{x_3} > P_{cr} \end{cases} \\[2em] \dot{\emptyset}_2 = \begin{cases} \dfrac{C_d P_s}{\sqrt{T}}\bar{\gamma}, & \dfrac{x_4}{P_s} \leq P_{cr} \\ \dfrac{C_d P_s}{\sqrt{T}}\bar{\gamma}\sqrt{1 - (\dfrac{x_4/P_s - P_{cr}}{1 - P_{cr}})^{(\gamma-1)/\gamma}}, & \dfrac{x_4}{P_s} > P_{cr} \end{cases} \qquad x_5 < 0 \end{cases} \tag{6-14}$$

The equilibrium point of (6-5) is:

$$x_1{}^{ss} = \frac{x_m}{1 + \frac{K_{ext}}{K_{adm}}}, x_2{}^{ss} = 0, x_5{}^{ss} = 0, x_7{}^{ss} = 0 \qquad (6\text{-}15)$$

$$A(x_3{}^{ss} - x_4{}^{ss}) - K_{ext} \frac{x_m}{1 + \frac{K_{ext}}{K_{adm}}} - \sigma_0 x_6{}^{ss} = 0 \qquad (6\text{-}16)$$

The LEs of (6-5) are calculated and summarized in Table 6-1. The calculation was continued for 5000 seconds to make sure all the numerical values of LEs reach their steady value. This is crucial, especially for the LEs that are equal to zero. In this case, the calculation continued until the value of zero LEs stays negative for more than half of the calculation time. The time evolution of λ_6 is shown in Figure 6-4 as an instant. As discussed in Chapter 4, for a nonlinear system to have valid Lyapunov exponents, the nonlinear equation and its linearized equation must have a solution which is unique. Also, at the instants when the nonlinear equation cannot be linearized, a variational equation has to be substituted based on [55, 50] which must have equal numerical values at the left and right sides of the nonsmooth instant. These conditions are verified for the systems in this thesis. The details have been omitted as they do not relate to the focus of the work.

Table 6-1. Numerical results of LEs for autonomous unilateral teleoperation employing admittance control.

	λ_1	λ_2	λ_3	λ_4	λ_5	λ_6	λ_7
(s^{-1})	0.0	0.0	-0.1	-17.8	-18.0	-75.5	-229.4
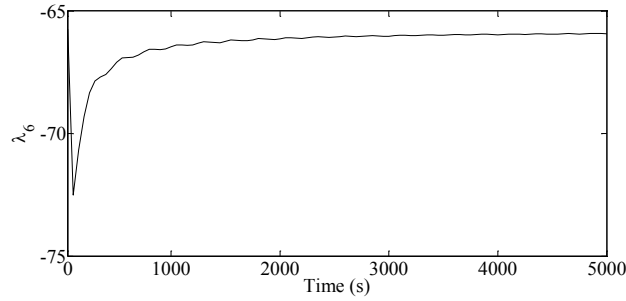
Figure 6-4. Time evolution of λ_6.

The signs of Lyapunov exponents determine the stability property of the dynamic system. Negative exponents correspond to exponential stability. The first largest exponent being zero indicates a stable system with a one-dimensional attractor. To understand the physical meaning of the results in Table 6-1, (6-15) and (6-16) are revisited. According to these equations, $x_1{}^{ss}$, $x_2{}^{ss}$ and $x_5{}^{ss}$ will eventually reach fixed values where the combination of $x_3{}^{ss}$, $x_4{}^{ss}$ and $x_6{}^{ss}$ will not hold fixed points but satisfy (6-16). Having three unknowns ($x_3{}^{ss}$, $x_4{}^{ss}$, $x_6{}^{ss}$) and one equation, (6-16) will have a two-dimensional solution; i.e., the equilibrium of (6-5) is two-dimensional [47, 37]. This explains the two zero LEs in Table 6-1. Finally, stability of the proposed control system in the presence of external force and model uncertainties is proven, as seen in Table 6-1. Referring to Chapter 4, because some LEs are zero and the rest are negative, and the nearby orbits stay within a constant distance from each other, the system is stable in the sense of Lyapunov (Lyapunov stable).

Parametric Stability Analysis

The concept of Lyapunov exponents can be used in parametric stability analysis, which is the stability analysis of a dynamic system as its parameters change [51]. Parametric analysis can assure the stability of the system when some of the physical parameters are not accurately known or measured. Likewise, it can be used to investigate the effect of changing controller gains on

overall stability. Also, by varying the physical and controller parameters, one can find the stability regions of a dynamic system [51].

As an instant, the LEs of the teleoperation method under question are calculated for different values of a physical parameter, the stiffness coefficient of the environment denoted by K_{ext}, and a controller gain, δ. Table 6-2 shows the numerical values of LEs for admittance unilateral teleoperation as K_{ext} varies. It is evident that changing K_{ext} does not have a notable effect on LEs. Table 6-3 shows the numerical values of LEs while the SMC bandwidth gain, δ, varies. The system behaves stably for the values of $\delta \leq 120$. However, the first LE becomes positive for $\delta = 140 \ \text{s}^{-1}$, which means the system is chaotic.

Table 6-2. Numerical results of LEs for admittance unilateral teleoperation as K_{ext} varies.

K_{ext}(N/m)	$\lambda_1(\text{s}^{-1})$	$\lambda_2(\text{s}^{-1})$	$\lambda_3(\text{s}^{-1})$	$\lambda_4(\text{s}^{-1})$	$\lambda_5(\text{s}^{-1})$	$\lambda_6(\text{s}^{-1})$	$\lambda_7(\text{s}^{-1})$
10	0.0	0.0	-0.1	-17.7	-18.0	-75.7	-229.3
50	0.0	0.0	-0.1	-17.8	-18.0	-75.7	-229.3
100	0.0	0.0	-0.1	-17.8	-18.0	-75.5	-229.4
150	0.0	0.0	-0.1	-17.8	-18.1	-75.5	-229.5
200	0.0	0.0	-0.1	-17.9	-18.1	-75.4	-229.6
300	0.0	0.0	-0.1	-17.9	-18.1	-75.3	-229.7
600	0.0	0.0	-0.1	-18.1	-18.6	-74.8	-230.1

Table 6-3. Numerical results of LEs for admittance unilateral teleoperation as δ varies.

δ (s^{-1})	$\lambda_1(\text{s}^{-1})$	$\lambda_2(\text{s}^{-1})$	$\lambda_3(\text{s}^{-1})$	$\lambda_4(\text{s}^{-1})$	$\lambda_5(\text{s}^{-1})$	$\lambda_6(\text{s}^{-1})$	$\lambda_7(\text{s}^{-1})$
20	0.0	0.0	-0.1	-19.8	-64.6	-64.7	-191.4
30	0.0	0.0	-0.1	-26.0	-56.1	-56.1	-202.3
40	0.0	0.0	-0.1	-34.3	-47.8	-47.8	-210.7
60	0.0	0.0	-0.1	-31.7	-31.9	-55.0	-222.2
80	0.0	0.0	-0.1	-17.8	-18.1	-75.5	-229.4
100	0.0	0.0	-0.4	-13.2	-14.5	-83.2	-230.0
120	0.0	0.0	-0.7	-7.5	-34.4	-70.9	-228.0
140	1.6	0.0	-0.1	-4.8	-47.4	63.4	-227.8

6.1.2 Non-autonomous System

Simulation studies

The system stability analysis using Lyapunov exponents is also studied when the system is non-autonomous in which the primary desired trajectory x_h, and external force F_{ext} are functions of time. For this reason, simulation study of the system is conducted. The non-autonomous external force is a sinusoidal wave which imposes the force in both an assistive and resistive manner.

$$F_{ext}(t) = A_1 \sin(A_2 t), \tag{6-17}$$

where $A_1 = 30$ N and $A_2 = 0.5$. The primary desired trajectory from the hand-controller is a function of time as follows:

$$x_h(t) = B_1 + B_2 \sin(B_3 t) , \tag{6-18}$$

where $B_1 = 0.07$ m, $B_2 = 0.18$ m and $B_3 = 0.025$. The numerical values of coefficients in (6-17) and (6-18) are chosen in a way to generate the desired trajectory similar to an experimental result that was conducted along with the experimental results in 6.2 but is not presented here. The master manipulator provides a preliminary time-varying desired trajectory formulated by (6-18) and shown in Figure 6-5. During the motion, it interacts with an external force that varies with time, Figure 6-5(b). The admittance module converts the external force to a relevant position which is shown in Figure 6-5(c). The admittance module is assumed similar to the one in the autonomous simulation. The desired position, shown in Figure 6-5(d), is the sum of Figure 6-5(a) and Figure 6-5(c).

Figure 6-6 shows the simulation results on the slave side. Displacement of the slave, Figure 6-6(a), is in reasonable agreement with the desired position, Figure 6-5(d). The position error, Figure 6-6, confirms this fact. The air pressures in the slave chambers are shown in Figure 6-6(b). The control signal, Figure 6-6(c), is unsaturated.
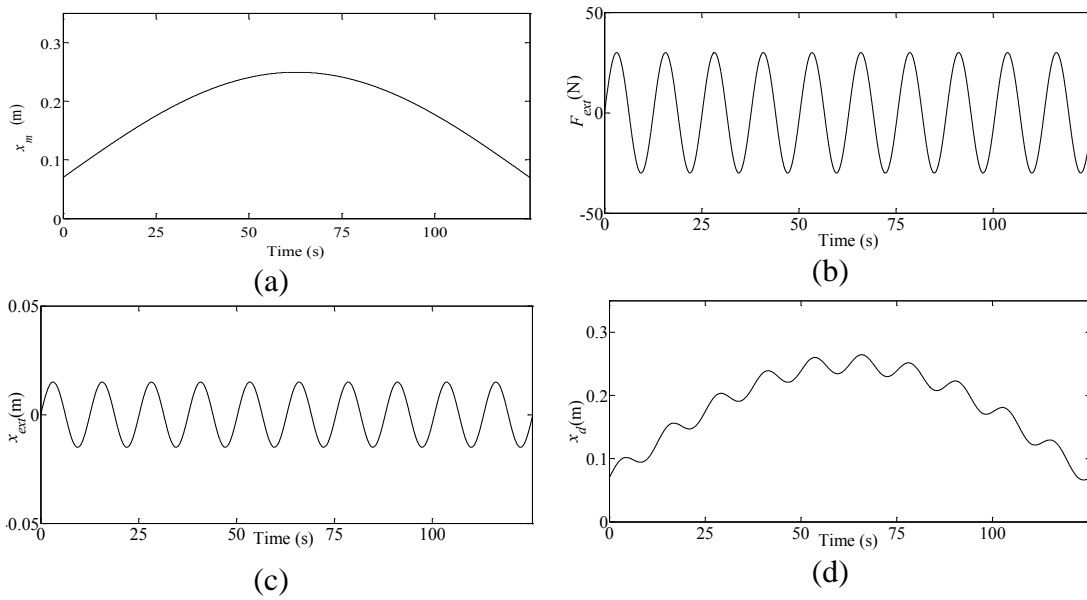
Figure 6-5. Admittance control variables pertaining to step tracking: (a) primary desired trajectory provided by the master manipulator, x_m; (b) external force, F_{ext}; (c) displacement corresponding to the external force, x_{ext}; (d) desired trajectory achieved from admittance model, x_d.
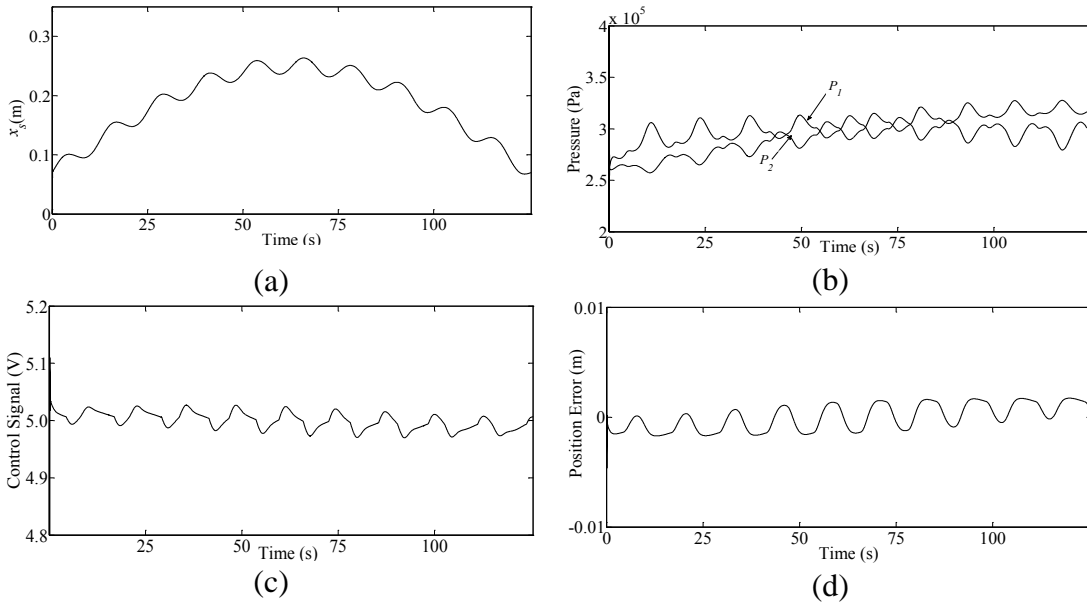
Figure 6-6. Step tracking with SMC: (a) piston position; (b) chamber pressures; (c) control signal; (d) position error.

Stability analysis

The state space vector for a non-autonomous unilateral admittance system with explicitly defined time as a state space variable is as follows:

$$\vec{x} = [x_1 \ \ x_2 \ \ x_3 \ \ x_4 \ \ x_5 \ \ x_6 \ \ x_7 \ \ x_8]^T = [t \ \ x_s \ \ v_s \ \ P_1 \ \ P_2 \ \ x_v \ \ z \ \ \int_0^t e \, d\tau]^T \quad . \tag{6-19}$$

The dynamic system equations of motion will be modified to:

$$
\begin{cases}
\dot{x}_1 = 1 \\[2mm]
\dot{x}_2 = x_3 \\[2mm]
\dot{x}_3 = \dfrac{1}{m_p}\left[A(x_4 - x_5) + F_{ext} - \left(\sigma_0 x_7 + \sigma_1 \left(x_3 - \dfrac{\sigma_0 |x_3| x_7}{F_c + (F_s - F_c)e^{-(x_3/vs)^2}} \right) + b x_3 \right) \right] \\[4mm]
\dot{x}_4 = +\gamma R T \dfrac{w x_6 \, \dot{\emptyset}_1}{V_0 + A x_2} - \alpha \gamma A \dfrac{x_3 x_4}{V_0 + A x_2} \\[4mm]
\dot{x}_5 = -\gamma R T \dfrac{w x_6 \, \dot{\emptyset}_2}{V_0 + A(L - x_2)} + \alpha \gamma A \dfrac{x_3 x_5}{V_0 + A(L - x_2)} \\[4mm]
\dot{x}_6 = \dfrac{1}{\tau}(-x_6 + K_v u) \\[3mm]
\dot{x}_7 = x_3 - \dfrac{\sigma_0 |x_3| x_6}{F_c + (F_s - F_c)e^{-(x_3/vs)^2}} \\[3mm]
\dot{x}_8 = e
\end{cases}
\tag{6-20}
$$

where

$$e = x_2 - (B_1 + B_2 \sin(B_3 x_1)) - A_1 \sin(A_2 x_1)/K_{adm} \quad , \tag{6-21}$$

$$\dot{e} = x_3 - B_2 B_3 \cos(B_3 x_1) - A_1 A_2 \cos(A_2 x_1)/K_{adm} \quad , \tag{6-22}$$

$$\ddot{e} = \dot{x}_3 + B_2 B_3^2 \sin(B_3 x_1) + A_1 A_2^2 \sin(A_2 x_1)/K_{adm} \quad , \tag{6-23}$$

$$\dddot{x}_d = -(B_2 B_3^3 \cos(B_3 x_1) + A_1 A_2^3 \cos(A_2 x_1)/K_{adm}) \quad , \tag{6-24}$$

$$Fx = -\frac{\alpha \gamma A^2}{m_p}\left(\frac{x_4}{V_0 + Ax_2} + \frac{x_5}{V_0 + A(L - x_2)}\right)x_3 - \frac{B}{m_p}\dot{x}_3$$

$$+ \frac{A_1 A_2}{m_p}\cos(A_2 x_1)$$

$\qquad$ (6-25)

,

$$F_{ext} = A_1 sin(A_2 x_1) \quad .$$

$\qquad$ (6-26)

The variables $\dot{m}_1, \dot{m}_2$, u and F_f are defined before. Since the system is non-autonomous, it does not have an equilibrium point. The numerical values of (6-20) are presented in Table 6-4. With all LEs being non-positive, Lyapunov stability of the system is proven.

Table 6-4. Numerical results of LEs for non-autonomous unilateral teleoperation employing admittance control

	λ_1	λ_2	λ_3	λ_4	λ_5	λ_6	λ_7	λ_8
(s^{-1})	0.0	0.0	0.0	-0.1	-0.3	-42.6	-47.4	-228.7

6.2 Experimental Results

Experiments were performed to evaluate the performance of the teleoperated pneumatic system under real test scenarios. The experimental setup, described in Chapter 4, consists of an omni-directional, PHANToM haptic device, driven by the operator at the master side. The slave is a double rod pneumatic actuator which is imposed by an external force generated by a human at the slave side. The master, slave, data acquisition board, and control station are connected to each other through an ideal network. An encoder and two pressure sensors are incorporated to provide the data of the slave actuator. The external force is measured by a load cell which is located between the piston rod and a shaft with a handle.

Different admittance parameter settings were tested. Two experimental scenarios are presented to show the performance of the admittance control in conjunction with SMC. In the first

experiment, the admittance parameters are set to study soft reaction to an external force. In the second experiment, an external force is applied to the actuator and the goal of the admittance model is a stiff actuator reaction.

Experiment 1: In this experiment, the operator moves the master and, at the same time, a human subject located at the slave side applies a force to the pneumatic actuator. The external force passes through the admittance model in (6-1), having parameters set as $M = 10$ Kg, $B = 50$ Ns/m and $K = 250$ N/m. Choosing numerical values of inertia, damping coefficient and stiffness is based on the desired acceleration, velocity, and displacement of the slave actuator as a result of imposing the external force.

The desired position trajectory originating from the master, x_m, is shown in Figure 6-7(a). Figure 6-7(b) shows the external force. The modified desired trajectory is shown in Figure 6-7(c). It is evident that the admittance control module effectively adjusts the primary desired trajectory according to the imposed external force. This figure also compares the modified desired trajectory with the actual position of the actuator and illustrates their reasonable agreement. Figure 6-7(d) shows the control signal, which is also bounded and unsaturated. This experiment shows the successful application of admittance control with soft stiffness.
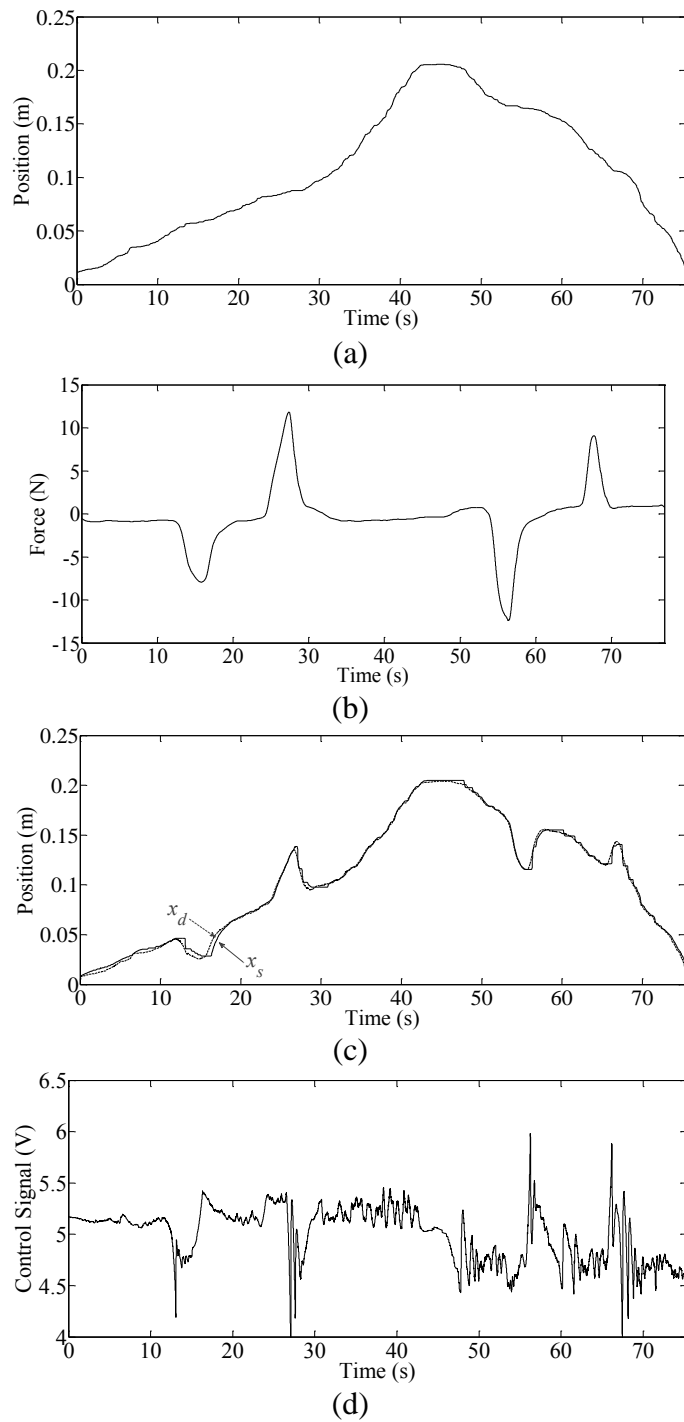
Figure 6-7. Experimental study of the low stiffness admittance model while tracking a human-guided trajectory: (a) primary desired position by the master manipulator, x_m; (b) external force, F_{ext}; (c) modified desired trajectory, x_d, versus position of actuator, x_s; (d) control signal, u.

Experiment 2: In this experiment, the parameters of the admittance model are set to $M = 10$ Kg, $B = 50$ Ns/m and $K = 10^4$ N/m. The goal is to study the behaviour of the system when the stiffness in the admittance model is set high. The actuator is subject to an external force with a magnitude of 100 N applied by a human subject. As Figure 6-8(a) shows, the primary desired position is fixed during the experiment. The external force is shown in Figure 6-8(b). The admittance model in (6-1) converts the external force to small displacement as shown in Figure 6-8(c). For an external force with a 100 N magnitude, the change in the primary desired trajectory is about 0.01 m. Comparing Figure 6-8(c) and Figure 6-7(c) shows the effect of changes in the parameters of the admittance control module. Figure 6-8(c) also shows the actual position of the slave actuator, x_s. Figure 6-8(d) shows the control signal corresponding to the position tracking shown in Figure 6-8(c).

The above experiments show the proposed control system can successfully control the slave actuator's desired position in the presence of the external force. The stability of the actuator motion was evident in the experiments. The SMC position controller worked effectively despite non-idealities such as friction and the compressibility of air. More experiments are conducted to assure the same result will be achieved.
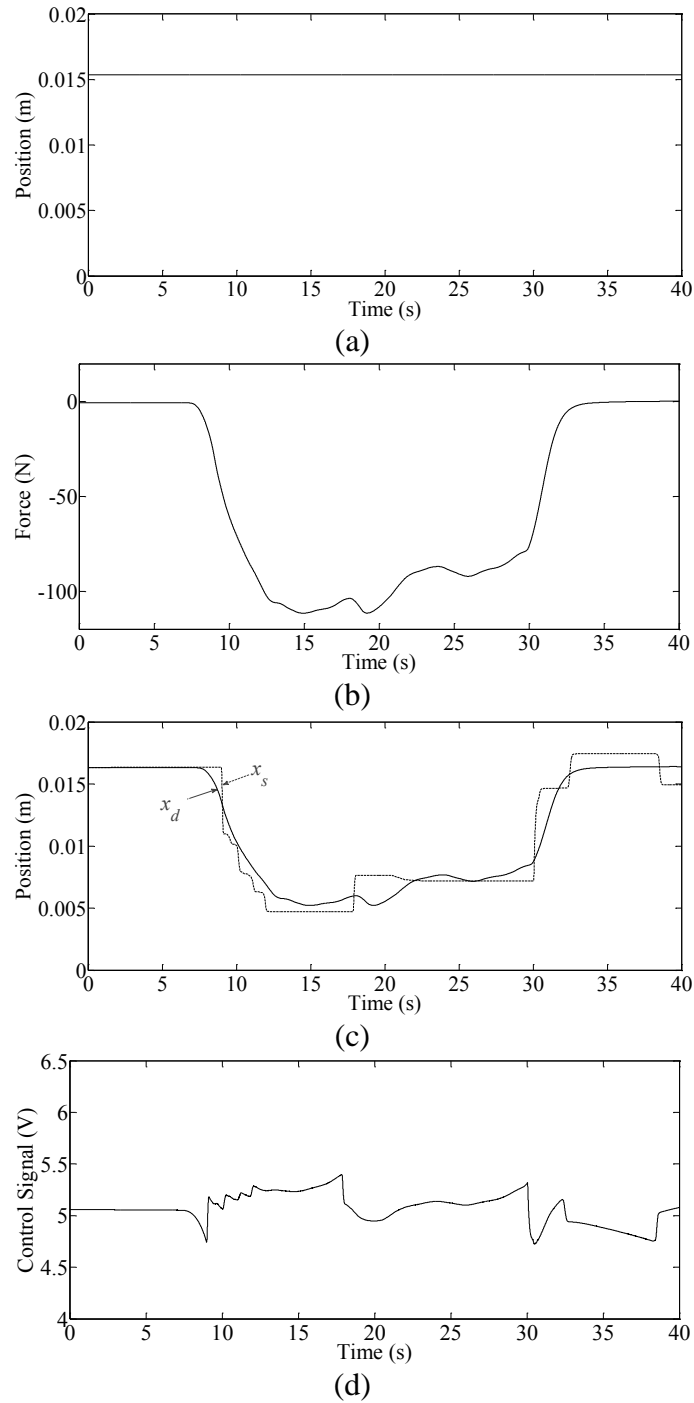
Figure 6-8. Experimental study of the high stiffness admittance model while tracking a human-guided trajectory: (a) primary desired position by the master manipulator, x_m; (b) external force, F_{ext}; (c) modified desired trajectory, x_d, versus the position of the actuator, x_s; (d) control signal, u.

71

Additional experimental results were conducted. Because the experimental results do not always

perform identically when they are repeated, this study was done to show that the experiments are

repeatable. The selected criteria of this study were average and maximum of control accuracy

(error). Statistical analysis including frequency distribution and scatter plot are presented.

The above experiments were repeated for different settings of admittance parameters. The

average position error, $\bar{e}$, and maximum position error, $\tilde{e}$, of the experiments are summarized in

Table 6-5. Then, the frequency distribution is obtained from Table 6-5 and also presented in a

scatter plot in Figure 6-9. It is evident that the population of average position error in $2 < \bar{e} \leq 3$

is the highest. The majority of the maximum position errors are in $10 < \tilde{e} \leq 20$ range which is

caused by the static friction of the pneumatic actuator.

Table 6-5. The average and maximum position error

of the unilateral admittance control experiments.

Experiment No.	Avg. Position Error, $\bar{e}$ (mm)	Max. Position Error, $\tilde{e}$ (mm)
1	2.5	17
2	4.7	25
3	2.8	20
4	3.6	40
5	2.5	15
6	5.6	2.5
7	2.1	14
8	4.4	26
9	1.7	6
10	2.3	9
11	2.5	18
12	2.6	17
13	2.2	10
14 (Figure 6-7)	1.9	14
15 (Figure 6-8)	0.8	5

Table 6-6. Frequency distribution table of the average and maximum position error of unilateral admittance control experiments.

Avg. Position error, $\bar{e}$ (mm)	Number	Percentage
≤ 2	3	20.0%
$2 < \bar{e} \leq 3$	8	53.3%
$3 < \bar{e} \leq 4$	1	6.7%
$4 < \bar{e} \leq 5$	2	13.3%
$\bar{e} > 5$	1	6.7%

Max. Position Error, $\tilde{e}$ (mm)	Number	Percentage
$\tilde{e} \leq 5$	2	13.3%
$5 < \tilde{e} \leq 10$	3	26.7%
$10 < \tilde{e} \leq 20$	7	40.0%
$20 < \tilde{e} \leq 30$	2	13.3%
$\tilde{e} > 30$	1	6.7%

(a)   (b)
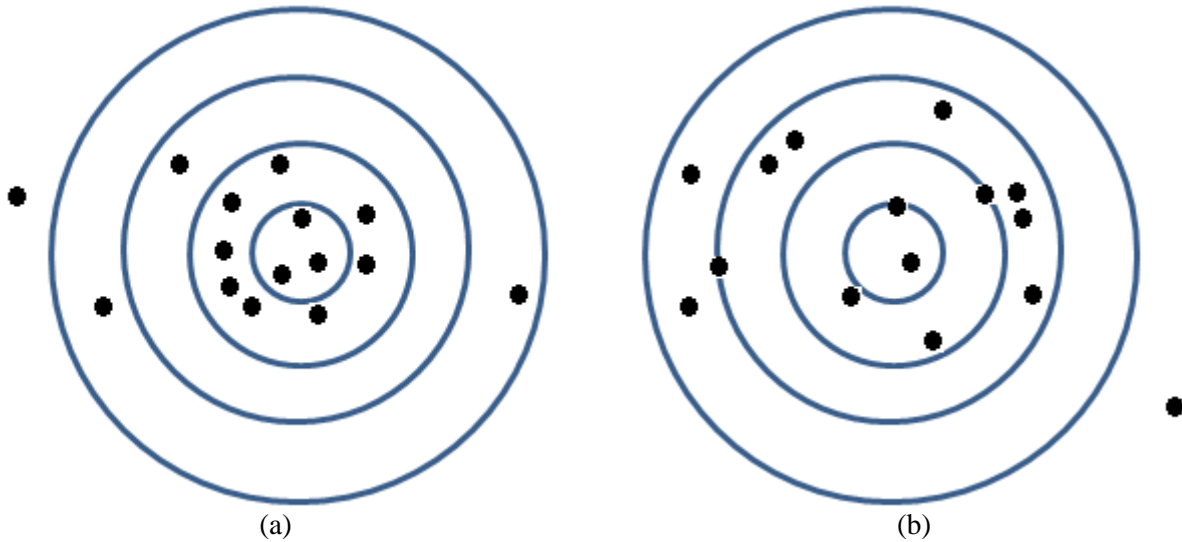
Figure 6-9. Scatter plot of the average and maximum position error of unilateral admittance control experiments: (a) average position error; (b) maximum position error.

6.3   *Summary*

In this chapter, the successful implementation of an admittance controller for unilateral control of a pneumatic actuator was presented. Admittance control, coupled with a sliding mode position controller, was employed to manage the actuator position and external force on the slave side. The proposed control system not only inherited the structural advantages of the unilateral teleoperation system with no need for a highly skilled operator, but also displayed satisfactory performance in scenarios involving various levels of environmental stiffness and interactions. Simulation and experimental results showed the effectiveness of the proposed unilateral teleoperation system both in position tracking and handling the external force. Repeatability of the experiments was assured by presenting scatter plot. Meanwhile, the stability of the entire control system was evaluated using the concept of Lyapunov exponents. Autonomous and non-autonomous cases were considered and studied. Parametric stability analysis showed that some values of control gain can make the system chaotic. By providing position tracking and handling the external force in an appropriate way, the proposed control method can potentially be applied to applications such as telerehabilitation.

7 UNILATERAL TELEOPERATION OF PNEUMATIC ACTUATORS; IMPLEMENTATION OF IMPEDANCE CONTROL[1]

This chapter focuses on the design and development of a unilateral pneumatic system based on impedance control. One objective of this chapter is to design a high-performance force controller suitable for applications such as teleoperation. The force controller should be able to handle modeling imperfections and uncertainties caused by friction and the compressibility of air. An impedance control scheme is then applied to deal with external force in a unilateral way. The schematic diagram of a unilateral control system is shown in Figure 7-1.
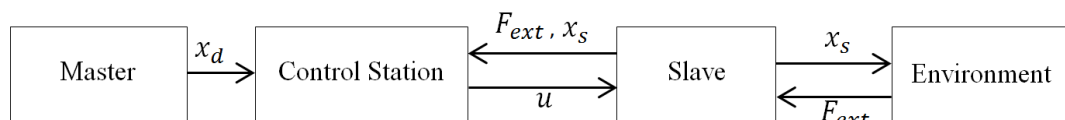
Figure 7-1. Schematic diagram of a unilateral pneumatic system.

---

[1] This paper is written based on a paper in press [82].

Similar to the admittance control mentioned in the previous chapter, impedance control simultaneously maintains desired force and position in the same direction [66]. Unlike admittance control, impedance control is formed using a force control loop. Figure 7-2 shows a general block diagram of force-based impedance control.
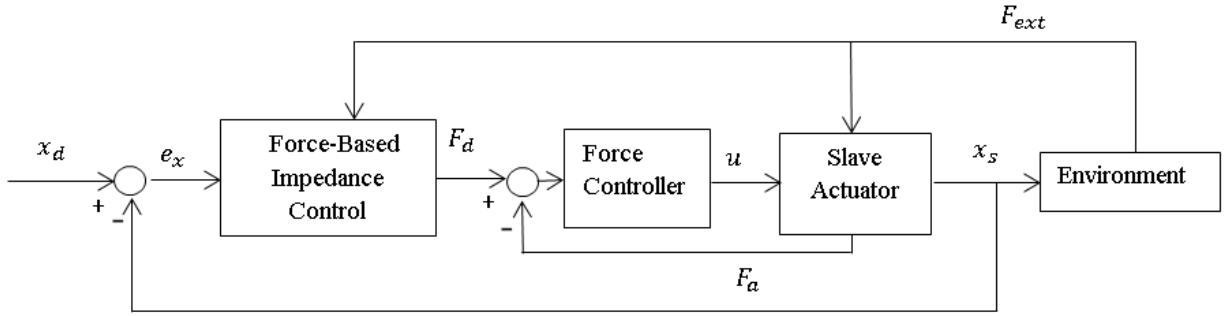
Figure 7-2. General block diagram of force-based impedance control.

In Figure 7-2, e_x is the position error defined as $e_x = x_d - x_s$ where x_d is the desired position generated by the hand-controller. F_a is the actuating force of the pneumatic actuator generated by the air pressure difference in the chambers. The slave actuator is modeled in Chapter 3. The environment can be anything depending on the application. The force controller and the corresponding control signal, u, will be detailed in this chapter. According to [67], the external force can be modeled as:

$$-F_{ext} = M(\ddot{x}_d - \ddot{x}_s) + B(\dot{x}_d - \dot{x}_s) + K(x_d - x_s) , \qquad (7\text{-}1)$$

where M, B and K are inertia, stiffness, and damping coefficients, corresponding to the impedance model. By extracting $\ddot{x}_s$ from (7-1) and inserting it in (3-2) and considering $e_x = x_d - x_s$, the formulation of the force-based impedance control is obtained:

$$F_d = m_p \left(F_{ext} + M\ddot{x}_d + B\dot{e}_x + Ke_x\right)/M + \left(F_f + b\dot{x}_s\right) - F_{ext} . \qquad (7\text{-}2)$$

It is evident that the impedance model in (7-2) is a combination of external force, position information, and position error.

7.1   Force Control

Efforts have been made toward the development of an efficient force controller for pneumatic systems. A first order linear controller was used to control the pressure of a pneumatic actuator [68]. Kazerooni [69] used the fact that the power of the actuator is a product of the actuator force and piston displacement. Through the precise measurement of the piston displacement and control of the actuator's power by a proportional controller, he controlled the actuator force.

A fuzzy controller was implemented to control the force of a pneumatic arm-exoskeleton [70]. Using a linearized model, a hybrid adaptive neuro-fuzzy model-reference controller was proposed towards the force control of pneumatic actuators [71]. Ben-Dov et al. [72], used a combination of linear and nonlinear models of valve dynamics and compressible flow to control air pressure in the chambers. Adaptive control was employed for pneumatic force actuation and trajectory tracking [73].

The SMC approach has been widely applied in the force control of pneumatic systems. In [74], a sliding mode force controller was augmented by a discontinuous, adaptive, robust controller to adopt the parameters to reduce the effect of the uncertainties of the pneumatic system. To eliminate the need for pressure sensors, a pressure estimation algorithm was developed and added to SMC [6]. A back-stepping sliding mode control was also used to simultaneously control the force and the stiffness of a pneumatic actuator [75]. An accurate sliding mode force control was designed for a pneumatic system with a low-cost solenoid valve [76]. Richer and Hurmuzlu [12] used SMC in the force control of a pneumatic muscle. A cascaded SMC scheme using observer-based disturbance compensation was used for a pneumatic muscle [77].

Sliding Mode Control is a robust control approach and has been applied to the force control of pneumatic systems [72, 25]. It generates the control signal based on the dynamic model of the

system. For a pneumatic actuator, as shown in Figure 7-1, the output is the actuating force, F_a, which is produced by the pressure difference in the chambers [25]:

$$F_a = A(P_1 - P_2) \ . \tag{7-3}$$

The sliding mode force control scheme makes F_a follow the desired force, F_d [25]. The control signal, u, is composed of Av_{eq}, the equivalent component, and Av_{rb}, the robust component [25]:

$$u = (Av_{eq} + Av_{rb})/(wK_v) \ . \tag{7-4}$$

The sliding surface is selected as follows:

$$S_f = (\frac{d}{dt} + \delta) \int_0^t e_f d\tau \ , \tag{7-5}$$

where δ is the control bandwidth. The force error is expressed as:

$$e_f = F_a - F_d \ . \tag{7-6}$$

The dynamics on the sliding surface is expressed as:

$$\dot{S}_f = \dot{e}_f + \delta e_f = 0 \ . \tag{7-7}$$

This leads to the equivalent part of the control signal:

$$Av_{eq} = \frac{\dot{F}_d - \delta e_f - \dot{F}_{ext} + (\dot{F}_f + b\ddot{x}_s) - F_x}{P_x} \tag{7-8}$$

where:

$$F_x = -\alpha\gamma A^2(\frac{P_1}{V_1} + \frac{P_2}{V_2})\dot{x}_s \ , \tag{7-9}$$

$$P_x = \gamma RTA(\frac{\dot{\emptyset}_1}{V_1} + \frac{\dot{\emptyset}_2}{V_2}) \ . \tag{7-10}$$

The dynamics of the pneumatic system is assumed faster than the rate of the change of the dry friction [14]. Thus, $\dot{F}_f$ can be neglected in (7-8) [14, 78]. This simplification is compensated by the robust part of SMC, which is formulated as follows:

$$Av_{rb} = -\frac{K_{rb}}{P_x}\text{sign}(S_f) \ , \tag{7-11}$$

In (7-11), K_{rb} is robustness gain. The discontinuity of the "sign" function can affect the implementation of Av_{rb}. Therefore, it is approximated by $\tanh(ax)$, where a is a large positive number.

$$\text{sign}(x) = \tanh(ax), a \gg 0 \ . \qquad (7\text{-}12)$$

7.2 Simulation Studies and Stability Analysis

7.2.1 Autonomous System

Simulation Results

The performance of an autonomous unilateral system applying impedance control is presented through simulation. The environment which the slave actuator is interacting with is assumed to be stiffness-dominant. Thus, the external force is proportional to the slave position:

$$F_{ext} = -K_{ext}x_1 \ , \qquad (7\text{-}13)$$

where K_{ext} is the environment stiffness gain. Figure 7-3(a) shows the slave actuator position tracking results. The force tracking result is shown in Figure 7-3(b). The desired force, F_d, is obtained from the impedance model expressed by (7-2). The actuating force, F_a, is formulated in (7-3). The control signal of the pneumatic actuator is shown Figure 7-3(c). The values of the SMC control bandwidth, δ, and robustness gain, K_{rb}, are 40 s^{-1} and 1100 mKg/s^3, respectively. The process of choosing the numerical values is explained before. K_{ext} is 100 N/m. Impedance parameters are $M = 1 \text{ Kg}, B = 20 \text{ Ns/m}$ and $K = 250 \text{ N/m}$. The reason for choosing this numerical value is to recreate the simulation of Chapter 6. Figure 7-3(d) shows the external force, as defined in (7-13). One can see the reasonable agreement between the motion of the master and slave and the reaction of the slave to the external force.
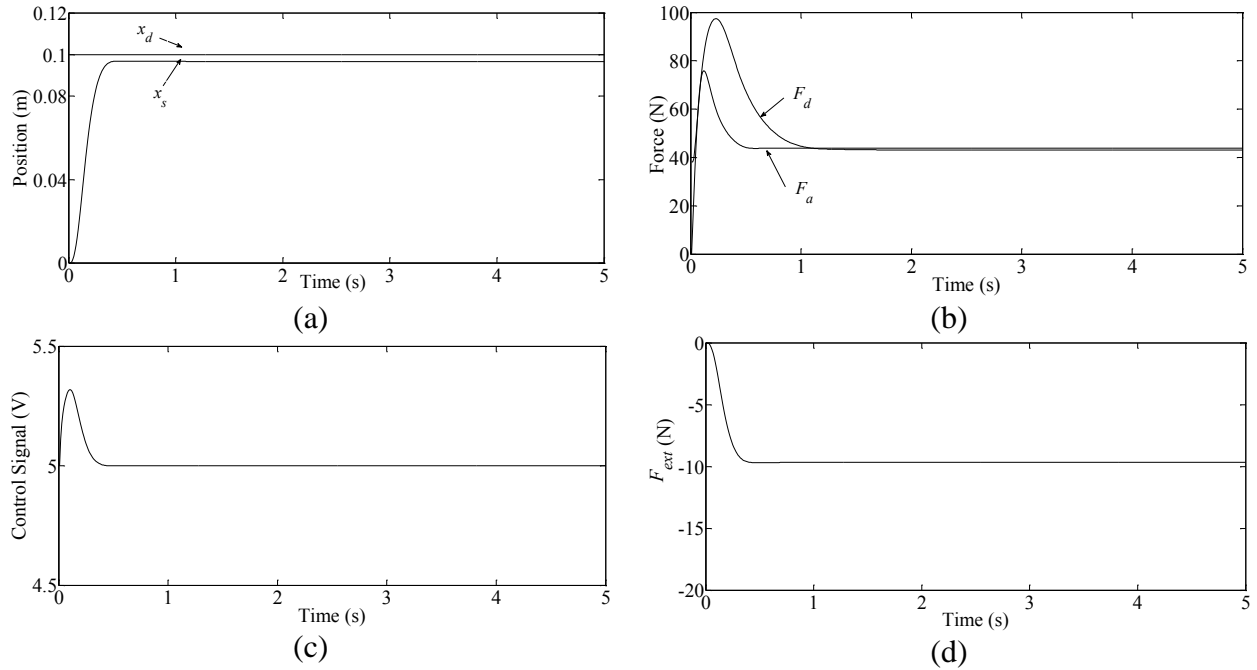
Figure 7-3. Simulation results of a step tracking: (a) piston position vs. desired position; (b) actuator force vs. desired force; (c) control signal; (d) external force.

Calculation of Lyapunov exponents

The state space is formed by defining the following state vector:

$$\vec{x} = [x_1 \ \ x_2 \ \ x_3 \ \ x_4 \ \ x_5 \ \ x_6 \ \ x_7 \ ]^T = [x_s \ \ v_s \ \ P_1 \ \ P_2 \ \ x_v \ \ z \ \ \int_0^t e_f \, d\tau]^T \quad , \qquad (7\text{-}14)$$

where $x_i(i = 1,..,7)$ are the state space and the right side variables (3-2) to (3-12) and (7-2) to (7-6) and (7-13), the state space model of the unilateral pneumatic system is constructed as follows:

$$\begin{cases} \dot{x}_1 = x_2 \\[4pt] \dot{x}_2 = \dfrac{1}{m_p}\left[A(x_3 - x_4) - K_{ext}x_1 - \left(\sigma_0 x_6 + \sigma_1\left(x_2 - \dfrac{\sigma_0|x_2|x_6}{F_c + (F_s - F_c)e^{-(x_2/vs)^2}}\right) + bx_2\right)\right] \\[10pt] \dot{x}_3 = +\gamma RT\dfrac{wx_5\,\dot{\emptyset}_1}{V_0 + Ax_1} - \alpha\gamma A\dfrac{x_2 x_3}{V_0 + Ax_1} \\[10pt] \dot{x}_4 = -\gamma RT\dfrac{wx_5\,\dot{\emptyset}_2}{V_0 + A(L - x_1)} + \alpha\gamma A\dfrac{x_2 x_4}{V_0 + A(L - x_1)} \\[10pt] \dot{x}_5 = \dfrac{1}{\tau}(-x_5 + K_v u) \\[10pt] \dot{x}_6 = x_2 - \dfrac{\sigma_0|x_2|x_6}{F_c + (F_s - F_c)e^{-(x_2/vs)^2}} \\[10pt] \dot{x}_7 = e_f \end{cases} \qquad , \quad (7\text{-}15)$$

where

$$u = \frac{1}{w.K_v}\left(\frac{\dot{F}_d - \delta e_f + K_{ext}x_2 + b\dot{x}_2 - Fx - K_{rb}\tanh(aS_f)}{\gamma RTA\left(\dfrac{\dot{\emptyset}_1}{V_0 + Ax_1} + \dfrac{\dot{\emptyset}_2}{V_0 + A(L - x_1)}\right)}\right) . \qquad (7\text{-}16)$$

In (7-16), S_f is defined as:

$$S_f = e_f + \delta x_7 . \qquad (7\text{-}17)$$

The force error is defined as:

$$e_f = A(x_3 - x_4) - K_{ext}x_1 - \left(\sigma_0 x_6 + \sigma_1\left(x_2 - \frac{\sigma_0|x_2|x_6}{F_c + (F_s - F_c)e^{-(x_2/vs)^2}}\right) + bx_2\right) - F_d . \qquad (7\text{-}18)$$

The desired force, F_d, is achieved from the impedance model as follows:

$$F_d = \frac{m_p}{M}\left(-K_{ext}x_1 + M\ddot{x}_d + B(\dot{x}_d - x_2) + K(x_d - x_1)\right) + \left(F_f + bx_2\right) \qquad (7\text{-}19)$$

$$+ K_{ext}x_1$$

The derivation of the desired force is formulated as follows:

$$\dot{F}_d = \frac{m_p}{M}\left(-K_{ext}x_2 + B(\dot{x}_2 - \ddot{x}_d) + K(x_2 - \dot{x}_d) + M\dddot{x}_d\right) + b\dot{x}_2 \qquad (7\text{-}20)$$

$$+ K_{ext}x_2$$

The steady state form definitions of the other variables in (7-15) are mentioned in Chapter 6.

The initial condition is $\vec{x}_0 = [0, 0, 3 \times 10^5, 3 \times 10^5, 0, 0, 0]^T$ and the equilibrium of (7-15) is $\vec{x}_{eq} = [x_1^{ss} \quad 0 \quad x_3^{ss} \quad x_4^{ss} \quad 0 \quad x_6^{ss} \quad x_7^{ss}]^T$ where:

$$\begin{cases} A(x_3^{ss} - x_4^{ss}) - K_{ext}x_1^{ss} - \sigma_0 x_6^{ss} = 0 \\ \dot{F}_d - K_{rb} \tanh(ax_7^{ss}) = 0 \end{cases} \quad . \tag{7-21}$$

To study the stability of the control system, the spectrum of the Lyapunov exponents are calculated. Table 7-1 shows the numerical values of Lyapunov exponents. It is evident that all Lyapunov exponents are zero or negative, which proves Lyapunov stability of the system despite the nonlinearity of the pneumatic actuator and the external force.

Table 7-1. Numerical results of LEs for autonomous unilateral teleoperation employing impedance control.

	λ_1	λ_2	λ_3	λ_4	λ_5	λ_6	λ_7
(s^{-1})	0.0	0.0	0.0	-23.4	-64.2	-64.2	-170.1

By revisiting (7-21), one can see that out of seven state space variables, x_2^{ss} and x_5^{ss} have numerical values at the steady state. Having two equations and five unknown variables means the solution of (7-21) is 3-dimensional. Knowing that the number of zero LEs for any dynamic system represents the dimension of the equilibrium point, one can see that the values in Table 7-1 are in line with the equilibrium of (7-15).

Parametric Stability Analysis

A parametric stability study is presented for the unilateral pneumatic system described in this chapter. First, environmental stiffness, K_{ext}, was changed as shown in Table 7-2. Then, LEs were calculated for each value of K_{ext}. It is observed that for all values of K_{ext}, LEs are non-positive. Table 7-2 shows that changing K_{ext} does not have a major effect on the rate of convergence/divergence of trajectories in the state space. Therefore, we can conclude that the dynamic system is stable for the range of K_{ext} in Table 7-2.

In the next set of studies, the value of the SMC control bandwidth, δ, was changed. Similar to the last sample, all LEs are non-positive for all values of δ presented in Table 7-3. Compared to Table 7-2, the rate of changes of LEs in this sample is higher. This indicates that the SMC control bandwidth can substantially influence the rate of convergence/divergence of state space trajectories.

Table 7-2. Numerical results of LEs for impedance unilateral teleoperation as K_{ext} varies.

K_{ext}(N/m)	$\lambda_1(s^{-1})$	$\lambda_2(s^{-1})$	$\lambda_3(s^{-1})$	$\lambda_4(s^{-1})$	$\lambda_5(s^{-1})$	$\lambda_6(s^{-1})$	$\lambda_7(s^{-1})$
10	0.0	0.0	0.0	-22.5	-64.1	-64.1	-171.1
50	0.0	0.0	0.0	-22.8	-64.2	-64.2	-170.6
75	0.0	0.0	0.0	-23.1	-64.2	-64.2	-170.3
100	0.0	0.0	0.0	-23.4	-64.2	-64.2	-170.1
125	0.0	0.0	0.0	-23.7	-64.1	-64.1	-169.9
150	0.0	0.0	0.0	-24.0	-64.0	-64.0	-169.7
200	0.0	0.0	0.0	-24.7	-63.8	-63.8	-169.4

Table 7-3. Numerical results of LEs for impedance unilateral teleoperation as δ varies.

$\delta(s^{-1})$	$\lambda_1(s^{-1})$	$\lambda_2(s^{-1})$	$\lambda_3(s^{-1})$	$\lambda_4(s^{-1})$	$\lambda_5(s^{-1})$	$\lambda_6(s^{-1})$	$\lambda_7(s^{-1})$
1	0.0	0.0	0.0	-1.0	-49.6	-49.7	-221.6
20	0.0	0.0	0.0	-13.7	-53.8	-53.8	-200.3
30	0.0	0.0	0.0	-19.9	-57.8	-57.8	-186.9
40	0.0	0.0	0.0	-23.4	-64.1	-64.2	-170.1
50	0.0	0.0	0.0	-27.0	-73.8	-73.8	-147.4
60	0.0	0.0	0.0	-30.0	-94.8	-98.7	-98.7
100	0.0	0.0	0.0	-38.0	-59.4	-112.4	-112.4

7.2.2 Non-Autonomous System

Simulation Results

Simulation studies are presented for the non-autonomous unilateral system employing impedance control. The external force and the displacement of the master manipulator are defined as the following. The reasoning of choosing coefficient was mentioned in the previous chapter.

$$F_{ext} = 30\sin(0.5t) \; , \tag{7-22}$$

$$x_m = 0.07 + 0.18\sin(0.025t) \; . \tag{7-23}$$

The numerical values of inertia, stiffness and damping ratio in (7-2) are $M = 1$ Kg, $B = 20$ Ns/m and $K = 3000$ N/m. The reason for choosing them was to recreate a simulation similar to the simulation of Chapter 6. Figure 7-4 shows the simulation results. The desired position trajectory given by the master manipulator and the actual displacement of the slave are presented in Figure 7-4(a). One can see that the slave follows the motion of the master with some adjustments related to the external force shown in Figure 7-4(d). Figure 7-4(b) shows that the desired and actual forces are in agreement. It is evident that the SMC controller works well even when the pneumatic actuator is under an external force. The control signal in Figure 7-4(c) is unsaturated.
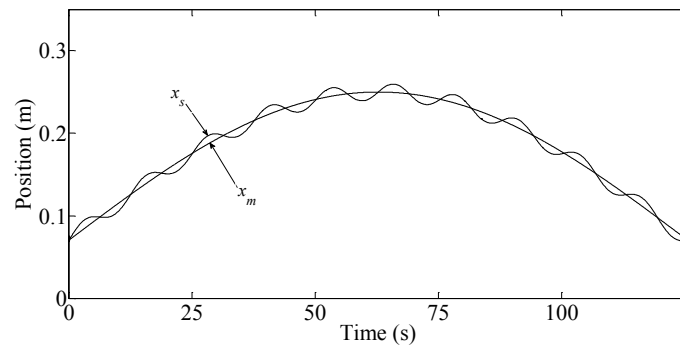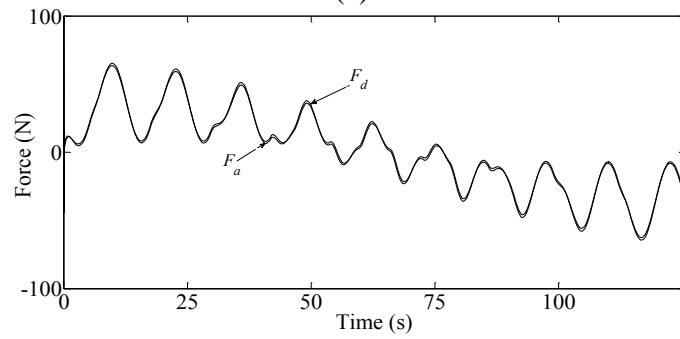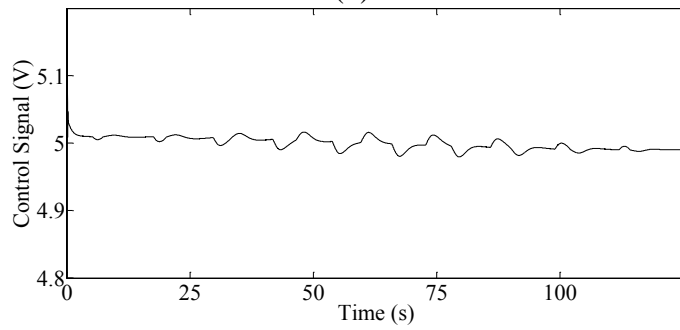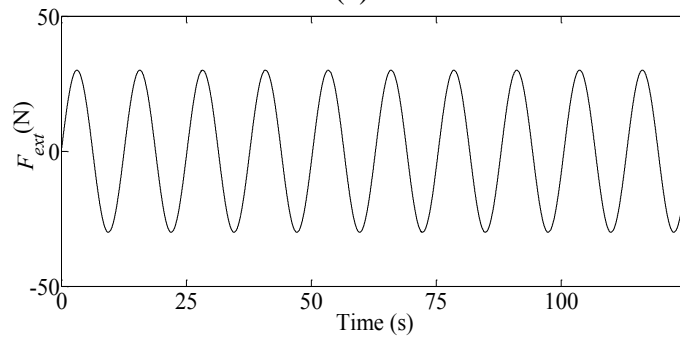
Figure 7-4. Simulation results of a sinusoidal tracking: (a) piston position vs. desired position; (b) actuator force vs. desired force; (c) control signal; (d) external force

Calculation of Lyapunov exponents

Stability analysis is conducted by modifying (6-4) to:

$$\vec{x} = [x_1 \; x_2 \; x_3 \; x_4 \; x_5 \; x_6 \; x_7 \; x_8]^T = [t \; x_s \; v_s \; P_1 \; P_2 \; x_v \; z \; \int_0^t e_f \, d\tau]^T \; . \quad (7\text{-}24)$$

The dynamic system is accordingly modified to:

$$
\begin{cases}
\dot{x}_1 = 1 \\[6pt]
\dot{x}_2 = x_3 \\[6pt]
\dot{x}_3 = \dfrac{1}{m_p}\left[A(x_4 - x_5) + F_{ext} - \left(\sigma_0 x_7 + \sigma_1 \left(x_3 - \dfrac{\sigma_0 |x_3| x_7}{F_c + (F_s - F_c)e^{-(x_3/vs)^2}} \right) + b x_3 \right) \right] \\[12pt]
\dot{x}_4 = +\gamma RT \dfrac{w x_6 \, \dot{\varnothing}_1}{V_0 + A x_2} - \alpha \gamma A \dfrac{x_3 x_4}{V_0 + A x_2} \\[12pt]
\dot{x}_5 = -\gamma RT \dfrac{w x_6 \, \dot{\varnothing}_2}{V_0 + A(L - x_2)} + \alpha \gamma A \dfrac{x_3 x_5}{V_0 + A(L - x_2)} \\[12pt]
\dot{x}_6 = \dfrac{1}{\tau}(-x_6 + K_v u) \\[12pt]
\dot{x}_7 = x_3 - \dfrac{\sigma_0 |x_3| x_6}{F_c + (F_s - F_c)e^{-(x_3/vs)^2}} \\[12pt]
\dot{x}_8 = e_f
\end{cases}
\quad . \quad (7\text{-}25)
$$

The variables and parameters of (7-25) are defined in (7-22), (7-23) and 6.2.1. The final numerical values of Lyapunov exponents of (7-25) are shown in Table 7-4. Since all exponents are negative or zero, the system under study is Lyapunov stable.

Table 7-4. Numerical results of LEs for non-autonomous unilateral teleoperation employing impedance control.

	λ_1	λ_2	λ_3	λ_4	λ_5	λ_6	λ_7	λ_8
(s^{-1})	0.0	0.0	0.0	0.0	-13.3	-65.6	-69.8	-163.8

7.3   Experimental Results

7.3.1   Force Control

Experiments are conducted on the test rig described in Chapter 3 to verify the practical utility of the proposed SMC force controller, (7-4). Desired force trajectories with different frequencies and magnitudes are experimented with. To avoid the effect of motion on the actuator force, the piston rod was placed in the middle of the stroke by a set of bolts as shown in Figure 7-5.
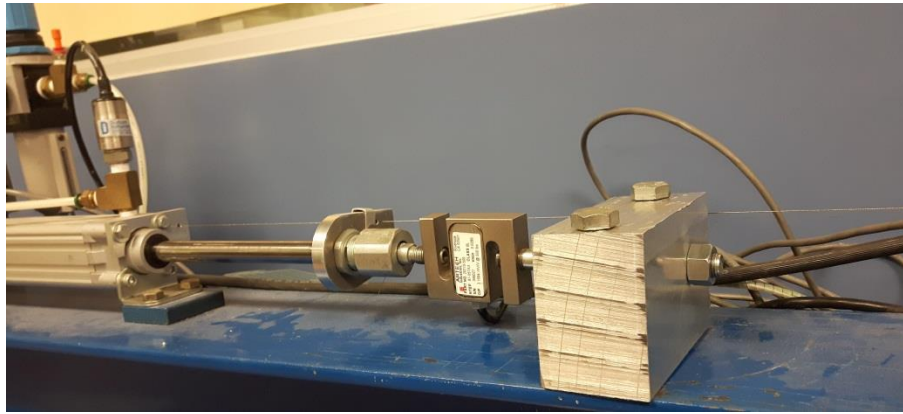
Figure 7-5 Experimental setup for SMC force tracking while the piston is fixed.

Figure 7-6 shows the force tracking experimental results for sinusoidal desired trajectories with the magnitudes of 20 N and 50 N and the frequencies of 0.1 rad/s and 0.9 rad/s. As can be seen, the proposed SMC force controller is able to track the desired force successfully. The oscillation on the force error and the control signals is caused by the oscillatory chamber pressure signals. Comparing the relative error displayed in Figure 7-6(a) to Figure 7-6(d), one can see that the performances of both force tracking experiments are similar. The control signals are always unsaturated and remain in the expected range. The above experiment shows that the proposed controller is capable of tracking the desired force with different amplitudes.
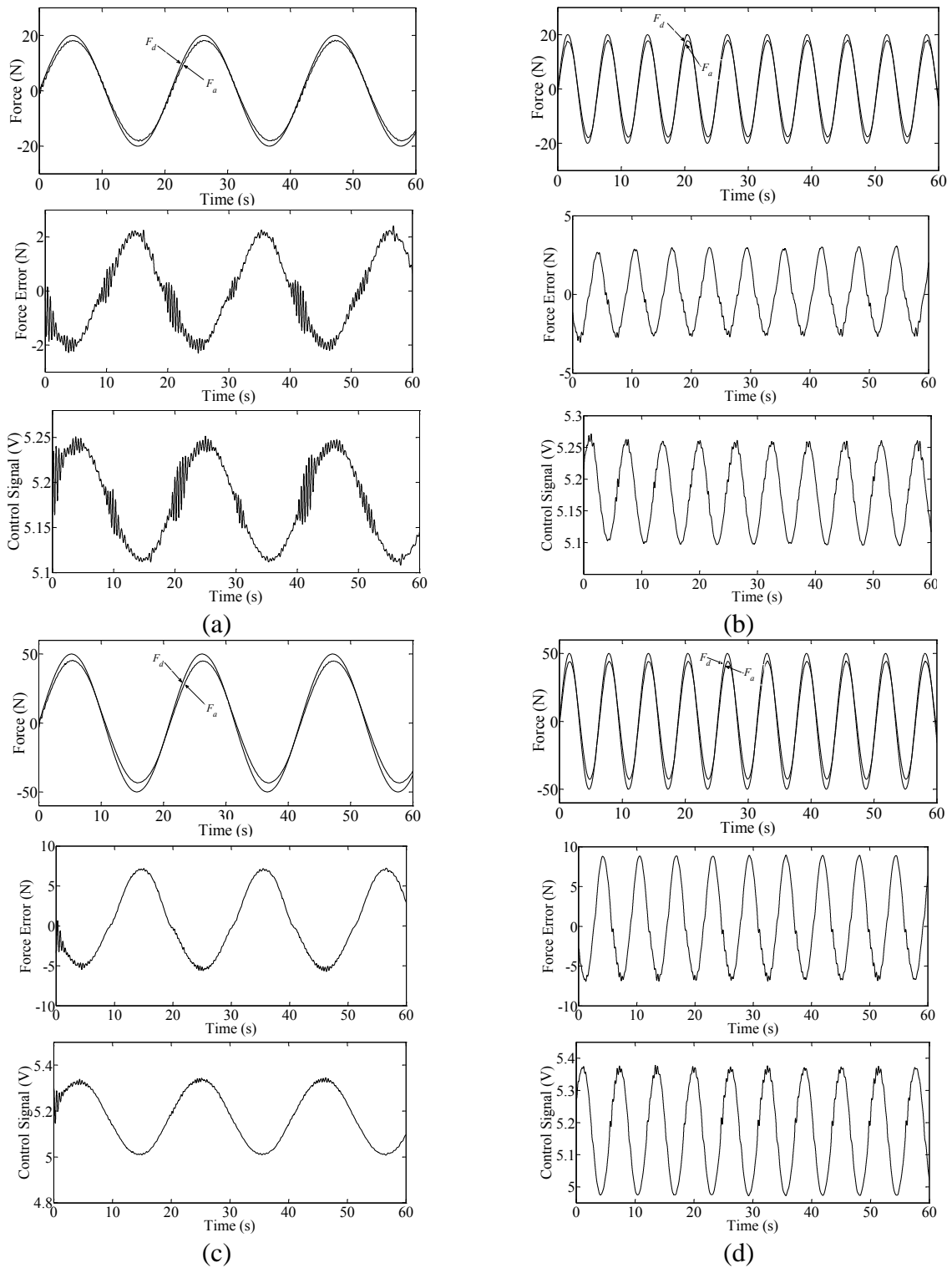
Figure 7-6. Sinusoidal force tracking response of SMC for a force with: (a) 20 N amplitude, 0.1 rad/s frequency; (b) 20 N amplitude, 0.9 rad/s frequency; (c) 50 N amplitude, 0.1 rad/s frequency; (d) 50 N amplitude, 0.9 rad/s frequency.

To further study the force tracking performance, the force tracking of 0.15 rad/s, 0.3 rad/s, 0.6 rad/s and 1.0 rad/s sinusoidal waves are experimented with. The results in the frequency domain are presented in Figure 7-7. It is observed that the force controller successfully follows the desired force for all tracking frequencies.

(a)   (b)
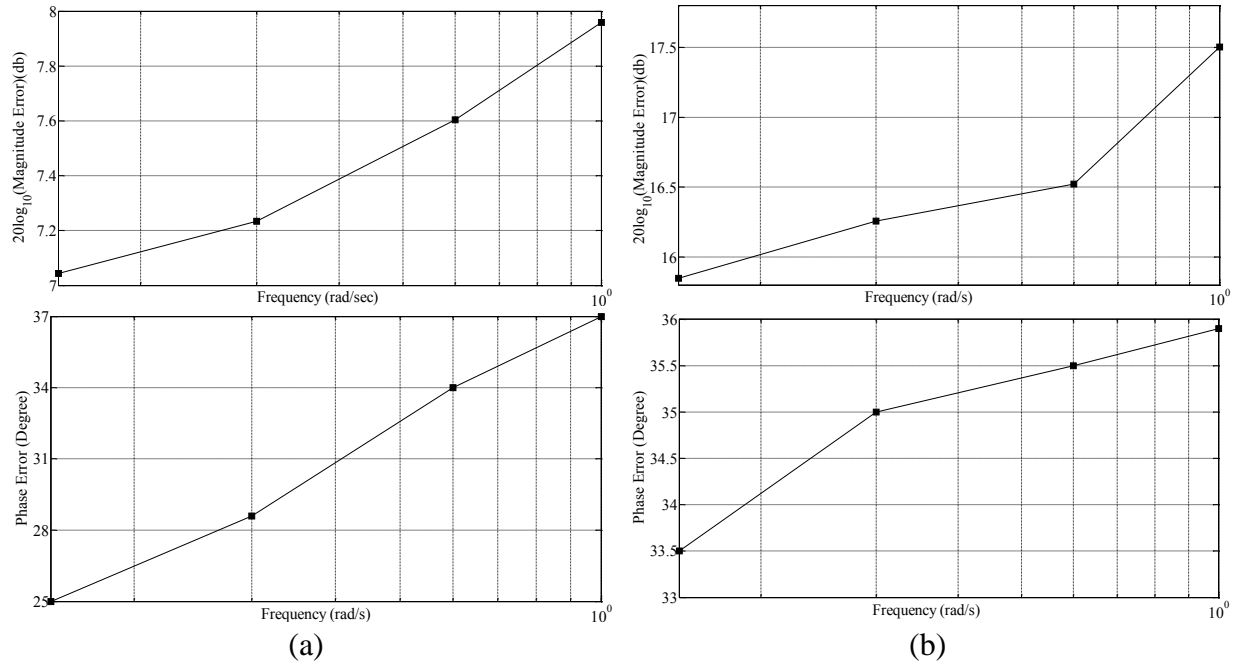
Figure 7-7. Frequency response of force tracking by SMC; (a) 20 N; (b) 50 N.

7.3.2 *Unilateral System*

In the next experiment, the SMC force controller is applied to an impedance control loop as shown in Figure 7-2 to track a desired position trajectory given by the master actuator. To observe the position tracking performance of the proposed controller, no external force is first applied to the slave actuator. The parameters of the impedance model shown in Figure 7-2 were set as $M = 1$ Kg, $B = 20$ Ns/m and $K = 3000$ N/m. Figure 7-8 shows the results. From Figure 7-8(a), it is obvious that the impedance control method tracked the desired position successfully. The position error during the experiment, as shown in Figure 7-8(b), is always less

than 0.02 m, which is possibly caused by the notable dry friction of the pneumatic actuator. The control signal in Figure 7-8(c) is bounded and not saturated.

(a)

(b)

(c)
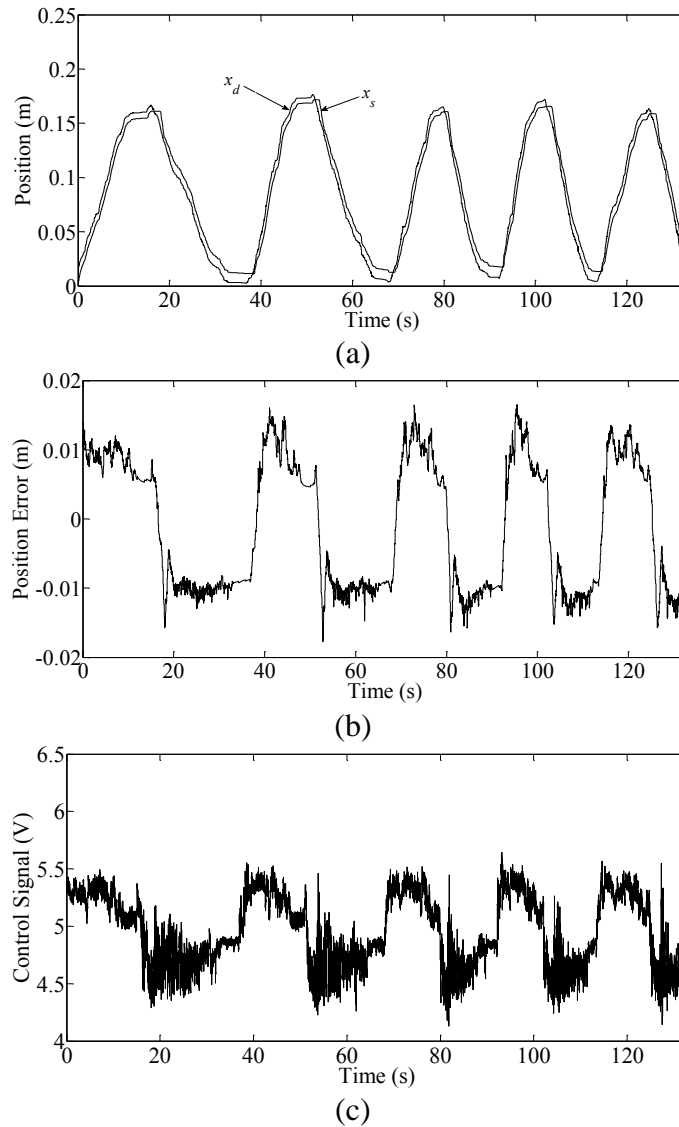
Figure 7-8. Experimental study of motion tracking in the absence of external force by impedance control: (a) position tracking; (b) position error; (c) control signal.

In the next experiment, a human subject applied an external force of 10 N magnitude to the slave actuator through an attached handle. A desired position trajectory, x_d, was given by the master actuator. The parameters of the impedance model are similar to those in the previous experiment. Figure 7-9 shows the positions of the master and the slave. One can observe a

reasonable position tracking in Figure 7-9(a). Further, at the instant of force exertion, the position of the slave actuator is adjusted according to the force.
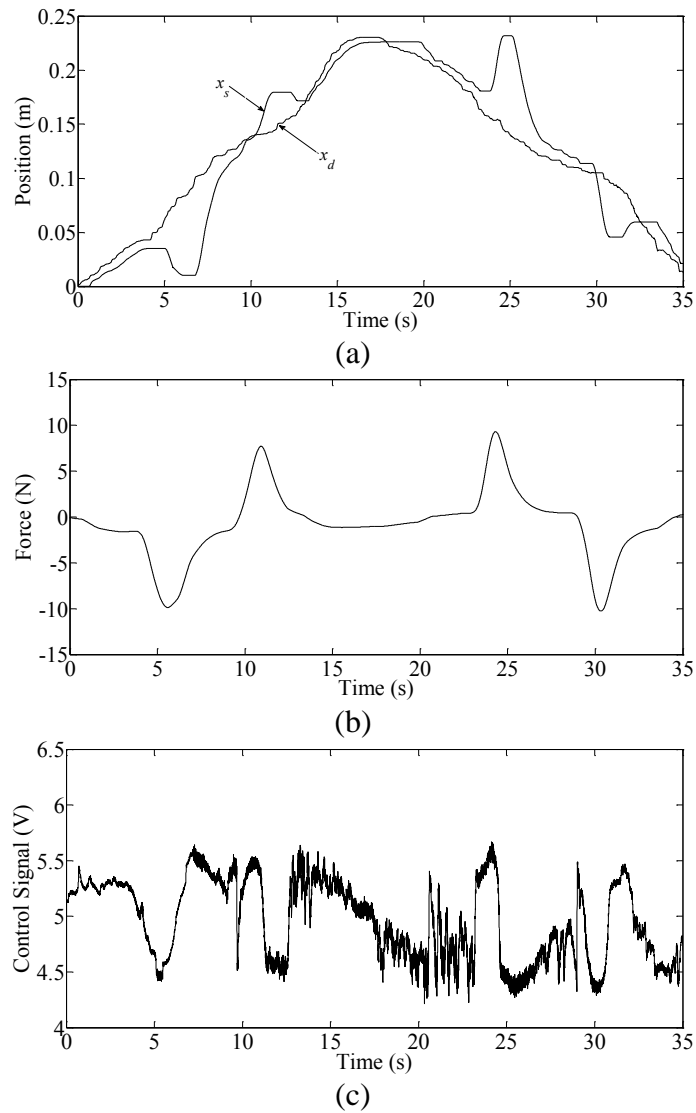
Figure 7-9. Experimental study of low stiffness impedance model: (a) position tracking; (b) external force; (c) control signal.

In the last experiment, the parameters of the impedance model are set to $M = 1 \text{ Kg}, B = 20 \text{ Ns/m}$ and $K = 5000 \text{ N/m}$. As shown in Figure 7-10(a), the slave actuator was moved by 0.03 m in reaction to a 50 N force, whereas in Figure 7-9(a) the same displacement is observed for a force of 10 N. This shows that the impedance model provided higher stiffness as a result of

increasing the value of K. The above experiments prove that the proposed impedance control can successfully control the position given by a hand-controller and at the same time incorporate the external force. Repeatability of the experimental results are confirmed by conducting more experiments.
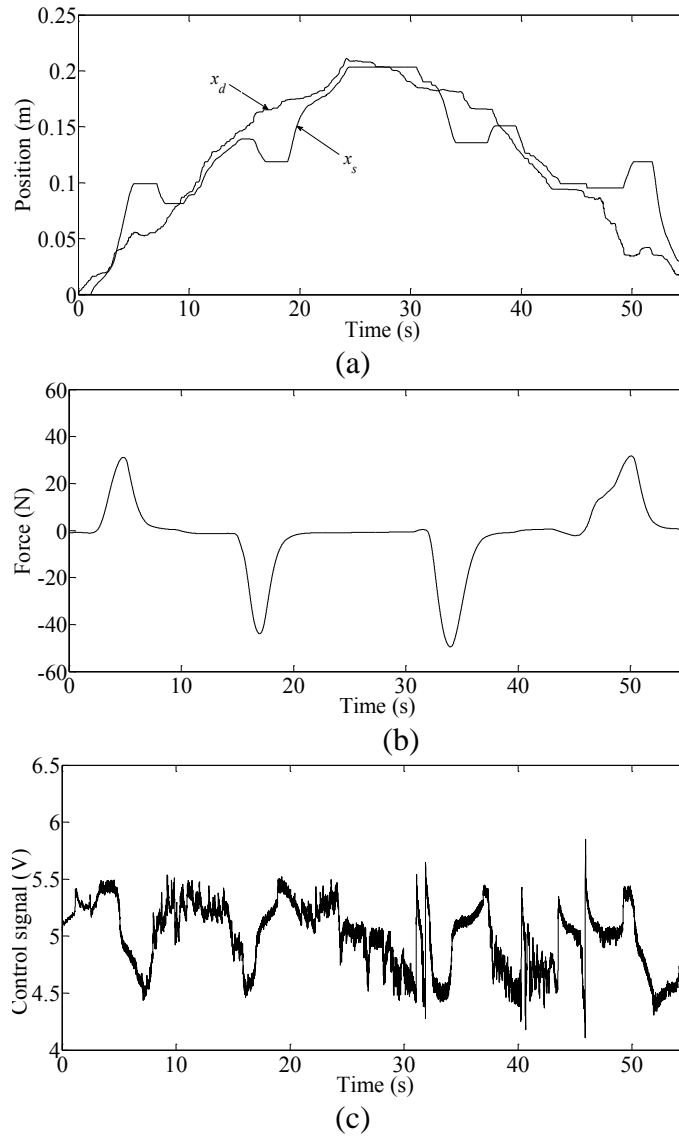
Figure 7-10. Experimental study of high stiffness behavior of impedance model: (a) position tracking; (b) external force; (c) control signal.

The above experiments were repeated to assure repeatability of the control system. Similar to the last chapter, a statistical study is conducted for unilateral impedance control using the average and maximum force tracking error of the experiments. The mentioned force errors are summarized in Table 7-5 and, the frequency distribution is derived accordingly and presented in Table 7-6. It is evident that the force errors are mostly in $5 < \bar{e}_f \leq 10$ range. The maximum force error is $30 < \bar{e}_f \leq 40$ range mostly caused by static friction force. All experiments show successful position tracking while dealing with the external force. Referring to the scatter plots shown in Figure 7-11, one can observe that the experimental results are convergent.

Table 7-5. The average and maximum force error of the unilateral impedance control experiments.

Experiment No.	Avg. Force Error (N)	Max. Position Error (N)
1	9.2	42
2	8.3	38
3	8.5	42
4	12	38
5	3.8	18
6	4.7	38
7 (Figure 7-9)	6.8	44
8 (Figure 7-10)	4.3	38

Table 7-6. Frequency distribution table of the average and maximum force error of the unilateral impedance control experiments.

Avg. Force error, $\bar{e}_f$ (N)	Number	Percentage
$\bar{e}_f \leq 2$	0	0.0%
$2 < \bar{e}_f \leq 5$	3	37.5%
$5 < \bar{e}_f \leq 10$	4	50.0%
$10 < \bar{e}_f \leq 20$	1	12.5%
$\bar{e}_f > 20$	0	0.0%

Max. Force Error , $\widehat{e}_f$ (N)	Number	Percentage
$\bar{e}_f \leq 10$	0	0.0%
$10 < \bar{e}_f \leq 20$	1	12.5%
$20 < \bar{e}_f \leq 30$	0	0.0%
$30 < \bar{e}_f \leq 40$	4	50.0%
$\bar{e}_f > 40$	3	37.5%

(a)

(b)
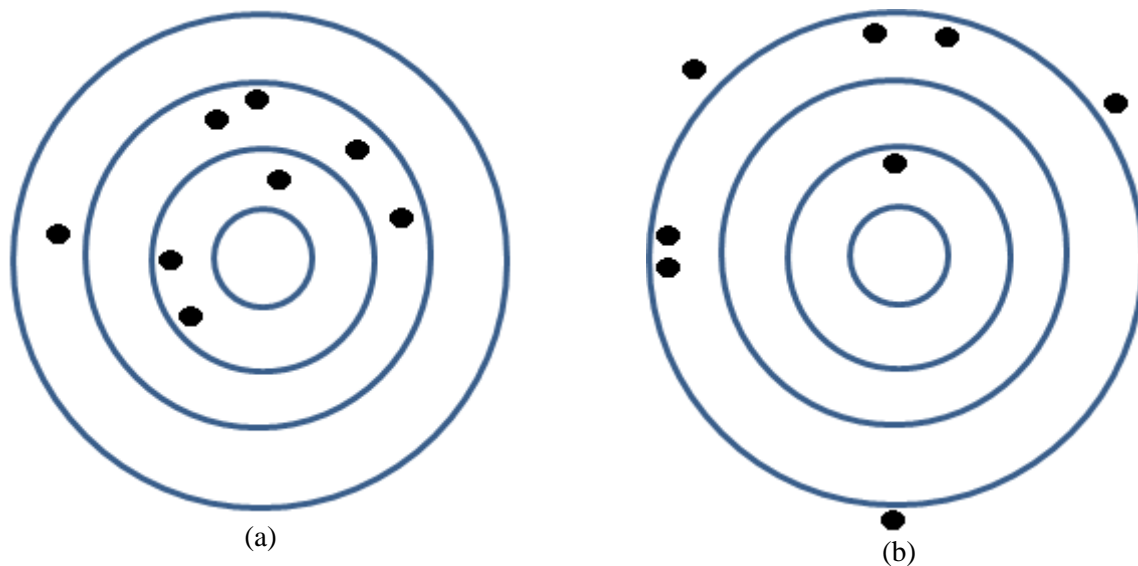
Figure 7-11. Scatter plot of average and maximum force error of the unilateral impedance control experiments.

7.4   Summary

In this chapter, a unilateral pneumatic system was developed, analyzed, and implemented employing an impedance control scheme. The goal was to develop a teleoperation system which, independent of the human operator, is capable of providing position tracking and simultaneously handling the external force at the slave side. The impedance control provided a combination of the external force and the desired position given by a hand-controller as the desired force to the sliding mode controller. The performance of the impedance unilateral teleoperation system was experimentally evaluated with different parameter settings. Simulation and experimental studies showed satisfactory performance of the proposed pneumatic unilateral system in position tracking and handling the external force. Stability analysis of the proposed control system was also conducted using the concept of Lyapunov exponents for an autonomous and a non-autonomous system. Parametric stability analysis showed that the controller gain has a notable effect on the stability of the teleoperation system.

8. BILATERAL CONTROL OF PNEUMATIC ACTUATORS[1]

This chapter presents the design, implementation and stability analysis of a bilateral teleoperation pneumatic actuation system whereby a low-cost pneumatic actuator, described in Chapter 3, is navigated by an operator using a commercially-available haptic device. The actuator is subject to an external force. As opposed to unilateral teleoperation, which was discussed in previous chapters, the value of the external force is scaled and rendered on the haptic device by the built-in controller in order to provide the operator with a feeling of the interaction at the remote site. As a result, the slave actuator does not need to deal with the external force but the operator should manually deal with the external force by changing the admittance of his hand. Figure 8-1 shows the schematic diagram of the bilateral pneumatic system.

---

[1] This chapter is built based on a published paper [81].
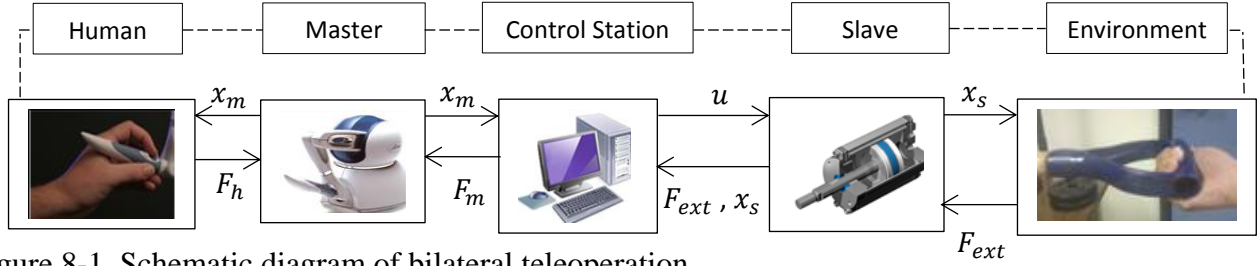
Figure 8-1. Schematic diagram of bilateral teleoperation.

8.1 Simulation Studies and Stability Analysis

Stability analysis of an autonomous and a non-autonomous bilateral teleoperation system including the dynamic of the operator's hand is presented. As mentioned before, autonomous and non-autonomous systems were studied separately because by including time in the equations, an extra state space variable should be defined.

8.1.1 Autonomous bilateral system

Simulation studies

Simulation studies are done to provide a better understanding of the performance of the teleoperation system described above. Figure 8-1 shows that the bilateral system has two inputs: the force of the operator's hand imposed to the master, F_h, and the external force imposed to the slave from the environment, F_{ext}. The environment is assumed to be spring-dominant in the simulation; thus, F_{ext} will be proportional to the displacement of the slave:

$$F_{ext} = -K_{ext} x_s \ ,$$

(8-1)

where K_{ext} is the stiffness coefficient of the environment. The system has two control signals. The first control signal is the force applied to the operator's hand by the master manipulator, F_m; its value is determined by the following equation:

$$F_m = K_{fs} F_{ext} \ ,$$

(8-2)

where K_{fs} is a scaling factor. The second control signal, u, positions the slave manipulator using the SMC scheme; its value is determined by equation (5-13).

96

Figure 8-2 shows the simulation results at the master side. The force of the operator`s hand, F_h, is considered to be constant and equal to 1 N as shown in Figure 8-2(a). As the results show, by this value of F_h, x_m is almost 0.1 m which is more or less equal to x_m in the simulation of Chapter 6. K_{fs} is considered 0.01; i.e. for 100 N of external force, the master generates 1 N force (the maximum force this particular haptic device generates is 3 N). Similar to the previous chapters, $K_{ext} = 100$ N/m. The force applied to the operator`s hand is shown in Figure 8-2(b). The displacement of the master manipulator caused by the combination of F_h and F_m is shown in Figure 8-2(c). Figure 8-2 (d) shows the external force.
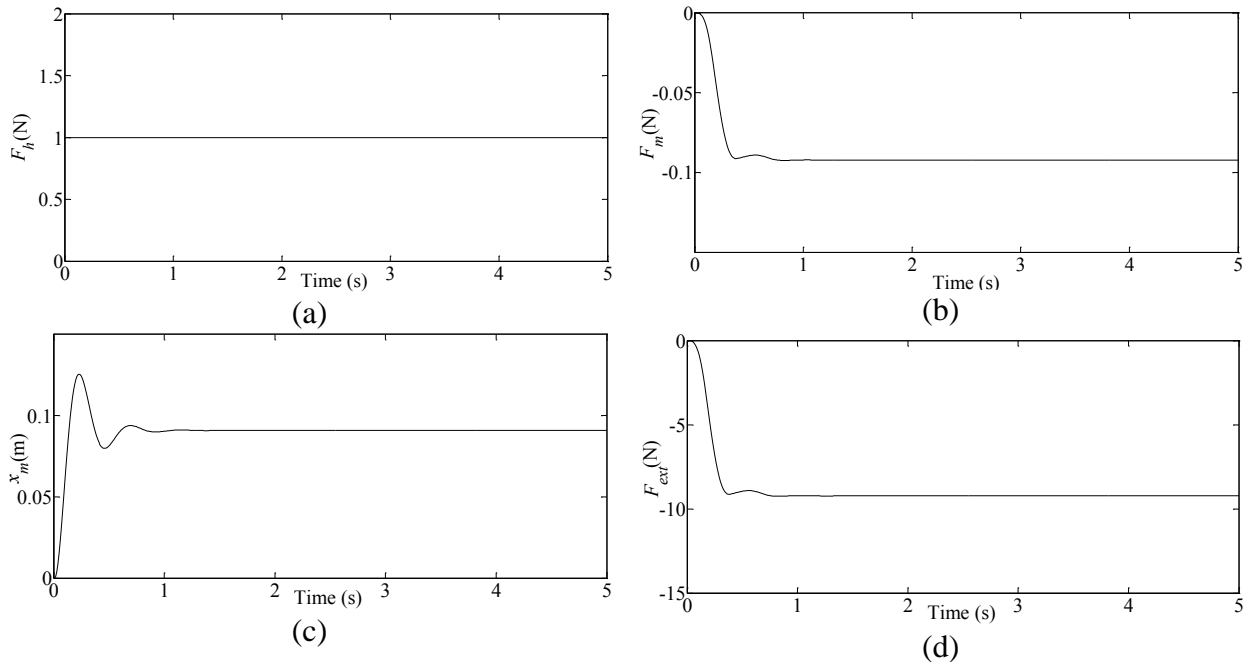
Figure 8-2. Simulation results of bilateral step tracking task: (a) force of operator`s hand; (b) force of the master manipulator; (c) displacement of the master manipulator; (d) external force.

Figure 8-3 shows the simulation results of the variables corresponding to the slave manipulator. Despite the controller gains of SMC in Chapter 6 ($\delta = 80$ s^{-1} and $K_{rb} = 2000$ m/s^3), δ is set to 60 s^{-1}, and $K_{rb} = 3000$m/s^3. The reason is to give more weight to the robust part of SMC than to the equivalent part in order to handle the uncertainties caused by

rendering the external force to the master actuator. It is seen in Figure 8-3(a) that the slave reasonably follows the motion of the master and handles the external force fairly well. The position error in Figure 8-3(b) converges to zero as a result of the integral part of SMC. The chattering observed in x_s is caused by the robust part of SMC. The air pressure in each chamber is shown in Figure 8-3(c). Figure 8-3(d) shows the control signal. The simulation shows that the entire bilateral system is stable and acts fast.
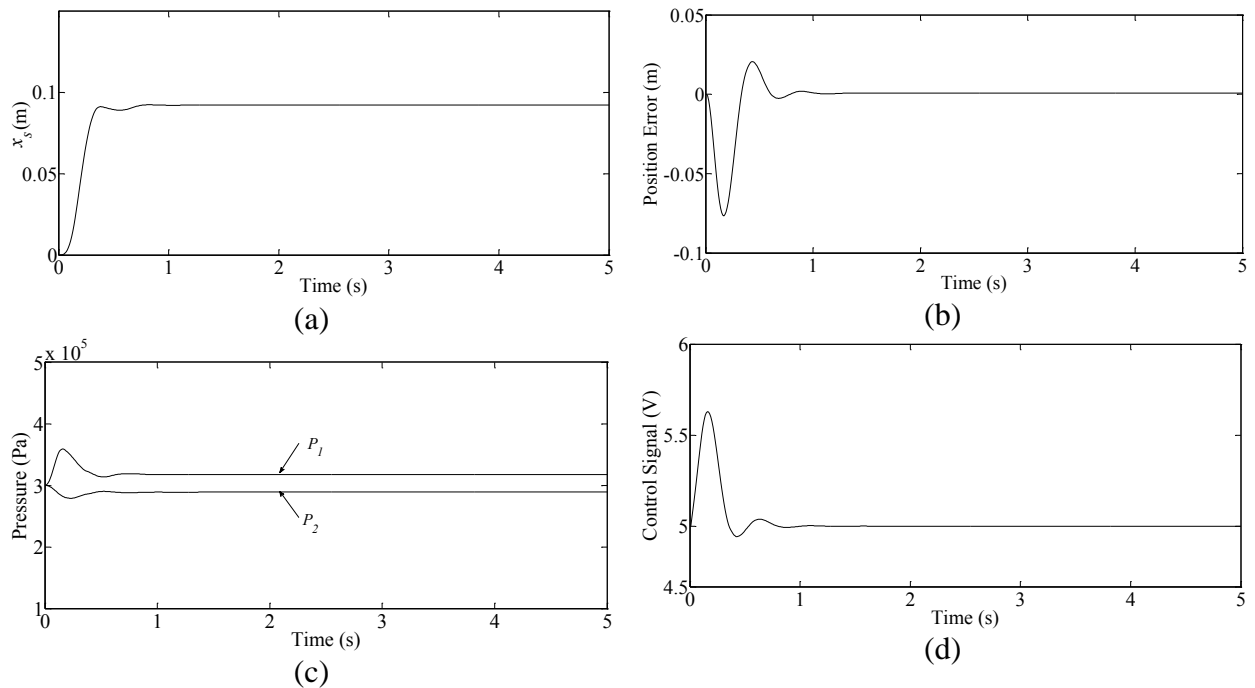
Figure 8-3. Simulation results of bilateral step tracking task: (a) displacement of the slave manipulator; (b) tracking error between master and slave, $e = x_s - x_m$; (c) chamber pressures; (d) control signal.

Calculation of Lyapunov exponents

The stability of the bilateral system is now studied through the use of the concept of the Lyapunov exponent. For this reason, the state space model of an autonomous bilateral pneumatic system is formed by defining the state space vector as:

$$\vec{x} = [x_1 \ x_2 \ x_3 \ x_4 \ x_5 \ x_6 \ x_7 \ x_8 \ x_9]^T = [x_s \ \dot{x}_s \ P_1 \ P_2 \ x_v \ z \ \int_0^t e\, d\tau \ e \ \dot{e}]^T \quad (8\text{-}3)$$

where x_s is the displacement of the slave, $\dot{x}_s$ is the velocity of the slave, P_1 and P_2 are air pressures, x_v is the displacement of the spool and z is the average bristle deflection in the friction model. e, is the position error:

$$e = x_s - x_m \ , \quad (8\text{-}4)$$

where x_m is the desired position of the slave actuator, which is equal to the position of the master actuator. Considering equations (8-3) and (8-4), one can see

$$x_m = x_1 + x_8 \ . \quad (8\text{-}5)$$

The dynamics of the master and slave and operator's hand are formulated in Equations (3-1) to (3-12). Using the state variables in (8-3) and combining (3-1) to (3-12), (8-1) to (8-5) and (4-12), the state space model is constructed as:

$$
\begin{cases}
\dot{x}_1 = x_2 \\
\dot{x}_2 = \dfrac{1}{m_p}\left[A(x_3 - x_4) - K_{ext}x_1 - \left(\sigma_0 x_6 + \sigma_1\left(x_2 - \dfrac{\sigma_0|x_2|x_6}{F_c + (F_s - F_c)e^{-(x_2/vs)^2}}\right) + bx_2\right)\right] \\
\dot{x}_3 = +\gamma RT \dfrac{wx_5\, \dot{\emptyset}_1}{V_0 + Ax_1} - \dfrac{\alpha\gamma Ax_2 x_3}{V_0 + Ax_1} \\
\dot{x}_4 = -\gamma RT \dfrac{wx_5\, \dot{\emptyset}_2}{V_0 + A(L - x_1)} + \dfrac{\alpha\gamma Ax_2 x_4}{V_0 + A(L - x_1)} \\
\dot{x}_5 = \dfrac{1}{\tau}(-x_5 + K_v u) \\
\dot{x}_6 = x_2 - \dfrac{\sigma_0|x_2|x_6}{F_c + (F_s - F_c)e^{-(x_2/v_{sv})^2}} \\
\dot{x}_7 = x_8 \\
\dot{x}_8 = x_9 \\
\dot{x}_9 = \dfrac{A(x_3 - x_4)}{M} - \dfrac{(K_{ext}x_1 + F_f + bx_2)}{M} - \dfrac{(F_h - K_{fs}K_{ext}x_1)}{m_m} \\
\qquad + \dfrac{b_m(x_2 - x_9)}{m_m} + \dfrac{k_m(x_1 - x_8)}{m_m}
\end{cases}
\quad (8\text{-}6)
$$

The dry friction is expressed in the state space as follows:

$$F_f = \sigma_0 x_6 + \sigma_1 x_2 - \frac{\sigma_0 \sigma_1 |x_2| x_6}{F_c + (F_s - F_c)e^{-(x_2/v_{sv})^2}} \quad . \tag{8-7}$$

The control signal in the state space model is defined as:

$$u = \frac{\ddot{x}_m - \delta^3 x_8 - 3\delta^2 x_9 - 3\delta\ddot{e} - Fx}{w K_v P x} + \frac{-K_{rb}\tanh{(aS)}}{w K_v P x} \quad . \tag{8-8}$$

The associated variables in (8-6) are:

$$\ddot{x}_m = \frac{-K_{fs}K_{ext}}{m_m}x_2 - \frac{b_m}{m_m^2}(F_h - K_{fs}K_{ext}x_1) + \left(\frac{b_m^2}{m_m^2} - \frac{k_m}{m_m}\right)(x_2 - x_9) + \frac{b_m k_m (x_1 - x_8)}{m_m^2} \quad , \tag{8-9}$$

$$\ddot{e} = \frac{A}{M}(x_3 - x_4) - \frac{1}{M}\left(F_f + Bx_2\right) + K_{ext}\left(\frac{K_{fs}}{m_m} - \frac{1}{M}\right)x_1 + \frac{b_m}{m_m}(x_2 - x_9) + \frac{k_m}{m_m}(x_1$$
$$- x_8) - \frac{F_h}{m_m} \quad , \tag{8-10}$$

$$Fx = -\frac{\alpha\gamma A^2}{M}\left(\frac{x_3}{V_0 + Ax_1} + \frac{x_4}{V_0 + A(L - x_1)}\right)x_2 - \frac{K_{ext}}{M}x_2$$
$$- \frac{B}{M^2}\left(A(x_3 - x_4) - K_{ext}x_1 - Bx_2 - F_f\right) \quad . \tag{8-11}$$

The other variables are defined in Chapter 6. The initial condition of (8-6) is:

$$\vec{x}_0 = [0, 0, 3 \times 10^5, 3 \times 10^5, 0, 0, 0, 0, 0]^T \quad . \tag{8-12}$$

The basin of attraction of (8-6) satisfies the following equation:

$$\begin{cases} x_2{}^{ss} = x_5{}^{ss} = x_7{}^{ss} = x_8{}^{ss} = x_9{}^{ss} = 0 \\ x_1{}^{ss} = \dfrac{F_h}{K_{ext}K_{fs} + K_m} \\ A(x_3{}^{ss} - x_4{}^{ss}) - K_{ext}x_1{}^{ss} - \sigma_0 x_6{}^{ss} = 0 \end{cases} \quad . \tag{8-13}$$

The Lyapunov exponents for the bilateral pneumatic system are calculated. The calculation was continued for 5000 seconds to find the final values of the Lyapunov exponents which are given in Table 8-1.

Table 8-1. Numerical results of LEs for autonomous bilateral teleoperation.

	λ_1	λ_2	λ_3	λ_4	λ_5	λ_6	λ_7	λ_8	λ_9
(s^{-1})	0.0	0.0	-0.1	-0.1	-5.3	-5.4	-46.2	-46.3	-228.6

To get a better understanding of the values of Table 8-1, (8-13) is revisited. The system has a set of equilibrium points where $x_1{}^{ss}$, $x_2{}^{ss}$, $x_5{}^{ss}$, $x_7{}^{ss}$, $x_8{}^{ss}$ and $x_9{}^{ss}$ will eventually have fixed values as time grows. However, a combination of $x_3{}^{ss}$, $x_4{}^{ss}$ and $x_6{}^{ss}$ must satisfy the following equation:

$$A(x_3{}^{ss} - x_4{}^{ss}) - K_{ext}x_1{}^{ss} - \sigma_0 x_6{}^{ss} = 0 \ . \tag{8-14}$$

Having three unknowns $(x_3{}^{ss}, x_4{}^{ss}, x_6{}^{ss})$ and one equation in (8-13), the solution of (8-13) is a two-dimensional plane. Therefore, the basin of attraction of equation (8-6) is two-dimensional. This fact justifies the two zero LEs observed in Table 8-1, since the number of zeros should be equal to the number of the dimension of the basin attraction [53, 47]. The values of the LEs in Table 8-1 clearly prove the entire control system is Lyapunov stable despite the friction, external force, chattering and replacement of non-smooth "sign" functions with smooth hyperbolic tangent functions.

Parametric Stability Analysis

Parametric stability analysis is done for the teleoperation system discussed in this chapter. Table 8-2 shows that the bilateral system is stable as K_{ext} varies between 10 N/m to 600 N/m. Table 8-3 shows the LEs of the bilateral teleoperation as controller gain changes. For $\delta = 20\ \mathrm{s}^{-1}$, the system has a positive LE, which means it is chaotic.

Table 8-2. Numerical results of LEs for bilateral teleoperation as K_{ext} varies.

K_{ext}(N/m)	$\lambda_1(s^{-1})$	$\lambda_2(s^{-1})$	$\lambda_3(s^{-1})$	$\lambda_4(s^{-1})$	$\lambda_5(s^{-1})$	$\lambda_6(s^{-1})$	$\lambda_7(s^{-1})$	$\lambda_8(s^{-1})$	$\lambda_9(s^{-1})$
10	0.0	0.0	-0.1	-0.1	-5.3	-5.3	-46.1	-46.1	-228.5
50	0.0	0.0	-0.1	-0.1	-5.3	-5.3	-46.1	-46.1	-228.5
100	0.0	0.0	-0.1	-0.1	-5.3	-5.3	-45.8	-45.8	-228.5
150	0.0	0.0	-0.1	-0.1	-5.3	-5.3	-46.0	-46.0	-228.5
200	0.0	0.0	-0.1	-0.1	-5.3	-5.3	-46.0	-46.0	-228.5
300	0.0	0.0	-0.1	-0.1	-5.3	-5.3	-46.0	-46.0	-228.5
600	0.0	0	-0.1	-0.1	-5.3	-5.3	-45.8	-45.8	-228.5

Table 8-3. Numerical results of LEs for bilateral teleoperation as δ varies.

δ (s^{-1})	$\lambda_1(s^{-1})$	$\lambda_2(s^{-1})$	$\lambda_3(s^{-1})$	$\lambda_4(s^{-1})$	$\lambda_5(s^{-1})$	$\lambda_6(s^{-1})$	$\lambda_7(s^{-1})$	$\lambda_8(s^{-1})$	$\lambda_9(s^{-1})$
20	59.2	0	0	-0.1	-2.4	-5.3	-16.4	-30.6	-228.6
30	0.0	0.0	-0.1	-1.6	-4.5	-5.3	-21.1	-23.5	-228.5
40	0.0	0.0	-0.1	-0.7	-5.3	-5.3	-31.6	-31.6	-228.5
60	0.0	0.0	-0.1	-0.1	-5.3	-5.3	-45.8	-45.8	-228.5
80	0.0	0.0	-0.1	-0.1	-5.3	-5.3	-46.0	-46.0	-228.5
100	0.0	0.0	-0.1	-0.1	-5.3	-5.3	-46.0	-46.0	-228.5
120	0.0	0.0	-0.1	-0.1	-5.3	-5.3	-46.0	-46.0	-228.5
140	0.0	0.0	-0.1	-0.1	-5.3	-5.3	-46.1	-46.1	-228.5

8.1.2   Non-autonomous bilateral system

Simulation Studies

The performance of the bilateral system in a non-autonomous environment is presented through simulation. Figure 8-4 shows the simulation results at the master side. Similar to non-autonomous systems in previous chapters, the force of the operator`s hand and external force, Figure 8-4(a) and Figure 8-4(d), are defined as follows:

$$F_h(t) = 1.5 + 0.8\sin(0.05t + 1.5\pi) \ , \tag{8-15}$$

$$F_{ext}(t) = 30\sin(0.5t) \ . \tag{8-16}$$

To make the simulation comparable to the simulation in the previous chapters, the gains in (8-15) are chosen in a way that x_m is similar to x_d in Figure 6-5(d). This definition is similar to previous chapters. Displacement of the master is shown in Figure 8-4(c) which is achieved from

(3-1). The force of the master actuator to the operator`s hand, Figure 8-4(b), is proportional to the external force.

$$F_m(t) = K_{fs}F_{ext}(t) \ . \tag{8-17}$$

Figure 8-5 shows the results at the slave side. K_{fs} in (8-17) is considered 0.02. Figure 8-5(a) and Figure 8-5 (b) show the displacement of the slave and the position error. It is evident that the slave successfully follows the movement of the master. Figure 8-5(c) shows the air pressure in slave chambers. The control signal of SMC is shown in Figure 8-5(d) and is unsaturated and bounded.

(a) (b) (c) (d)
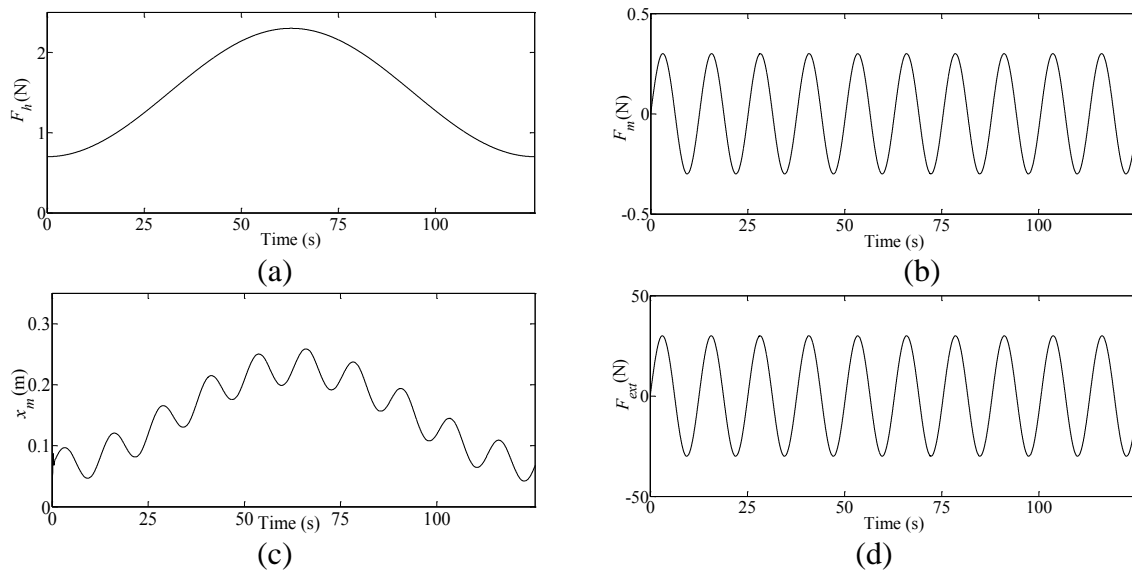
Figure 8-4. Simulation result for bilateral sinusoidal tracking task: (a) force of operator's hand, F_h; (b) haptic force, F_m; (c) displacement of the master, x_m; (d) external force F_{ext}.
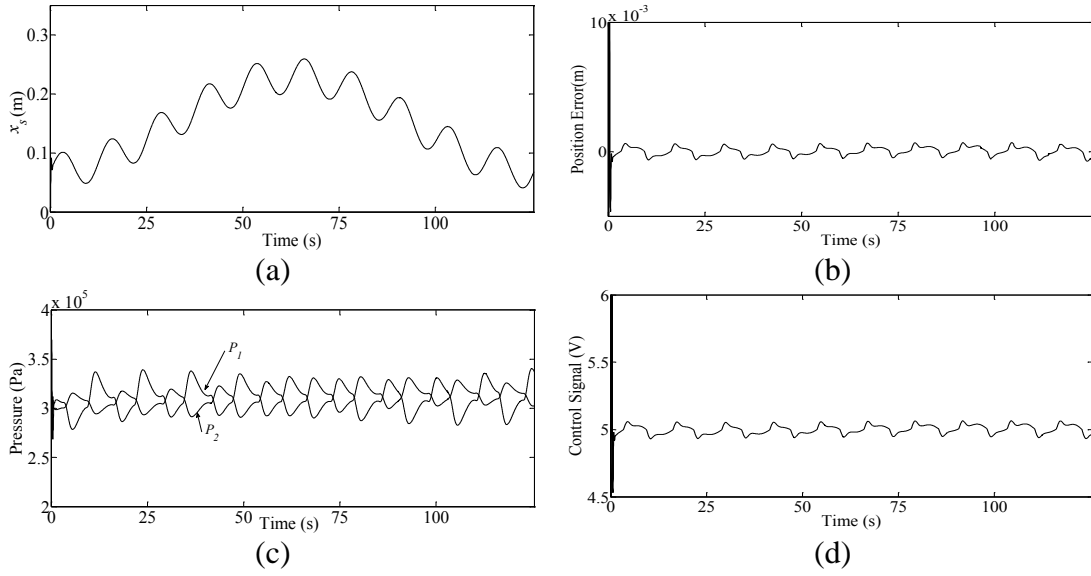
Figure 8-5. Simulation result for bilateral sinusoidal tracking task: (a) displacement of the slave, x_s; (b) position error; (c) pressure of chambers; (d) control signal.

Calculation of Lyapunov exponents

The stability analysis is conducted for the non-autonomous bilateral system by adding a variable to (8-6) corresponding to time. The state space variables are defined as:

$$\vec{x} = [x_1 \quad x_2 \quad x_3 \quad x_4 \quad x_5 \quad x_6 \quad x_7 \quad x_8 \quad x_9 \quad x_{10}]^T$$

$$= [t \quad x_s \quad \dot{x}_s \quad P_1 \quad P_2 \quad x_v \quad z \quad \int_0^t e \, d\tau \quad e \quad \dot{e}\,]^T \qquad (8\text{-}18)$$

The dynamic system in (8-6) is rewritten as:

104

$$\begin{cases} \dot{x}_1 = 1 \\[4pt] \dot{x}_2 = x_3 \\[4pt] \dot{x}_3 = \dfrac{1}{m_p}\big[A(x_4 - x_5)+F_{ext} - F_f - bx_3\big] \\[6pt] \dot{x}_4 = +\gamma RT\dfrac{wx_6\,\dot{\emptyset}_1}{V_0 + Ax_2} - \dfrac{\alpha\gamma Ax_3 x_4}{V_0 + Ax_2} \\[8pt] \dot{x}_5 = -\gamma RT\dfrac{wx_6\,\dot{\emptyset}_2}{V_0 + A(L - x_2)} + \dfrac{\alpha\gamma Ax_3 x_5}{V_0 + A(L - x_2)} \\[8pt] \dot{x}_6 = \dfrac{1}{\tau}(-x_6 + K_v u) \\[6pt] \dot{x}_7 = x_3 - \dfrac{\sigma_0|x_3|x_7}{F_c + (F_s - F_c)e^{-(x_3/v_{sv})^2}} \\[8pt] \dot{x}_8 = x_9 \\[4pt] \dot{x}_9 = x_{10} \\[4pt] \dot{x}_{10} = \dfrac{A}{m_p}(x_4 - x_5) - \dfrac{1}{m_p}\big(-F_{ext} + F_f + bx_3\big) - \dfrac{1}{m_m}\big(F_h + K_{fs}F_{ext}\big) \\[8pt] \qquad\quad + \dfrac{b_m}{m_m}(x_3 - x_{10}) + \dfrac{k_m}{m_m}(x_2 - x_9) \end{cases} \qquad , \qquad (8\text{-}19)$$

where

$$F_h = 1.5 + 0.8\sin(0.05x_{10} + 1.5\pi) \ , \qquad (8\text{-}20)$$

$$F_{ext} = 30\sin(0.5x_{10}) \ . \qquad (8\text{-}21)$$

The other variables in (8-19) are defined in 7.1.1.2. The parameters are similar to 7.1.1.1. Because the system is non-autonomous, there is not a certain equilibrium point. The final numerical values of Lyapunov exponents are shown in Table 8-4. With all exponents being negative or zero, one can conclude that the system does not show chaotic behavior and satisfies Lyapunov stability.

Table 8-4. Numerical values of LEs for non-autonomous bilateral teleoperation.

	λ_1	λ_2	λ_3	λ_4	λ_5	λ_6	λ_7	λ_8	λ_9	λ_{10}
(s^{-1})	0.0	0.0	0.0	-0.1	-0.1	-4.3	-5.4	-30.7	-35.1	-228.6

8.2   Experimental Results

Experiments were conducted to study the performance of the bilateral pneumatic system. In the first experiment, the master manipulator was moved periodically and the slave manipulator followed this movement. A spring was mounted in front of the slave manipulator to generate an external force proportional to actuator displacement. The stiffness of the spring was approximately 1.2 kN/m. The experiment started by moving the actuator in free space, then making contact with the spring and applying a force. This is done to examine the performance of the system in the transition between the two states. Figure 8-6(a) shows the displacement of the master and the slave manipulators in the presence of the external force that is shown in Figure 8-6(b). Figure 8-6(c) shows an adequate tracking quality. The control signal generated by SMC, and shown in Figure 8-6(d), is unsaturated and bounded. The chattering of the control signal is due to the robust part of the SMC. As mentioned before, the control signal varies between 0 V and 10 V; a 5 V control signal corresponds to the valve being in the neutral (closed) position.

A similar bilateral tracking task was repeated with a spring of 10 kN/m stiffness. Figure 8-7(a) shows the displacement of the master and the slave manipulators. The external force was higher than the previous experiment as shown in Figure 8-7(b). The external force was rendered to the operator`s hand, which provided a feeling of the distant environment. Subsequently, the operator could decide to move the haptic device further. It is worthy to note that the maximum external force should not be more than the maximum force of the actuator, which is equal to $A(P_s - P_a) = 440$ N. The control signal is shown in Figure 8-7(d). This experiment shows that the bilateral system maintains the performance in dealing with the stiff environment. Because the maximum force of the haptic device is 3 N, K_{fs} was considered 0.005 in this experiment.
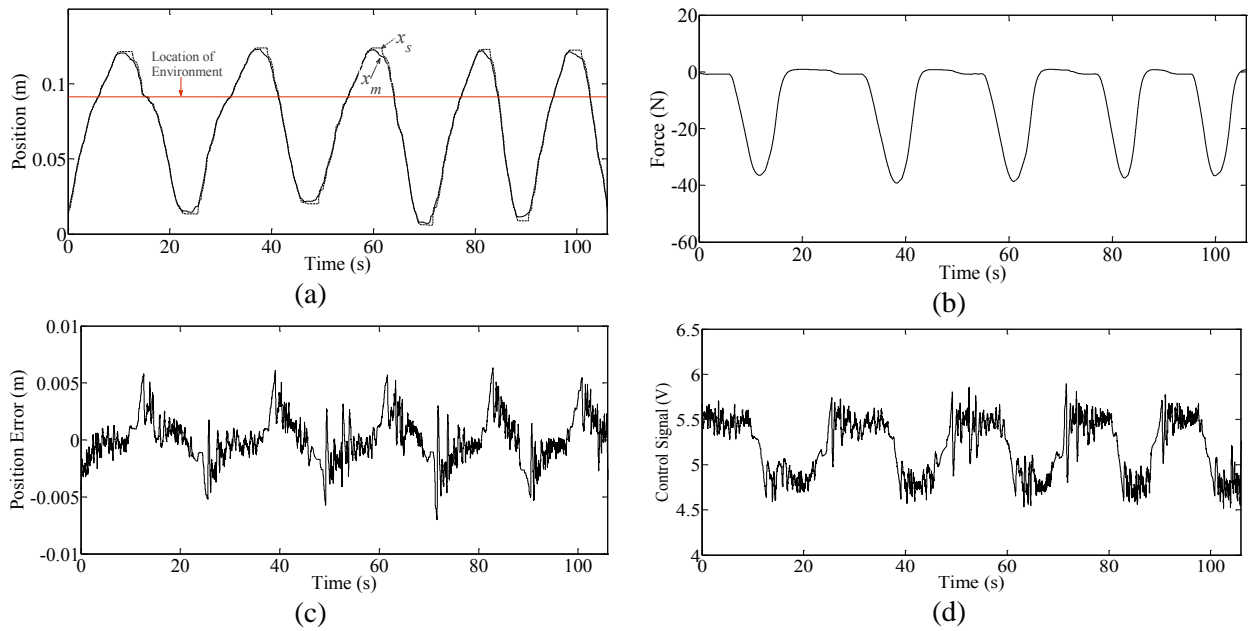
Figure 8-6. Experimental results of periodic tracking while interacting with a soft spring: (a) tracking response; (b) external force; (c) position error between master and slave; (d) control signal applied to the slave manipulator.
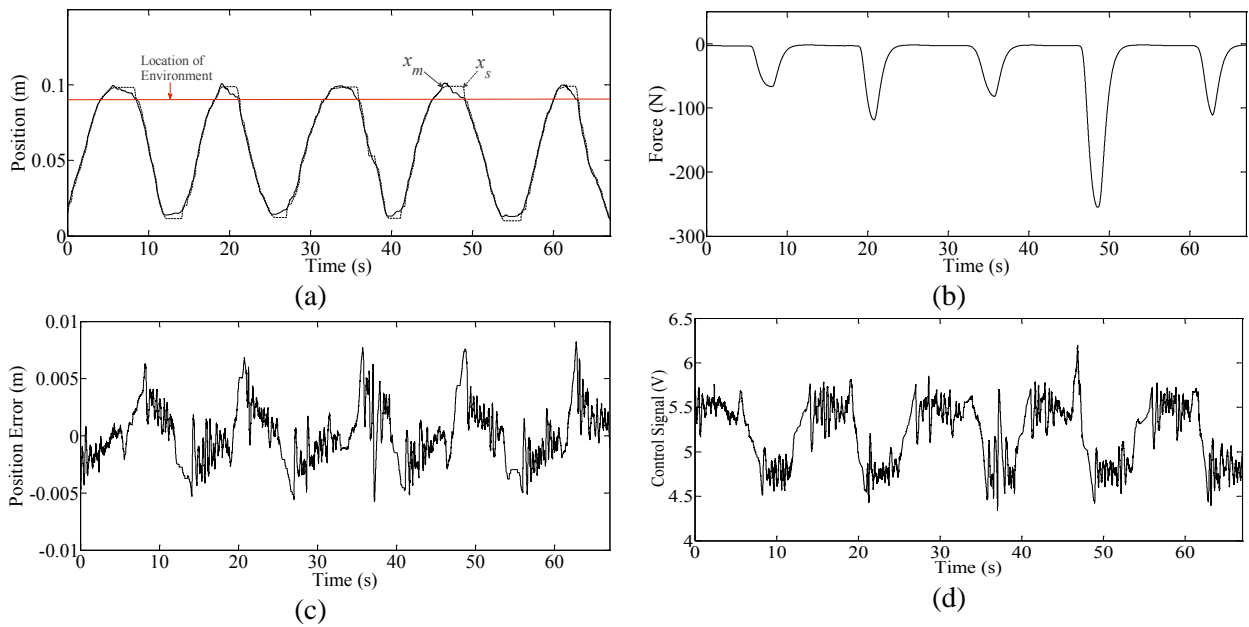
Figure 8-7. Experimental results of periodic tracking while interacting with a stiff spring: (a) tracking response; (b) external force; (c) position error between master and slave; (d) control signal to the slave manipulator.

In the next experiment, the slave was subject to a variable external force. Figure 8-8(a) shows the position tracking of the master and the slave. As shown in Figure 8-8(b), the external force with the maximum magnitude of 70 N was repeatedly imposed to the slave by a human in both resistive and assistive directions. Figure 8-8(d) shows the control signal. These experiments further confirm that the proposed bilateral pneumatic system works stably for various tracking tasks and different external force profiles. Performance of the system is assured by doing more experiments on bilateral teleoperation with different external force and desired position trajectory.

(a)   (b)

(c)   (d)
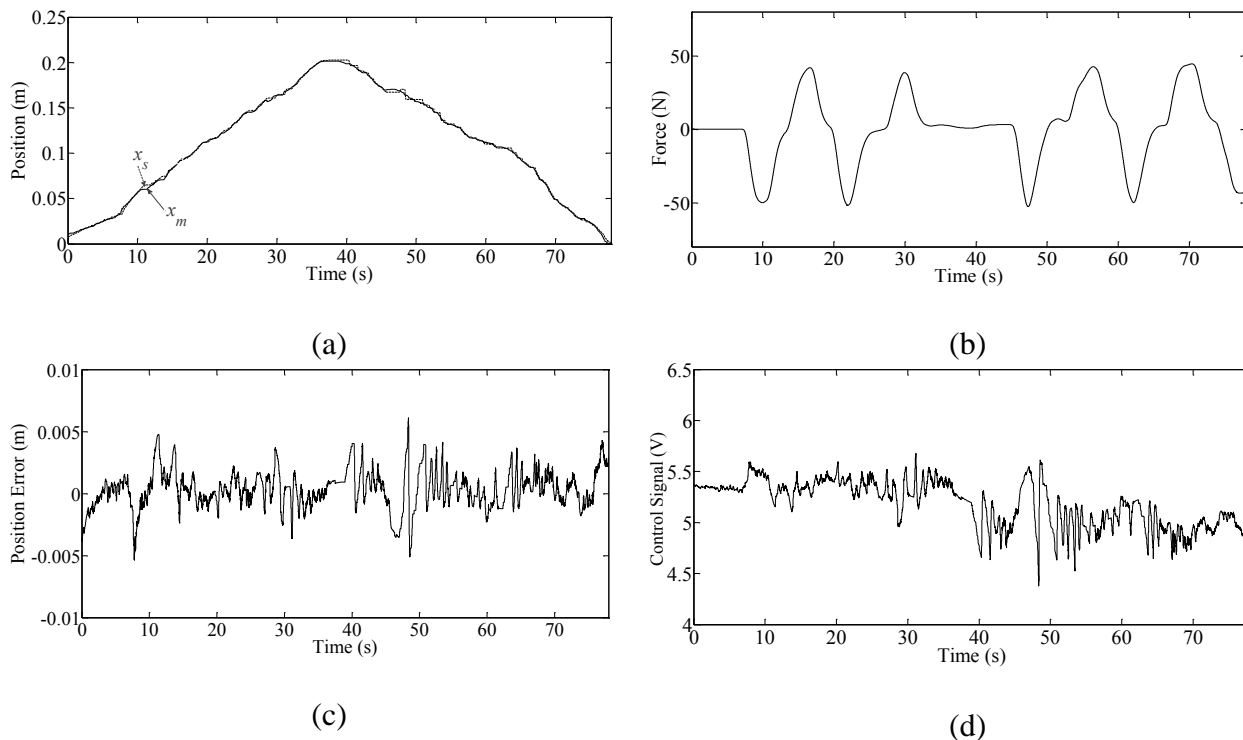
Figure 8-8. Experimental results of haptic-navigated tracking task while interacting with an arbitrary resistive-assistive external force applied to the actuator: (a) tracking response; (b) external force; (c) position error between master and slave; (d) control signal to the slave manipulator.

Similar to unilateral control methods, additional bilateral teleoperation experiments are conducted. The goal is to verify the repeatability of the performance of the experiment presented in Figure 8-8. Table 8-5 shows the average and maximum position error of all bilateral teleoperation experiments conducted for this purpose. The frequency distribution, shown in Table 8-6 states that the average position errors are mostly equal or less than 2 mm. It shows that most of the maximum position errors are in $5 < \widetilde{e} \leq 10$, caused by static friction. Figure 8-9 shows this information on a scatter plot. one can conclude that the experimental results are matching.

Table 8-5. The average and maximum position error of the

bilateral teleoperation experiments.

Experiment No.	Avg. Position error (mm)	Max. Position Error (mm)
1	3.5	20
2	2.6	6
3	3.0	12
4	1	5
5	1.6	5
6	2.4	7
7	1.8	6
8	2.1	7
9	1.8	8
10 (Figure 8-8)	1.2	6

Table 8-6. Frequency distribution table of the average and maximum position error of the bilateral

teleoperation experiments.

Avg. Position error, $\bar{e}$ (mm)	Number	Percentage
≤ 2	5	50.0%
$2 < \bar{e} \leq 3$	4	40.0%
$3 < \bar{e} \leq 4$	1	10.0%
$4 < \bar{e} \leq 5$	0	0.0%
$\bar{e} > 5$	0	0.0%

Max. Position Error, $\widetilde{e}$ (mm)	Number	Percentage
$\widetilde{e} \leq 5$	2	20.0%
$5 < \widetilde{e} \leq 10$	6	60.0%
$10 < \widetilde{e} \leq 20$	2	20.0%
$20 < \widetilde{e} \leq 30$	0	0.0%
$\widetilde{e} > 30$	0	0.0%
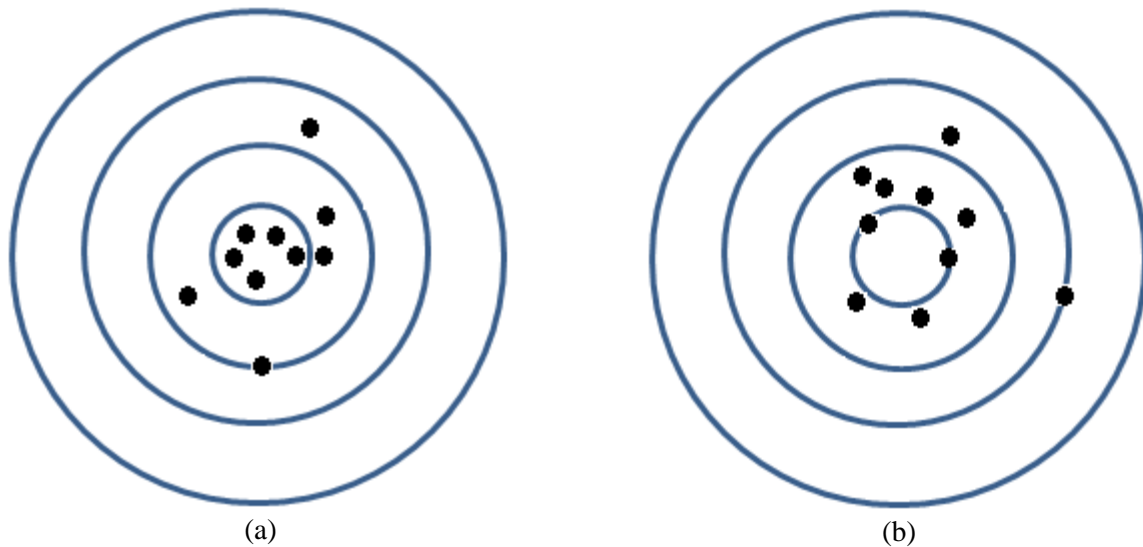
Figure 8-9. Scatter plot position error of the bilateral teleoperation experiments: (a) average position error; (b) maximum position error.

8.3 Summary

In this chapter, a bilateral teleoperation control system was proposed and experimentally evaluated. A low-cost pneumatic slave actuator, subjected to external force and friction, was navigated by a commercially-available haptic device. The interaction force on the slave side was rendered to the master actuator via the built-in controller and felt by the operator. The performance of the control system was evaluated experimentally using scenarios involving various environmental effects, namely, soft and stiff spring forces, and arbitrary forces generated directly by a human at the slave side. It was shown that in addition to stability, the control scheme satisfied the position tracking and provided stiffness reasonably. Owing to the unstructured force imposed to the slave side by the environment, and the nonlinearity of the pneumatic system, stability analysis was conducted for autonomous and non-autonomous systems using the concept of the Lyapunov exponent, which showed the stability of the system despite the mentioned non-idealities. Parametric stability analysis was also conducted, which showed the range of controller gains by which the system is stable.

9. COMPARISON OF ADMITTANCE AND IMPEDANCE UNILATERAL TELEOPERATION

Admittance and impedance control schemes are complementary. Although they are derived from the same concept and share fundamental similarities, their performance can be different in applications. Richardson [9] suggested the use of admittance control for pneumatic systems. In a more recent research, impedance control was preferred over admittance for pneumatic actuators [67]. This chapter is dedicated to comparison of the admittance and impedance schemes in the context of teleoperation. Position accuracy, energy dissipation, and responsiveness to external force are compared.

9.1 Positioning Accuracy

Positioning accuracy is an important factor in evaluating every teleoperation system since the slave is expected to follow the motion of the master to the greatest possible accuracy. The

positioning accuracies of admittance and impedance methods are achieved by calculating the average position error of the experiments presented in Figures 6-7, 6-8, 7-9,7-10 while the external force is almost zero. The results are summarized in Table 9-1:

Table 9-1. Comparison of the position errors

Method	Avg. Position Error (mm)	Max. Position Error (mm)	Min. Position Error (mm)	Standard Deviation (mm)	Variation (mm^2)	Root Mean Square (mm)
Admittance	1.3	13	0.04	1.98	3.93	1.7
Impedance	9.1	14	7	5.61	31.43	10.4

According to Table 9-1, admittance unilateral teleoperation provides higher tracking accuracy. This is expected since admittance unilateral teleoperation utilizes an SMC position controller. Whereas, in impedance unilateral, an SMC force controller is in charge of tracking the position.

9.2   Energy Dissipation

The sum of the Lyapunov exponents shows the generalized convergence/divergence of the trajectories in the phase space, which is related to energy dissipation. Energy dissipation in mechanical systems corresponds to the damping characteristic of the system [44]. Therefore, a system with a lower sum of LEs has a faster exponential divergence of the disturbance imposed on the initial states [28]. Referring to Table 6-1, Table 6-4, Table 7-1 and Table 7-4, the sum of LEs for the under-question teleoperation methods are given below.

Table 9-2. Comparison of the sum of LEs

Method	Sum of LEs
Autonomous Admittance Unilateral	-341.6
Non-Autonomous Admittance Unilateral	-319.1
Autonomous Impedance Unilateral	-321.9
Non-Autonomous Impedance Unilateral	-312.5

Referring to Table 9-2, admittance unilateral has a higher energy dissipation characteristic, which corresponds to more damping characteristic. It is evident from Table 9-2 that for admittance and impedance, the energy dissipation of the regulating task is higher than the tracking task.

9.3   Sensitivity to External Force

For teleoperation systems, it is crucial to know how fast each method incorporates the external force to the movement of the slave actuator, i.e. how long it takes the slave actuator to adjust its displacement in reaction to an external force. For this purpose, the experimental results in Chapter 6 and 7 are compared here. According to Figure 9-1, the average time admittance unilateral teleoperation takes to reflect the effect of the external force in the slave displacement is 0.2 seconds. The admittance unilateral teleoperation passes the external force through the admittance model, which, in fact, is a low pass filter. Therefore, the output of the admittance model is slightly delayed. Furthermore, the slave manipulator, which is in charge of dealing with the external force, is controlled by SMC. Depending on the tracking performance of SMC, especially in the presence of friction, the reaction to the external force can be delayed even more. With reference to Figure 9-2, the delay between force exertion and change in the slave displacement is almost 1.0 second.   Similar to the admittance unilateral teleoperation, the reaction of the impedance unilateral teleoperation to external force can be delayed by the SMC force controller. Another issue with the impedance unilateral teleoperation can be explained by rewriting the impedance model:

$$F_d = \frac{m_p}{M}(M\ddot{x}_d + B\dot{e}_x + Ke_x) + \left(F_f + b\dot{x}_s\right) + (\frac{m_p}{M} - 1)F_{ext} \quad . \tag{9-1}$$

The effect of the external force in F_d depends on the values of the other terms of the impedance model, especially friction. When the direction of the motion is opposite to the

direction of the external force, i.e. external force and friction are in the same direction but F_f has a positive sign and F_{ext} has a negative sign ($m_p/M - 1 < 0$), F_{ext} should be big enough to be able to make a notable change in F_d and change the direction of motion.
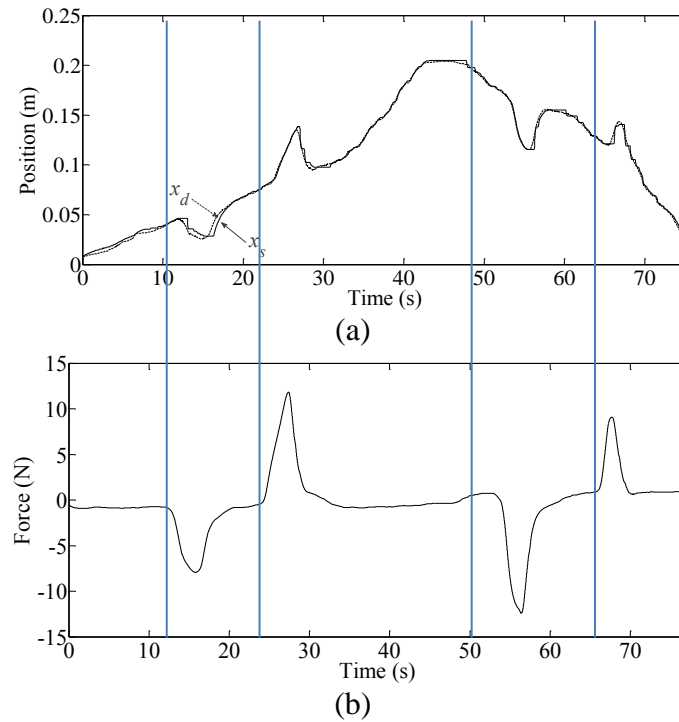
Figure 9-1. Experimental result of admittance unilateral teleoperation: (a) position of slave manipulator, x_s; (b) external force, F_{ext}.
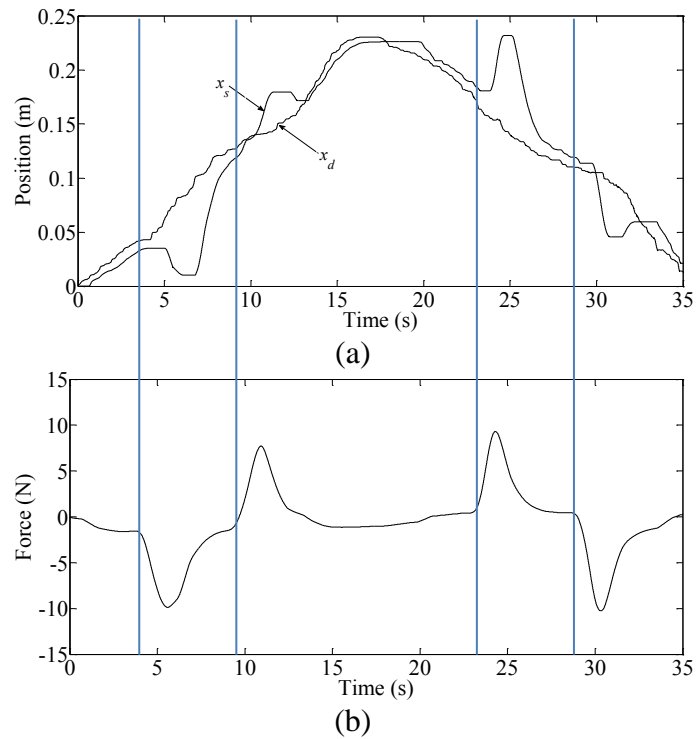
Figure 9-2. Experimental result of impedance unilateral teleoperation: (a) position of

slave manipulator, x_s; (b) external force, F_{ext}.

9.4   Summary

Admittance and impedance unilateral teleoperation methods applied to a pneumatic system were compared in this chapter. The comparison showed that admittance unilateral teleoperation provides higher positioning accuracy because it is formed around a position tracking loop. Using the concept of LEs, the energy dissipation of the two methods were compared. The numerical results showed that the admittance control has a higher damping characteristic than impedance control. Experimental results presented earlier in chapters 6 and 7 were used to compare the methods in terms of sensitivity to external force. It was shown that using the admittance control, the slave reaction to the external force is faster than the impedance control. Therefore, for the pneumatic teleoperation system in question, admittance control performs better than impedance control.

10. CONCLUSIONS

10.1 Contribution of this Thesis

The focus and novelty of this thesis is developing a human-haptic-pneumatic system using a solenoid valve-driven, industrial pneumatic actuator, and a commercial electrical haptic device, with one potential application in rehabilitation studies and not necessary that one only. This is unlike the available pneumatic teleoperation systems in which both slave and master are identical. An electrical master actuator is available, noiseless, and more affordable in comparison to a pneumatic master actuator. Development of a bilateral control, development of unilateral systems with two configurations and comparing them together under the same environment and stability studies of all using the concept of LE for the first time for such systems are novelties of this thesis. The contribution of the thesis is listed as follows:

I.   In order to find a suitable controller for teleoperation application, three position controllers were compared to each other. One controller was a novel model-free, intelligent positioning method, BELBIC, which was implemented in this application for

the first time. Another controller was a nonlinear PI, which was previously applied to the same experimental setup. The third controller, SMC, belongs to the group of robust, model-based controllers. It was shown that although both controllers were comparable in terms of implementation challenges, BELBIC outperforms the nonlinear PI controller. BELBIC and SMC position controllers were compared through several experiments including tracking joystick-generated trajectories while exposed to the external force. In terms of the performance, SMC was shown to be more accurate than BELBIC. The reason is that, unlike BELBIC, SMC incorporates system parameters and measurements such as the pressure of air in the chambers. In particular, SMC provided 0.005 m less average position error than BELBIC in teleoperation configurations. The two controllers are comparable in terms of implementation difficulties. While BELBIC requires the definition of the emotional signal, SMC requires knowledge of system models and parameters.

II. Three teleoperation schemes were designed, developed and implemented on the pneumatic system employing an electrically-actuated joystick. The schemes are: (*i*) unilateral teleoperation incorporating an admittance controller, (*ii*) unilateral teleoperation incorporating an impedance controller, and (*iii*) bilateral teleoperation. The performances of the developed schemes were validated through experiments, followed by theoretical stability analysis using the concept of Lyapunov exponents. It was shown that all three methods are successful in tracking the desired position trajectory as well as handling the external force.

III. The theoretical stability analysis of the entire teleoperation system included the effect of changing certain parameters on the stability of the entire system using the concept of LEs. The concept of LEs investigates the stability of system without limiting the

parameters and control gain. It also provides a quantitative measurement of stability that allows comparison of different systems in terms of damping characteristic. The external force, the model of operator`s hand, friction, and SMC controller are considered in the stability analysis as well as the master and slave models.

IV. .Chapter 9 compares the performance of the two unilateral teleoperation methods that were presented previously. Using experimental results, it was shown that admittance unilateral teleoperation provides the better positioning accuracy (on average 0.008 m lower positioning error) than its counterpart. With regard to sensitivity to external force, it was observed that the effect of external force appears in the slave position after 0.2 seconds for admittance unilateral teleoperation. This value was 1.0 second for the impedance unilateral teleoperation. Considering that the sum of the LEs is a quantification of energy dissipation in a stable system, it was shown that admittance unilateral has higher energy dissipation than impedance teleoperation. It was discussed that the performance of impedance unilateral teleoperation was affected by static friction and also the fact that the impedance controller uses a force control loop to control the position.

10.2 Future Work

Future work of this thesis includes, but is not limited to:

i.   Development of a teleoperation system by combining the teleoperation systems discussed earlier.

ii.   Improving BELBIC by considering friction in the formulation of the controller.

iii. Investigating the meaning of each LE.

iv.   Applying the teleoperation methods developed in this thesis to a rehabilitation platform.

v. Improving the impedance/admittance schemes by reformulating the corresponding model in a way that provides a comfortable feeling to the human subject at the slave side (Having fixed gains in admittance and impedance formulation offers a single stiffness reaction, whereas it is desirable to have variable stiffness for rehabilitation purposes).

vi. Substitute the joystick, which works using a built-in controller, with a programmable joystick.

vii. Considering network delay.

REFERENCES

[1] K. Zarei-nia and N. Sepehri, "Lyapunov stable displacement-mode haptic manipulation of hydraulic actuators: theory and experiment," *International Journal of Control,* vol. 85, no. 9, pp. 1313-1326, 2012.

[2] K. Tadano and K. Kawashima, "Development of a master–slave system with force-sensing abilities using pneumatic actuators for laparoscopic surgery," *Journal of Advanced Robotics,* vol. 24, no. 30, pp. 1763-1783, 2010.

[3] M. Kontz, J. Beckwith and W. Book, "Evaluation of a teleoperated haptic forklift," in *IEEE/ASME International Conference on Advanced Intelligent Mechatronics*, Monterey, CA, US, 2005, 295-300.

[4] R. Anderson, "Bilateral control of teleoperators with time delay," *IEEE Transaction on Automatic Control,* vol. 34, pp. 494-501, 1989.

[5] R. Morales, F. Badesa, N. Aracil, J. Sabater and C. Vidal, "Pneumatic robotic systems for upper limb rehabilitation," *Journal of Medical & Biological Engineering & Computing,* vol. 49, no. 10, p. 1145–1156, 2011.

[6] T. Driver and X. Shen, "Pressure estimation-based robust force control of pneumatic actuators," *International Journal of Fluid Power,* vol. 14, no. 1, pp. 37-45, 2014.

[7] V. Durbha and P. Li, "Passive bilateral teleoperation and human power amplification with pneumatic actuators," in *Proceedings of the ASME Dynamic Systems and Control Conference*, Hollywood, CA, US, 2009, 1-8.

[8] M. Le, M. Pham, M. Tavakoli and R. Moreau, "Development of a hybrid control for a pneumatic Teleoperation system using on/off solenoid valves," in *IEEE/RSJ International Conference on Intelligent Robots and Systems*, Taipei, Taiwan, 2010, 5818-5823.

[9] R. Richardson, Control and actuation for robotic physiotherapy, PhD, Dissertation, University of Leeds, Faculty of Engineering, 2001.

[10] M. Rahman, R. Milasi, C. Lucas, B. Araabi and T. Rawan, "Implementation of emotional controller for interior permanent-magnet synchronous motor drives," *IEEE Transaction on Industry Applications,* vol. 44, no. 5, pp. 1466-1476, 2008.

[11] M. Karpenko and N. Sepehri, "Development and experimental evaluation of a fixed-gain nonlinear control for a low-cost pneumatic actuator," *IEE Proceedings of Control Theory Applications,* vol. 153, no. 6, pp. 629-640, 2006.

[12] E. Richer and Y. Hurmuzlu, "A high performance pneumatic force actuator system: part II—nonlinear controller design," *Journal of Dynamic Systems, Measurement and Control,* vol. 122, no. 3, pp. 426-434, 2000.

[13] Z. Rao and G. Bone, "Nonlinear modeling and control of servo pneumatic actuators," *IEEE Transaction on Control Systems Technology,* vol. 16, no. 3, pp. 562-569, 2008.

[14] R. Rahman, L. He and N. Sepehri, "Design and experimental study of a dynamical adaptive backstepping-sliding mode control scheme for position tracking and regulating of a low-cost pneumatic cylinder," *International Journal of Robust and Nonlinear Control,* vol. 26, p. 853–875, 2016.

[15] K. Khayati, P. Bigras and L. Dessaint, "LuGre model-based friction compensation and positioning control for a pneumatic actuator using multi-objective output-feedback control

via LMI optimization," *Journal of Mechatronics,* vol. 19, p. 535–547, 2009.

[16] Z. Qiu, B. Wang, X. Zhang and J. Han, "Direct adaptive fuzzy control of a translating piezoelectric flexible manipulator driven by a pneumatic rodless cylinder," *Journal of Mechanical Systems and Signal Processing,* vol. 36, p. 290–316, 2013.

[17] Y. Liua, T. Kung, K. Chang and S. Chen, " Observer-based adaptive sliding mode control for pneumatic servo system," *Journal of Precision Engineering,* vol. 37, p. 522– 530, 2013.

[18] G. Bone, M. Xue and J. Flett, "Position control of hybrid pneumatic–electric actuators using discrete-valued model-predictive control," *Journal of Mechatronics,* vol. 25, p. 1–10, 2015.

[19] S. Salim, M. Rahmat, A. Faudzi and Z. Ismail, "Position control of pneumatic actuator using an enhancement of NPID controller based on the characteristic of rate variation nonlinear gain," *International Journal of Advanced Manufacturing Technology,* vol. 75, p. 181–195, 2014.

[20] C. Shang, G. Tao and D. Meng, "Adaptive robust trajectory tracking control of a parallel manipulator driven by pneumatic cylinder," *Advances in Mechanical Engineering,* vol. 8, no. 4, p. 1–15, 2016.

[21] X. Shen, "Nonlinear model-based control of pneumatic artificial muscle servo systems," *Control Engineering Practice,* vol. 18, pp. 311-317, 2010.

[22] V. Jouppila, S. Gadsden, G. Bone, A. Ellman and S. Habibi, "Sliding mode control of a pneumatic muscle actuator system with a PWM strategy," *International Journal of Fluid Power,* vol. 15, no. 1, pp. 19-31, 2014.

[23] N. Gulati and E. Barth, "A globally stable, load-independent pressure observer for the servo control of pneumatic actuators," *IEEE/ASME Transaction on Mechatronics,* vol. 14, no. 3, pp. 295-306, 2009.

[24] R. Moreau, M. Pham, M. Tavakoli, M. Le and T. Redarce, "Sliding-mode bilateral teleoperation control design for master–slave pneumatic servosystems," *Control Engineering Practice,* vol. 20, p. 584–597, 2012.

[25] M. Le, M. Pham, M. Tavakoli, R. Moreau, J. Simon and T. Redarce, "Bilateral control of nonlinear pneumatic teleoperation system with solenoid valves," *IEEE Transaction on Control Systems Technology,* vol. 21, no. 4, pp. 1463-1470, 2013.

[26] S. Hodgson, M. Le, M. Tavakoli and M. Pham, "Improved tracking and switching performance of an electro-pneumatic positioning system," *Journal of Mechatronics,* vol. 22, pp. 1-12, 2012.

[27] N. Hogan and S. Buerger, "Impedance and Interaction Control," in *Robotics and Automation Handbook*, Boca Raton, FL, United States, CRC Press, 2004, pp. 368-391.

[28] H. Khalil, Nonlinear Systems, Upper Saddle River, NJ, US: Prentice Hall, 1995.

[29] N. Hogan, "Controlling impedance at the man/machine interface," in *Proceeding of IEEE International Conference on Robotics and Automation*, Scottsdale, AZ, US, 1989, 1626-1631.

[30] K. Tadano and K. Kawashima, "Development of 4-DOFs forceps with force sensing using pneumatic servo system," in *Proceeding of IEEE International Conference on Robotics and Automation*, Orlando, FL, US, 2006, 2250-2255.

[31] M. Lyapunov, The general problem of the stability of motion (In Russian), PhD dissertation, University of Kharkov, Kharkov Mathematics Society, 1892.

[32] X. Shen and M. Goldfarb, "On the enhanced passivity of pneumatically actuated impedance-type haptic interfaces," *IEEE Transaction on Robotics,* vol. 22, no. 3, pp. 470-480, 2006.

[33] A. Haddadi and K. Hashtrudi-Zaad, "A new robust stability analysis and design tool for bilateral teleoperation control systems," in *IEEE International Conference on Robotics and Automation*, Pasadena, CA, US, 2008, 663-670.

[34] R. Adams and B. Hannaford, "Stable haptic interaction with virtual environments," *IEEE Transaction on Robotics and Automation,* vol. 15, no. 3, pp. 465 -474, 1999.

[35] Y. Sun and Q. Wu, "A radial-basis-function network-based method of estimating Lyapunov exponents from a scalar time series for analyzing nonlinear systems stability," *Journal of Nonlinear Dynamics,* vol. 70, p. 1689–1708, 2012.

[36] W. Story, application of Lyapunov exponents to strange attractors and intact & damaged ship stability, MSc dissertation, Virginia Polytechnic and State university,College of Engineering, 2009.

[37] P. Sekhavat, N. Sepehri and C. Wu, "Calculation of Lyapunov exponents using nonstandard finite difference discretization scheme: a case study," *Journal of Difference Equations and Applications,* vol. 10, no. 4, pp. 369-378, 2006.

[38] C. Yang, C. Wu and P. Zhang, "Estimation of Lyapunov exponents from a time series for n-dimensional state space using nonlinear mapping," *Journal of Nonlinear Dynamics,* vol. 69, p. 1493–1507, 2012.

[39] M. Tufail and C. De Silva, "Haptic teleoperation using impedance control with application in homecare robotics," *Control and Intelligent Systems,* vol. 41, no. 3, 2013.

[40] I. Aliaga, A. Rubio and E. Sanchez, "Experimental quantitative comparison of different control architectures for master–slave teleoperation," *IEEE Transaction of Control Systems Technology,* vol. 12, no. 1, pp. 2-11, 2004.

[41] C. De Wit, H. Olsson, K. Astrom and P. Lischinsky, "A new model for control of systems with friction," *IEEE Transaction of Automation and Control,* vol. 40, no. 3, pp. 419-25, 1995.

[42] S. Liu and J. Bobrow, "An analysis of a pneumatic servo system," *Transaction of ASME Journals on Dynamic Systems Measurement and Control,* vol. 110, pp. 228-235, 1988.

[43] F. Sanville, "A new method of specifying the flow capacity of pneumatic fluid power valves," *BHRA 2nd International Fluid Power Symposium,* pp. 337-D347, 1971.

[44] J. Shin and K. Hammond, "The instantaneous Lyapunov exponent and its application to chaotic dynamical systems," *Journal of Sound and Vibration,* vol. 218, no. 3, pp. 389-403, 1998.

[45] S. F. Bockman, "Lyapunov exponents for system described by Differential Equations with discontinuous right-hand sides," in *American Control Conference*, Boston, MA, US, 1991, 1673-1678.

[46] T. S. C. L. O. Parker, Practical Numerical Algorithms for Chaotic Systems, New York, US: Springer-Verlag New York, 1989.

[47] J. P. Eckmann and D. Ruelle, "Ergodic theory of chaos and strange attractors," *Reviews of Modern Physics,* vol. 57, pp. 617 -656, 1985.

[48] A. M. Stuart and A. R. Humphries, Dynamical Systems and Numerical Analysis.

CømbrÌdge, Cambridge, UK: Cambridge University Press, 1998.

[49] A. Medio and M. Lines, Nonlinear dynamics: a primer, Cambridge, UK: Cambridge University Press, 2001.

[50] M. Kunze, Non-smooth dynamical systems, Berline, Germany: Springer Berlin Heidelberg, 2000.

[51] A. Wolf, J. Swift, H. Swinney and J. Vastano, "Determining Lyapunov exponents from a time series," *Journal of Physica,* vol. 16, no. 4, pp. 285-317, 1985.

[52] V. Oseledec, "A multiplicative ergodic theorem: Lyapunov characteristic numbers for dynamical system," *Transaction of Moscow Math Society,* vol. 19, pp. 197-231, 1968.

[53] P. Sekhavat, N. Sepehri and C. Wu, "Overall stability analysis of hydraulic actuator's switching contact control using the concept of Lyapunov exponents," in *International Conference on Robotics and Automation*, Barcelona, Spain, 2005, 550-556.

[54] A. Filippov, Differential equations with discontinuous right-hand sides, Aalipine, Netherlands: Springer Netherlands, 1988.

[55] P. Muller, "Calculation of Lyapunov exponents for dynamic systems with discontinuities," *Journal of Chaos, Solitans and Fractals,* vol. 5, no. 9, pp. 1671-1681, 1995.

[56] A. Filippov, "Differential equations with discontinuous right-hand sides," *Math Sbornnik,* pp. 51-99, 1960.

[57] J. Moren, *Emotion and Learning,* PhD Dissertation, Cognitive Science Department, Lund University, 2002.

[58] C. Lucas and D. Shahmirzadi, "Introducing BELBIC: Brain Emotional Learning Based Intelligent Controller," *International Journal of Intelligent Automation and Soft Computing,* vol. 10, no. 1, pp. 11-22, 2004.

[59] M. Valipor, K. Maleki and S. Ghidary, "Optimization of emotional learning approach to control systems with unstable equilibrium," in *Software Engineering, Artificial Intelligence, Networking and Parallel/Distributed Computing*, Switzerland, Springer International Publishing, 2015, pp. 45-56.

[60] M. Khalghania and M. Khoobanb, "A novel self-tuning control method based on regulated bi-objective emotional learning controller's structure with TLBO algorithm to control DVR compensator," *Applied Soft Computing,* vol. 24, p. 912–922, 2014.

[61] T. Jaksch, R. Ortner and P. Auer, "Near-optimal regret bounds for reinforcement learning," *Journal of Machine Learning Research,* vol. 11, p. 1563–1600, 2010.

[62] K. Dakkan, E. Barth and M. Goldfarb, "Dynamic constraint based energy saving control of pneumatic servo systems," *ASME Journal of Dynamic Systems, Measurement and Control,* vol. 128, no. 3, pp. 655-662, 2006.

[63] J. Wu, M. Goldfarb and E. Barth, "On the observability of pressure in a pneumatic servo actuator," *ASME Journal of Dynamics System, Measurement and Control,* vol. 126, p. 921–924, 2004.

[64] S. Chiavervini and L. Sciavicco, "The parallel approach to force/position control of robotic manipulators," *IEEE Transaction on Robotics and Automation,* vol. 9, no. 4, p. 61–373, 1993.

[65] G. Ferretti, G. Magnani and P. Rocco, "Toward the implementation of hybrid force/position control in industrial robots," *IEEE Transaction on Robotics and Automation,* vol. 13, no. 6,

p. 838–845, 1997.

[66] N. Hogan, "Impedance control: an approach to manipulation part I,II,III," *Journal of Dynamic Systems, Measurements and Control,* vol. 107, no. 1, pp. 1-24, 1985.

[67] R. Richardson, M. Brown, B. Bhakta and M. Levesley, "Impedance control for a pneumatic robot-based around pole-placement, joint space controllers," *Journal of Control Engineering Practice,* vol. 13, p. 291–303, 2005.

[68] N. Yu, C. Hollnagel, A. Blickenstor, S. Kollias and R. Riener, "Comparison of MRI-compatible mechatronic systems with hydrodynamic and pneumatic actuation," *IEEE/ASME Transaction on Mechatronics,* vol. 13, no. 3, pp. 268-277, 2008.

[69] H. Kazerooni, "Design and analysis of pneumatic force generators for mobile robotic systems," *IEEE/ASME Transaction on Mechatronics,* vol. 10, no. 4, pp. 411-418, 2005.

[70] C. Ying, Z. Jia-fan, Y. Can-jun and N. Bin, "Design and hybrid control of the pneumatic force-feedback systems for Arm-Exoskeleton by using on/off valve," *Journal of Mechatronics,* vol. 17, p. 325–335, 2007.

[71] S. Kaitwanidvilai and M. Parnichkun, "Force control in a pneumatic system using hybrid adaptive neuro-fuzzy model reference control," *Journal of Mechatronics,* vol. 15, pp. 23-41, 2005.

[72] D. Ben-Dov and S. Salcudean, "A force-controlled pneumatic actuator," *IEEE Transaction on Robotics and Automation,* vol. 11, no. 6, pp. 906-911, 1995.

[73] J. Bobrow and F. Jabbari, "Adaptive pneumatic force actuation and position control," *Journal of Dynamic System, Measurement and Control,* vol. 113, pp. 367-272, 1991.

[74] D. Meng, G. Tao, W. Ban and P. Qian, "Adaptive robust output force tracking control of pneumatic cylinder while maximizing/minimizing its stiffness," *Journal of Central South University,* vol. 20, no. 6, p. 1510−1518, 2013.

[75] B. Taheri, D. Case and E. Richer, "Force and stiffness backstepping-sliding mode controller for pneumatic cylinders for wearable robotic applications," *IEEE/ASME Transaction on Mechatronics,* vol. 19, no. 6, pp. 1799-1809, 2012.

[76] T. Nguyen, J. Leavitt, F. Jabbari and J. Bobrow, "Accurate sliding-mode control of pneumatic systems using low-cost solenoid valves," *IEEE/ASME Transaction on Mechatronics,* vol. 12, no. 2, 2007.

[77] H. Aschemann and D. Schindele, "Sliding-mode control of a high-speed linear axis driven by pneumatic muscle actuators," *IEEE Transaction on Industrial Electronics,* vol. 55, no. 11, pp. 3855-3864, 2008.

[78] Y. Zhu and E. Barth, "Impedance control of a pneumatic actuator for contact tasks," in *IEEE International Conference on Robotics and Automation*, Barcelona, Spain, 2005, 987-992.

[79] M. Kunze, Non-smooth dynamical systems, Springer-Verlag, 2000.

[80] N. Garmsiri and N. Sepehri, "Emotional learning based position control of pneumatic actuators," *International Journal of Automation and Soft Computing,* vol. 20, no. 3, pp. 433-450, 2014.

[81] N. Garmsiri, Y. Sun, C. Yang and N. Sepehri, "Bilateral teleoperation of a pneumatic actuator: experiment and stability analysis," *International Journal of Fluid Power,* vol. 16, no. 2, pp. 99-110, 2015.

[82] N. Garmsiri, Y. Sun and N. Sepehri, "Impedance control of a teleoperated pneumatic

actuator: Implementation and stability analysis," *Journal of Control and Intelligent Systems,* 2017 (In Press).

[83] N. Garmsiri, Y. Sun, P. Sekhavat, C. Yang and N. Sepehri, "Implementation and stability analysis of an admittance-controlled pneumatic teleoperation system," *International Journal of Control,* 2017 (Submitted.).

APPENDIX: LINEARIZATION AND SOLUTION ANALYSIS

The required conditions for validity of applying the concept of Lyapunov Exponents are mentioned in Chapter 4. They are the existence of solution of the nonlinear system; existence and uniqueness of solution of the linearized system. These conditions are studied here for the unilateral teleoperation system employing admittance control that is formulated by (6-5). The same analysis can be applied to the systems mentioned in Chapters 7 and 8.

I. *Solution analysis for nonlinear equation*

Equation (6-5) is continuous, fully-defined, bounded, but nonsmooth at the following instants: : (i) $x_2 = 0,$ in friction model described by (6-13); (ii) $P_d/P_u = P_{cr}$, in the mass flow rate model described by (6-14), when the valve alters between sonic and subsonic flow regimes; (iii) $x_5 = 0,$ in (6-14), which makes $\dot{m}_1$, $\dot{m}_2$ and u nonsmooth (as the result of discontinuity of Px). Being bounded, and continuous, and measurable, (6-5) satisfies Filippov's solution theory [54] which states that a solution exists for nonlinear equation of motion, (6-5).

II. *Solution analysis for linearized equation*

To study existence and uniqueness of the solution of the linearized equations of motion for (6-5), the theory of Caratheodory for differential equations is used [54]. By inspecting (6-5), it is observed that the linearized equation is defined and piecewise continuous. According to this theory, since all the elements of the linearized equations of motion are defined and piecewise

continuous, and measurable, and $|F(x(t)) \le m(t)|$, where the function $m(t)$ is summable (piece-wise integrable) on each finite interval, the solution of linearized function of (6-5) and is unique.

III. *Linearization of dynamic model at nonsmooth instants*

As mentioned above, (6-5) cannot be linearized in three instants. To find the numerical value of principal axes length, the extension method of calculating the variational equation of nonsmooth systems [79, 55] is used. Since all of the states evolve continuously in time, the Jacobian of the transition condition, G, is always the identity matrix. According to Fillipov [56], the numerical value of variational equations at nonsmooth instants can be defined as:

$$\delta x^+ = G(x^-)\delta x^- + [G(x^-)f_1(x^-) - f_2(x^+)]\frac{H(x^-)\delta x^-}{H(x^-)f_1(x^-)} \tag{A.1}$$

where δx^+ and δx^- are the numerical values of variational equations before and after the nonsmooth instant. f_1 and f_2 are the nonlinear equations of motion before and after the nonsmooth instant, and the plus and minus signs characterize the right and left-sided limits, respectively. The matrix $H(x^-)$ is the Jacobian of the indicator function, $h(x)$, which indicates the switching to the next manifold of motion [55]. Precise examination of (6-5) shows that the right-hand sides of equations never experience discontinuity. In other words, $f_1 = f_2 = f$, and (A.1) yields:

$$\delta x^+ = \delta x^- \tag{A.2}$$

At the nonsmooth instants of motion, where Jacobian does not exist, equation (A.2) can be used.